

Inaugural dissertation
for
obtaining the doctoral degree
of the
Combined Faculty of Mathematics, Engineering and
Natural Sciences
of the
Ruprecht – Karls – University
Heidelberg

Presented by
M.Sc. Roberto Saleppico
born in: Terni, Italy

Oral examination: 6.12.2022

Molecular analysis of the unconventional secretory pathway of FGF2 employing TIRF microscopy

Referees: Prof. Dr. Walter Nickel
Prof. Dr. Thomas Söllner

Table of Contents

Summary	6
Zusammenfassung.....	7
1. Introduction.....	8
<i>1.1 Conventional ER/Golgi secretory pathway.....</i>	<i>8</i>
<i>1.2 Unconventional protein secretion.....</i>	<i>11</i>
1.2.1 Type I UPS.....	11
1.2.2 Type II UPS.....	14
1.2.3 Type III UPS	14
1.2.4 Type IV UPS	16
<i>1.3 Fibroblast Growth Factor 2.....</i>	<i>16</i>
<i>1.4 Na-K-ATPase.....</i>	<i>20</i>
<i>1.5 Glypican 1.....</i>	<i>23</i>
<i>1.6 Plasma membrane lipid composition.....</i>	<i>25</i>
1.6.1 Cholesterol	25
1.6.2 Sphingolipids.....	27
1.6.3 Liquid-ordered domains	28
2. Aims of the thesis	32
3. Materials and Methods.....	33
<i>3.1 Materials.....</i>	<i>33</i>
3.1.1 Consumables	33
3.1.2 Chemicals and biological reagents	34
3.1.3 Biochemical kits and Assays	36
3.1.4 Antibodies	36
3.1.5 Plasmids	37
3.1.6 Cell Lines.....	38
3.1.7 Equipment.....	39
3.1.8 Softwares	40
<i>3.2 Methods.....</i>	<i>41</i>
3.2.1 Molecular Biology techniques.....	41
3.2.2 Cell Biology techniques.....	44
3.2.3 Biochemical techniques.....	48
3.2.4 Microscopy techniques.....	51
3.2.5 Statistical analysis.....	53
4. Results	54
<i>4.1 The $\alpha 1$ subunit of the Na,K-ATPase is the first physical contact of FGF2 at the inner plasma membrane leaflet.....</i>	<i>54</i>
4.1.1 Ouabain-dependent inhibition of the Na,K-ATPase have an impact on the unconventional secretion of FGF2	61
<i>4.2 The role of cysteine 77 and 95 on the unconventional secretory pathway of FGF2</i>	<i>63</i>
<i>4.3 Glypican 1 is a rate limiting factor of FGF2 secretion from cells.....</i>	<i>66</i>

<i>4.4 The importance of plasma membrane lipid composition on the unconventional secretion of FGF2</i>	69
4.4.1 The role of cholesterol in the unconventional secretory pathway of FGF2.....	69
4.4.2 The role of sphingomyelin in the unconventional secretory pathway of FGF2	80
5. Discussion	90
<i>5.1 The $\alpha 1$ subunit of the Na,K-ATPase is the first physical contact of FGF2 at the inner plasma membrane leaflet</i>	90
<i>5.2 Two different roles for two cysteine residues?</i>	92
<i>5.3 A possible involvement of liquid-ordered domains on the unconventional secretion of FGF2</i>	95
<i>5.4 Lipidomic analysis</i>	99
6 Conclusion and future perspective	100
7. References	102
8. Acknowledgments	118

Summary

Protein secretion has been for long believed to be exclusively taking place through the conventional ER/Golgi-dependent secretory pathway. However, in the last few decades, more and more studies pointed at several different routes for protein lacking a signal peptide to get secreted from cells. It is now accepted from the scientific community that protein secretion from cells can also follow unconventional, ER/Golgi-independent pathways. These processes have been collectively termed Unconventional Protein Secretion (UPS).

Fibroblast Growth Factor 2 (FGF2) is a cell survival factor involved in hematopoiesis, wound repair, and tumor-induced angiogenesis. It exerts its biological functions in the extracellular space, in an autocrine and paracrine manner. Despite this, it lacks a signal peptide and does not follow the conventional ER/Golgi-dependent secretory pathway. FGF2 has been in fact one of the first protein found to follow a UPS pathway. It directly translocates across the plasma membrane in a complete folded state. FGF2 gets recruited to the plasma membrane through interaction with the $\alpha 1$ subunit of the Na,K-ATPase. Following interaction with Tec kinase, FGF2 gets phosphorylated. Subsequently, FGF2 oligomerizes in a PI(4,5)P₂-dependent manner. The resulting oligomer is able to span the membrane, forming a toroidal lipidic pore. At this stage, membrane-proximal heparan sulfate chains capture FGF2 on cell surfaces.

Within this study, employing a recently established single molecule TIRF recruitment assay, I found the $\alpha 1$ subunit of the Na,K-ATPase to be the first physical contact of FGF2 at the inner plasma membrane leaflet. I found this interaction to be a prerequisite for the subsequent FGF2 binding to PI(4,5)P₂.

Two surface cysteine residues on FGF2, in position 77 and 95, have been for long a mystery in our laboratory with regards to their specific role. With a combination of cell-based recruitment and secretion assays, I contributed to elucidate their respective role. I found both residues to be involved in FGF2 recruitment to the inner plasma membrane leaflet, as well as in translocation to cell surfaces. Nevertheless, comparing FGF2 variants carrying either single substitutions or a double substitution of these cysteines, I observed the residue in position 95 to contribute in a stronger manner to both parameters. Combining my results with other findings from our laboratory, cysteine 95 appears to be involved in intermolecular disulfide bridge formation, while cysteine 77 seems to be involved in the interaction with the $\alpha 1$.

Glypican-1 has been recently discovered to be the dedicated HSPGs for FGF2 secretion. Under conditions of low FGF2 expression levels, I found Glypican-1 to increase FGF2 secretion from cells in a much higher manner compared to conditions of overexpressed FGF2. With this finding, I contributed to the conclusion that Glypican-1 is the rate-limiting factor for the unconventional secretion of FGF2.

Finally, I found many hints pointing at a possible involvement of liquid-ordered domains in the unconventional secretion of FGF2. This was based on my findings on the positive modulation of both cholesterol and sphingomyelin, two important components of liquid-ordered domains on the plasma membrane, on the unconventional secretion of FGF2.

Zusammenfassung

Lange Zeit ging man davon aus, dass die Proteinsekretion ausschließlich über den herkömmlichen ER/Golgi-abhängigen Sekretionsweg erfolgt. In den letzten Jahrzehnten jedoch wiesen immer mehr Studien darauf hin, dass Proteine, denen ein Signalpeptid fehlt, auf verschiedenen Wegen aus den Zellen sezerniert werden können. In der wissenschaftlichen Gemeinschaft ist man sich inzwischen einig, dass die Sekretion von Proteinen aus Zellen auch über unkonventionelle, ER/Golgi-unabhängige Wege erfolgen kann. Diese Prozesse werden unter dem Begriff Unconventional Protein Secretion (UPS) zusammengefasst.

Der Fibroblasten-Wachstumsfaktor 2 (FGF2) ist ein Zellüberlebensfaktor, der an der Hämatopoese, der Wundheilung und der tumorinduzierten Angiogenese beteiligt ist. Er übt seine biologischen Funktionen im extrazellulären Raum auf autokrine und parakrine Weise aus. Trotzdem fehlt ihm ein Signalpeptid und es folgt nicht dem konventionellen ER/Golgi-abhängigen Sekretionsweg. FGF2 ist in der Tat eines der ersten Proteine, die einem UPS-Weg folgen. Es transloziert direkt durch die Plasmamembran in einem vollständig gefalteten Zustand. FGF2 wird durch Interaktion mit der $\alpha 1$ -Untereinheit der Na,K-ATPase an die Plasmamembran rekrutiert. Nach der Interaktion mit der Tec-Kinase wird FGF2 phosphoryliert. Anschließend oligomerisiert FGF2 in einer PI(4,5)P₂-abhängigen Weise. Das resultierende Oligomer ist in der Lage, die Membran zu überbrücken und eine toroidale Lipidpore zu bilden. In diesem Stadium fangen membrannahe Heparansulfatketten FGF2 auf der Zelloberfläche ein.

In dieser Studie habe ich mit Hilfe eines kürzlich etablierten Einzelmolekül-TIRF-Rekrutierungstests festgestellt, dass die $\alpha 1$ -Untereinheit der Na,K-ATPase der erste physische Kontakt von FGF2 am inneren Plasmamembranblatt ist. Diese Interaktion erwies sich als Voraussetzung für die anschließende Bindung von FGF2 an PI(4,5)P₂.

Zwei Oberflächen-Cysteinreste auf FGF2, in Position 77 und 95, waren in unserem Labor lange Zeit ein Rätsel hinsichtlich ihrer spezifischen Rolle. Mit einer Kombination aus zellbasierten Rekrutierungs- und Sekretionstests habe ich dazu beigetragen, ihre jeweilige Rolle aufzuklären. Ich fand heraus, dass beide Reste sowohl an der Rekrutierung von FGF2 an der Innenseite der Plasmamembran als auch an der Translokation an Zelloberflächen beteiligt sind. Beim Vergleich von FGF2-Varianten, die entweder eine einfache oder eine doppelte Substitution dieser Cysteine tragen, konnte ich jedoch feststellen, dass der Rest in Position 95 stärker zu beiden Parametern beiträgt. Kombiniert man meine Ergebnisse mit anderen Erkenntnissen aus unserem Labor, so scheint Cystein 95 an der intermolekularen Disulfidbrückenbildung beteiligt zu sein, während Cystein 77 an der Interaktion mit dem $\alpha 1$ beteiligt zu sein scheint.

Kürzlich wurde entdeckt, dass Glypican-1 das dedizierte HSPG für die FGF2-Sekretion ist. Ich fand heraus, dass Glypican-1 unter Bedingungen mit geringer FGF2-Expression die FGF2-Sekretion aus den Zellen wesentlich stärker erhöht als unter Bedingungen mit überexprimiertem FGF2. Mit diesem Ergebnis trug ich zu der Schlussfolgerung bei, dass Glypican-1 der ratenlimitierende Faktor für die unkonventionelle Sekretion von FGF2 ist.

Schließlich fand ich viele Hinweise, die auf eine mögliche Beteiligung von Flüssigkeitsdomänen an der unkonventionellen Sekretion von FGF2 hinweisen. Dies basierte auf meinen Erkenntnissen über die positive Modulation von Cholesterin und Sphingomyelin, zwei wichtigen Komponenten von Flüssigkeitsdomänen auf der Plasmamembran, auf die unkonventionelle Sekretion von FGF2.

1. Introduction

1.1 Conventional ER/Golgi secretory pathway

The classical manner by which eukaryotic proteins get secreted to the extracellular space is the ER/Golgi secretory pathway¹⁻³. A schematic representation of this classical secretory mechanism is shown in figure 1. Proteins that follow this pathway usually possess an N-terminal signal peptide, an aminoacidic sequence, including a hydrophobic motif, consisting in 16–30 residues^{4,5}. This sequence is recognized and bound by the Signal Recognition Particle (SRP), a highly conserved ribonucleoprotein consisting of 6 polypeptides complexed with RNA^{4,6-8}. After SRP binding to the signal peptide, translation is transiently arrested and the SRP binds to its receptor [SRP Receptor (SR)], targeting the whole complex to the endoplasmic reticulum (ER) membrane⁵. Here, ribosomes bind to their receptor, stabilizing the complex at the ER membrane⁹. At this point, the nascent peptide is transferred into the translocon pore and SRP gets released from its receptor in a GTP-dependent manner^{10,11}. The translocon is a protein channel formed by a complex of Sec61 α (a pore-forming subunit), Sec61 β , and Sec61 γ (two accessory proteins)¹². Hydrophilic peptide chains pass through the translocon channel into the ER lumen, due to its aqueous environment, and once protein synthesis is completed, the signal peptide gets cleaved by a resident signal peptidase¹³, allowing the newly synthesized polypeptide chain to get released into the ER lumen. Proteins containing a transmembrane domain contain a stop-transfer sequence, which opens the later gate in the Sec61 α subunit allowing the peptide chain to access the lipid bilayer¹⁴⁻¹⁶. Translation of the protein continue, resulting in a protein containing a transmembrane domain, with the N-terminus in the ER-lumen and the C-terminus in the cytosolic side. There are also proteins containing internal, non-removable signal peptides. In these cases, the signal sequence acts as a transmembrane domain and, based on its orientation, can allow for different orientation of the protein (having the N-terminal either at the lumen side or at the cytosol side). Finally, proteins with multiple transmembrane domains, contain both an internal signal sequence (one or more based on the number of the transmembrane domains) as well as a stop-transfer sequence (which can also be more than one)¹⁷. During translation, molecular chaperones bind to newly synthesized peptide chains, right after their translocation into the ER-lumen¹⁸. Molecular chaperones, like BiP, facilitate protein folding in an ATP-dependent manner¹⁹. Parallel to protein translation, ER-resident enzymes catalyze N-glycosylation of the nascent polypeptide chain in the ER-lumen, through an N-glycosylic link between asparagine residues and N-acetylglucosamine²⁰. A number of post-translational modifications take place in the ER-lumen, like the formation of disulfide bridges between cysteine residues²¹. Furthermore, Glycosylphosphatidylinositol (GPI) anchors are synthesized in the ER and added to polypeptides with a C-terminal signal for GPI anchor attachment²². GPI

anchor consists of conserved core glycan, glycan side chains and phosphatidylinositol (PI), which anchors the GPI to the lipid bilayer through its fatty acid chains. Once protein translation is concluded, the C-terminal transmembrane signal is removed and the new C-terminal is linked to the primary amine group of the GPI's ethanolamine. In this way, the newly synthesized protein remains anchored to the lipid bilayer through the GPI anchor, and it is not inserted through a transmembrane domain.

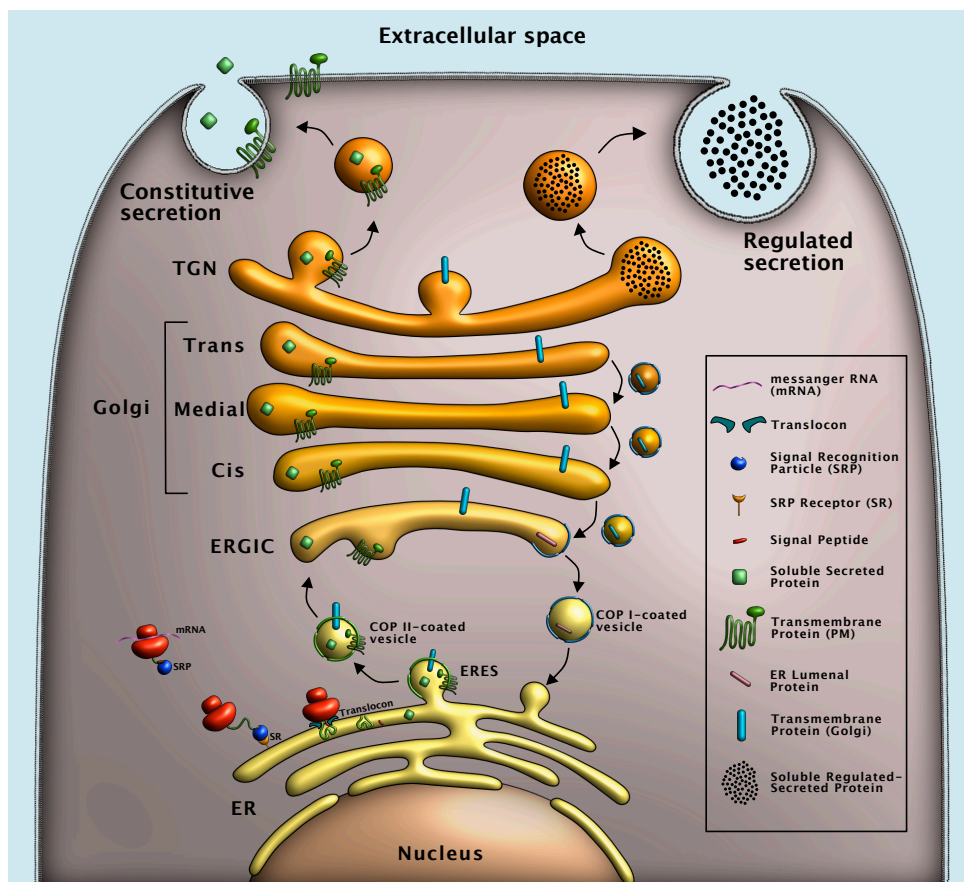


Figure 1: ER/Golgi-dependent conventional secretory pathway. Protein translation of secreted proteins starts in the cytosol and, following binding of the SRP, they translocate in the ER lumen through the translocon. The signal sequence is then cleaved off and protein folding occurs in the ER. Proteins are subsequently packaged in COPII vesicles, where they reach the ERGIC and the Golgi apparatus. Following further maturation into the Golgi, proteins are sorted in secretory vesicles (SVs) and delivered to the extracellular space. *Adapted from Viotti, 2016²³.*

All of these covalent changes are also important for correct folding of the proteins. Before exit from the ER, proteins undergo to a strict “quality control” system mediated by molecular chaperones and folding sensors, including calnexin and BiP, which recognize improperly folded proteins and target them to the cytosol for proteasome-mediated degradation²⁴. At this point, properly folded and modified proteins are exported from ER exit sites (ERES), specific smooth ER protuberances coated with Coat protein complex II (COP II). COP II-coated vesicles, which mediate ER to Golgi transport of newly synthesized proteins, are generated at the ERES²⁵. Vesicles formation is dependent on a small GTPase, Sar1, which recruits COP II

components, Sec12, which catalyzes the activation of Sar1 at the ERES, as well as the Sec23/24 heterodimeric bow tie-shaped subcomplex and the Sec 13/31 hetero-tetrameric subcomplex, which constitute the inner and the outer coat complex, respectively²⁶. Proteins are sorted into COP II vesicles through binding of specific cargo receptors, which differ for transmembrane and soluble cargo proteins. Transmembrane proteins are sequestered into COP II vesicles via binding of Sec24 to their cytoplasmic tail, whereas soluble proteins bind to cargo receptors belonging to ERGIC-53 family, Erv family, or p24 family²⁷. After release of cargo proteins into the ER-Golgi intermediate compartment (ERGIC), these cargo receptors recycle back to the ER into COP I vesicles²⁸. ERGIC is exclusively present in mammalian cells, while is absent in yeast and plant cells, where COP II vesicles directly fuse with *cis*-Golgi²⁹. This difference is probably due to the higher distance between ER and Golgi in mammalian cells, compared to yeast and plant cells, making it necessary to have an intermediate compartment. Cargo protein-containing vesicles are then carried to the *Cis*-Golgi Network (CGN) in a microtubule-dependent manner³⁰. In the CGN, O-glycosylation is initiated through binding between N-acetyl-galactosamine (GalNAc) and the hydroxyl group of a serine or a threonine residue³¹. The Golgi apparatus consists of closely packed membrane *cisternae*, with a various number of stacks based on cell type (usually between four and seven *cisternae*)³². The Golgi apparatus has a specific polarity from *cis*- (facing the ER), *medial*- (in between), and *trans*-Golgi *cisternae* (in the direction of the plasma membrane), which is mainly reflected by different enzyme localization, causing specific post-translational modifications for each stack. Transport through the Golgi is currently debated, since it may occur by vesicular transport or cisternal maturation³³⁻³⁷, with the latter being more accepted. In this model, the cargo proteins remain in the same compartment, which undergo remodeling due to loss of early-acting enzymes and acquisition of late-acting enzymes. To achieve this, Golgi proteins are packaged into COP I vesicles and move with a retrograde direction into the more proximal compartment (i.e., from *trans*- to *medial*-Golgi and so on)³⁸. In the *cis*-Golgi *cisternae*, mannose is removed by the early acting mannosidase II, and lysosomal protein phosphorylation, which begins in the CGN, continues. In the *medial-cisternae*, O-glycosylation is continued with binding of N-acetyl-glucosamine (GlcNAc) to the hydroxyl group of a serine or a threonine residue. In the *trans-cisternae*, galactose is added by the late-acting galactosyl-transferase. Furthermore, in the Golgi apparatus and in the *Trans*-Golgi Network (TGN), other post-translational modifications occur, for example sialic acid addition and tyrosine sulfation. Within the TGN, the modified proteins get sorted into their final destination. They can be inserted in the plasma membrane as transmembrane proteins, directed to the endolysosomal system as lysosomal enzyme pools, or get secreted to the extracellular space. For the last ones, there are two different pathways: a constitutive secretion (which is present in each cell type), and a regulated secretion (only occurring in specialized cell types). Constitutive secretion leads to a bulk flow of secretion of the vesicles content (e.g., glycoproteins)³⁹, whereas regulated secretion is restricted to specialized cells and consists in

the rapid secretion of granules content (e.g., hormones and digestive enzymes) in a signal-dependent manner⁴⁰.

1.2 Unconventional protein secretion

The majority of secreted proteins have a signal peptide and follow the previously described classical ER/Golgi-dependent secretory pathway. Nevertheless, in the last few decades, a number of proteins have been shown to have an extracellular localization, even though they lack a signal peptide⁴¹. For this reason, these proteins have been classified as unconventionally secreted proteins⁴²⁻⁴⁴. The majority of unconventionally secreted cargos have a function also inside the cell, and not only at the extracellular space, and most of them get unconventionally secreted only upon a certain stimulus (e.g., starvation or inflammation). In some cases, a finely regulated secretion is necessary, since the presence of the unconventionally secreted cargo at the cell exterior may be harmful for the organism [this is the case, among others, for IL-1 β and Insulin Degrading Enzyme (IDE)]. Over the years, more and more proteins have been shown to be secreted upon unconventional protein secretion (UPS), and there are now four different pathways of UPS: type I, type II, type III and type IV⁴²⁻⁴⁵ (Fig. 2). Type I UPS consists in direct translocation across plasma membrane of the cargo; protein secreted through type II UPS uses ABC transporters; type III UPS involves secretion through endocytic compartments; type IV UPS refers to transmembrane proteins which bypass the Golgi apparatus and directly go from the ER to the plasma membrane.

1.2.1 Type I UPS

The most studied protein following type I UPS is Fibroblast Growth Factor 2 (FGF2), which directly translocate across the plasma membrane through the formation of a toroidal lipidic pore⁴⁶ (the unconventional secretory pathway of FGF2 will be discussed in more detail in section 1.3). Other proteins that reach the extracellular space following type I UPS are HIV-Tat (the Trans-activator of transcription of the Human Immunodeficiency Virus), annexins and, under certain circumstances, IL-1 β and Tau, which can also follow type III UPS.

The first step into the discovery of unconventional secretory pathways among eukaryotic cells was the cloning of IL-1 β , a pro-inflammatory cytokine that gets secreted to exert its biological functions, but that was found to lack a signal peptide⁴⁷⁻⁴⁹. IL-1 β has been proposed to follow either type I or type III UPS pathway, based on the immune cell being involved in the secretion, the immune stimulation type, as well as the time scale exposure to Damage- or Pathogen-Associated Molecular Patterns (DAMPs and PAMPs, respectively)⁵⁰. A type I UPS of IL-1 β is triggered in macrophages by the presence of DAMPs (like extracellular ATP) and/or PAMPs (like bacterial lipopolysaccharides), which lead to inflammasome activation⁵¹. Under these

conditions, the IL-1 β precursor (pro-IL-1 β), as well as gasdermin D, are proteolytically cleaved into their active forms: mature IL-1 β (mIL-1 β), and N-terminal gasdermin D (gasdermin N)^{52,53}.

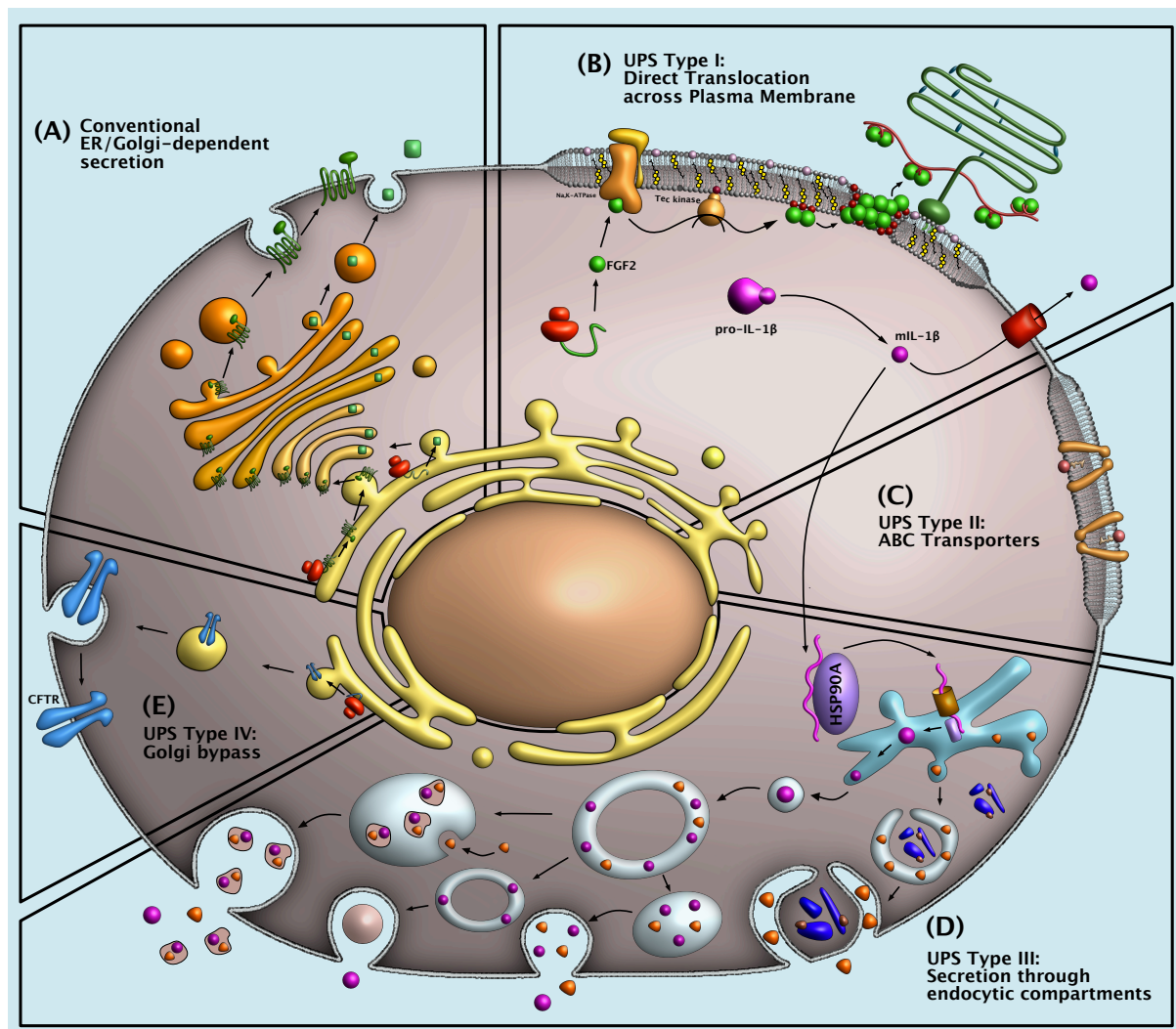


Figure 2: Pathways of Unconventional Protein Secretion. Beyond the classical ER/Golgi-dependent secretory pathway (A), the four different types of Unconventional Protein Secretion (UPS) are shown. (B) Type I UPS: for direct translocation of the cargo across the plasma membrane; Type II UPS (C), for ABC transporters-mediated protein translocation across the plasma membrane; Type III UPS (D), for proteins secreted through endocytic compartments; and Type IV UPS (E) for proteins that reaches the plasma membrane through Golgi bypass. Inspired by Dimou and Nickel, 2018⁴³, and Pallotta and Nickel, 2020⁵⁴.

Gasdermin N can bind to acidic membrane lipids (like phosphoinositide), oligomerize and form membrane pores. IL-1 β has been proposed to directly translocate into the extracellular space through these Gasdermin pores⁵². Pyroptosis is a direct consequence of the formation of Gasdermin N pores, and is connected to cell death. Nevertheless, cell death can be

prevented in the presence of pyroptosis through the activation of repair mechanisms⁵⁴, showing that IL-1 β type I unconventional secretion is an active mechanism by which intact and viable immune cells can trigger immune response. Type III UPS mechanism for IL-1 β will be discussed in more detail on section 1.2.3.

Another cargo protein that has been shown to follow a type I UPS is HIV-Tat⁵⁵. The specific role of extracellular HIV-Tat is currently unknown, but its presence in the extracellular space has been correlated with the development of Acquired Immune Deficiency Syndrome (AIDS), and it has been shown to be neurotoxic^{56,57}. The unconventional secretion of HIV-Tat consists in a direct translocation across the plasma membrane in a PI(4,5)P₂-dependent manner⁵⁸. HIV-Tat oligomerizes and forms a lipidic membrane pore, and is then sequestered by membrane proximal heparan sulfate proteoglycans (HSPGs). Furthermore, the α 1 subunit of the Na,K-ATPase has recently been shown to play a role in this unconventional secretory pathway⁵⁹. Beyond translocation mediated by pore formation, recent studies suggested other two possible ways by which HIV-Tat can be secreted from cells. One possible alternative way is mediated by spontaneous translocation of a single monomer of HIV-Tat following its interaction with PI(4,5)P₂ and subsequent membrane destabilization⁵⁸. The other one involves incorporation of HIV-Tat into exosomes⁵⁸. There are currently only a restricted number of studies exploring these two possible alternative pathways for HIV-Tat unconventional secretion and further investigations will be needed.

Annexins have also been proposed to be translocated following a type I UPS pathway⁶⁰. They are a family of phospholipid binding proteins, an activity that they exert, commonly, in a Ca⁺⁺-dependent manner⁶¹. Annexins have a role in membrane organization, and extracellularly they act as receptors for extracellular proteins (e.g., regulators of blood coagulation and serum proteases)^{62,63}. As previously mentioned, annexins bind to phospholipids in a Ca⁺⁺-dependent manner. This binding has been proposed to be the initial step for their unconventional secretion from cells. A recent study from the Moreau group showed how cinnamycin, a stimulator of phospholipid flipping, was able to significantly increase secretion of both annexin A2 and annexin A5⁶⁰. Furthermore, they demonstrated how annexin A2 and A5 secretion was inhibited in a TMEM16F (a lipid scramblase) knock-out. Both results pointed at an involvement of phospholipid flipping in the unconventional secretion of annexins A2 and A5.

Tau, a member of the microtubule associated protein (MAP) family, was also shown to get secreted via direct translocation across the plasma membrane, and thereby to follow type I UPS⁶⁴⁻⁶⁶. Under physiological conditions, Tau interacts with tubulin to stabilize microtubules in neuronal cells, and it plays a role in axonal transport and cytoskeletal organization. In pathological conditions, Tau detaches from microtubules after creating insoluble aggregates, due to an abnormal phosphorylation⁶⁶. There are a number of tauopathies involving

hyperphosphorylation and aggregation of Tau, including Alzheimer's disease (AD). The direct translocation of Tau across the plasma membrane has been shown to be dependent on its hyperphosphorylation, its interaction with PI(4,5)P₂ at the inner plasma membrane leaflet and the binding to HSPGs at cell surfaces⁶⁴, similarly to FGF2 and HIV-Tat. Furthermore, both cholesterol and sphingomyelin seemed to be effective in increasing its secretion from cells, another feature in common between the unconventional secretion of Tau and FGF2⁶⁵.

1.2.2 Type II UPS

As opposed to type I UPS, there is a very limited number of cargo proteins known to follow a type II UPS. In this type of UPS, plasma membrane translocation of lipidated cargoes is facilitated by ATP-binding cassette (ABC) transporters⁴³. ABC transporters consist of two transmembrane domains and two ATP-binding domains⁶⁷. The best studied cargo that uses this type of UPS is the α -factor of *Saccharomyces cerevisiae*, a mating pheromone. This polypeptide (36 amino acid) is expressed by yeast cells of the haploid mating type MAT α and undergoes to a series of modifications, resulting in a 12 amino acid carboxymethylated and prenylated mature form. This mature form is then exported from yeast cells via Ste6p ABC transporter⁶⁸. The current model for this ABC transporter-mediated secretion proposes the α -factor to be associated with the inner plasma membrane leaflet, due to its hydrophobic nature, and flipped by the Ste6p transporter in an ATP-dependent manner to reach the outer leaflet. Another ABC transporter, MAM1, is responsible for a very similar pathway of type II UPS in the yeast *Schizosaccharomyces pombe*, where the M-factor is S-farnesylated and carboxymethylated prior its MAM1-facilitated translocation⁶⁹.

One of the few examples of type II UPS cargoes in mammalian cells is represented by Heat shock 70-kDa protein (HSP70), which, following heat shock, has been proposed to enter endo-lysosomal vesicles in an ABC transporter-dependent manner and to be secreted from cells via these vesicles^{70,71}.

1.2.3 Type III UPS

One of the first cargo protein characterized to follow a type III UPS was the acyl-CoA binding protein (AcbA in *Dictyostelium discoideum*, Acb1 in yeast, and ACBP in mammalian cells)⁴⁹. When the Malhotra group started investigating the role of GRASP proteins (Golgi Reassembly-Stacking Protein) in *Dictyostelium discoideum*, since only one form of GRASP is expressed (in contrast to yeast and mammals, where two GRASP forms are expressed), they found that GrpA (the respective GRASP orthologue) Knock-out *Dictyostelium discoideum* cells were incapable to form viable spores following starvation⁷². The starting point of spore formation upon

starvation in these cells is the release of AcbA, which is then cleaved and capable of starting a feedback loop which brings to the formation of spores. The AcbA orthologue in yeast, Acb1, was also found to get secreted unconventionally in a Grh1 (the yeast GrpA orthologue)-dependent manner upon starvation. Subsequent studies revealed the involvement in this pathway of several autophagy-related proteins⁷³ and the Endosomal Sorting Complexes Required for Transport (ESCRT)-I, -II, and -III⁷⁴, as well as the membrane t-SNARE Ssol. Starvation-induced secretion of Acb1 also resulted in the formation of a new Grh1 positive compartment, which has been called CUPS (Compartment of Unconventional Protein Secretion)^{75,76}. In early steps of starvation, Grh1-containing vesicles starts to cluster in what has been named I-CUPS (Immature CUPS). In a subsequent state, these Grh1-containing vesicles get surrounded by curved saccules⁷⁴, and are referred to as M-CUPS (Mature CUPS). Acb1 has been shown to be associated with M-CUPS, pointing at an involvement of these compartments in this type III UPS pathway⁷⁵. In the final steps of Acb1 unconventional secretion, M-CUPS fuses with the plasma membrane in a Ssol-dependent manner, resulting in Acb1 secretion into the extracellular space.

SuperOxide Dismutase 1 (SOD1), a factor that has been linked to propagation of amyotrophic lateral sclerosis (ALS) in humans, was also shown to follow a type III UPS pathway, and to share the same machinery of Acb1 starvation-induced unconventional secretion⁷⁷. In an attempt to identify a possible common motif between Acb1 and SOD1, the Malhotra group identified a diacidic motif in SOD1, conserved between *S. cerevisiae* and humans, which mutation decreased SOD1 secretion⁷⁷. A diacidic motif was also found in Acb1, and also this cargo protein was shown to decrease its secretion upon mutation of these two residues⁷⁷.

As mentioned before, the pro-inflammatory cytokine IL-1 β follows unconventional secretory pathways to get secreted into the extracellular space. It has been shown to follow different pathways⁵⁴ (type I UPS pathway for IL-1 β has been discussed in more detail on section 1.2.1). A type III secretion was proposed after a pool of mIL-1 β was found in intracellular vesicles⁷⁸. For long, the nature of the intracellular vesicular intermediates involved in this pathway have been discussed, with multivesicular bodies (MVBs)⁷⁹, secretory autophagosomes^{80,81}, and secretory lysosomes^{82,83} being proposed to play a role. A recent study elucidated the way how IL-1 β enters intracellular vesicular compartments⁸⁴. In this study, TMED10, a member of the p24 integral membrane proteins family, was identified to be involved in the early secretory pathway, as responsible for mIL-1 β translocation across the membrane of an intracellular vesicular compartment. Downregulation and knockouts of TMED10 were reported to drastically reduce IL-1 β secretion in different cell lines, as well as in primary macrophages and in mice. mIL-1 β was found to interact, in its unfolded state, with the cytoplasmic domain of TMED10, through the cytoplasmic chaperon HSP90A. In this model, following activation via DAMPs and/or PAMPs, mIL-1 β undergoes unfolding, interaction with HSP90A and translocation across the membrane of ERGIC through TMED10, which is proposed to

oligomerize and form a protein-conducting channel in this compartment. In the lumen of ERGIC, the lumen-resident chaperone HSP90B1 interacts with unfolded mL-1 β , promoting its folding⁸⁴ (similarly to Sec61-mediated co-translational translocation in the lumen of the ER, in which proteins are folded with the help of BiP).

1.2.4 Type IV UPS

As opposed to the other three pathways of unconventional protein secretion, type IV UPS refers to proteins that have a signal peptide and are able to enter the ER co-translationally⁴⁴. Nevertheless, proteins that follow this pathway are directly transported to the plasma membrane, bypassing the Golgi apparatus⁸⁵. One of the most known examples of proteins that can follow a type IV UPS pathway is CFTR (Cystic Fibrosis Transmembrane Conductance Regulator), an anion channel of the ABC transporters family that allows the diffusion of chloride (Cl⁻) and hydrogen carbonate (HCO₃⁻). Under particular conditions, CFTR can reach the plasma membrane without going through the Golgi apparatus. This has been shown under conditions of ER stress and ER to Golgi blockage⁸⁵. This pathway has been shown to be dependent on GRASP⁸⁵ and the protein that reaches the plasma membrane following it, even if in the same immature form as in the ER, seemed to be functional⁸⁶. CFTR is of particular interest, since its mutations are directly related to cystic fibrosis, one of the most common fatal genetic diseases among humans. Cystic fibrosis causes the production of a thick and sticky mucus that accumulates in the lungs, leading to infections, as well as blocks the pancreas⁸⁷. There are over 900 CFTR mutations reported in the literature, the most common of which is the deletion of the phenylalanine in position 508 (CFTR Δ F508), which leads to a normal protein synthesis, but also to an incorrect folding, causing its retention in the ER and its subsequent degradation⁸⁶. This deletion does not influence the functionality of CFTR, and therefore an upregulation of this UPS pathway might be a potential approach in the treatment of cystic fibrosis, rescuing its localization to the plasma membrane⁸⁵.

1.3 Fibroblast Growth Factor 2

Fibroblast Growth Factor 2 (FGF2) is a potent mitogen involved in cellular growth and proliferation, wound repair, hematopoiesis, and angiogenesis^{88,89}. It is mainly expressed during development^{90,91}, tissue remodeling and injuries. It is also involved in pathological processes, such as cancer development and chemotherapy resistance⁹². This is mainly due to the formation of new vessels to support the tumor mass with nutrients and oxygen, and the inhibition of apoptosis.

The FGF family contains 23 members, most of them exerting their biological functions in the extracellular space through binding to FGF receptors. FGF1 and FGF2, despite being secreted from cells, lack a signal peptide. They have been described to follow a type I UPS. The FGF2 isoform that gets secreted is the small molecular weight isoform of 18 kDa. This is the only one that is translated from a canonical AUG starting codon. All the higher molecular weight isoforms (which will not be discussed in this work), that vary from 22 kDa to 34 kDa, have an alternative starting codon. Secreted FGFs bind to the FGFR receptor (FGFR), exerting their biological functions. There are four highly conserved FGFRs (FGFR 1–4), with diverse tissue and developmental stage expression. The extracellular domains of FGFRs contain three immunoglobulin-like (Ig) loops⁹³. Each FGFR dimerize upon ligand binding, triggering intracellular phosphorylation of the receptor kinase domains. Intracellular phosphorylation starts the signaling cascade, eventually leading to gene transcription activating survival and proliferation pathways⁹⁴, like the Ras–Raf–MAPK pathway, the JAK–STAT pathway, and the PI3–AKT–mTOR pathway. FGF/FGFR signaling complex is stabilized by heparan sulfate chains (HS) of heparan sulfate proteoglycans (HSPGs) at the extracellular matrix, creating a ternary signaling complex⁹⁵. HS also protect secreted FGFs from proteolytic degradation⁹⁶. All FGF2 isoforms contain a nuclear localization signal (NLS), with the highest molecular weight form (34 kDa) containing three NLS, the 22 kDa, 22.5 kDa and 24 kDa containing two NLS and the 18 kDa secreted isoform only containing one NLS. The high molecular weight isoforms mainly localize in the nucleus, where they regulate cellular processes involved in cell proliferation and survival⁹⁷, while the 18 kDa secreted isoform localizes both in the cytosol and in the nucleus⁹⁸, beyond getting secreted, exerting its functions in an autocrine and paracrine way.

As already mentioned, FGF2 lacks a signal peptide, and does not get secreted through the classical ER/Golgi-dependent secretory pathway. It gets secreted from cells through an unconventional secretory pathway, and, in particular, with a type I UPS pathway (for details on different type of UPS, see section 1.2)⁴⁶. FGF2 has been one of the first proteins identified to reach the extracellular space in an unconventional manner^{99–101}. Over the years, with a combination of several *in vitro* and cell-based assays, Walter Nickel and his group were able to detailly characterize this process, identifying the main components of the FGF2 export machinery^{46,54,102,103} (Fig. 3). FGF2 translation occurs in the cytosol, and it follows its type I UPS pathway in its folded state, including the translocation across the plasma membrane (a characteristic of type I UPS cargo, as opposed to the translocation into the ER of conventionally secreted cargoes). FGF2 is recruited to the inner leaflet of the plasma membrane via interaction with the $\alpha 1$ -subunit of the Na,K-ATPase^{104,105}. Another component of this machinery is Tec kinase^{106,107}, a non-receptor tyrosine kinase, which gets recruited to the plasma membrane through interaction of its PH domain with PI(3,4,5)P₃. Tec kinase phosphorylates the tyrosine in position 81 on FGF2, but the specific role of this phosphorylation is still not fully understood. *In vitro* studies showed how phosphorylation of tyrosine 81 leads to a more efficient insertion of FGF2 oligomers into liposomes¹⁰⁶, while an inhibition of FGF2/Tec kinase

interaction caused a decrease in FGF2 secretion efficiency from cells¹⁰⁷. Both Tec kinase and the $\alpha 1$ -subunit of the Na,K-ATPase have been identified as strong hits of a genome-wide RNAi screen designed to find new potential components involved in the unconventional secretion of FGF2¹⁰⁶. Additionally, the Na,K-ATPase was already suggested to potentially take part in the machinery involved in the unconventional secretion of FGF2, as ouabain, an inhibitor of this ATPase, was found to inhibit FGF2 secretion from cells¹⁰⁸. Furthermore, a cell line expressing a variant form of the Na,K-ATPase which is resistant to ouabain, was able to rescue FGF2 secretion in the presence of ouabain¹⁰⁹ (as the Na,K-ATPase represents a substantial part of this thesis, its structure and functions, as well as the inhibition by ouabain, will be discussed in more detail in section 1.4). These studies did not provide a specific role for the Na,K-ATPase, but indeed put forward first hints for its possible involvement in the unconventional secretion of FGF2. After finding $\alpha 1$ as the strongest hit of this RNAi screen, subsequent studies confirmed its interaction with FGF2, and the specific domain involved in this interaction was found in the third intracellular loop of the Na,K-ATPase, which was called CD3 (for Cytoplasmic Domain 3)¹⁰⁴. Additionally, a subsequent study revealed a sub-domain within CD3, referred to as sub-CD3, to be both necessary and sufficient for the interaction with FGF2¹⁰⁵. In figure 4, a schematic representation of the Na,K-ATPase is depicted, with these domains being highlighted. NMR spectroscopy performed in order to find the binding interface on FGF2 for sub-CD3, revealed two lysine residues, in position 54 and 60, on the surface of FGF2 to be involved in this interaction. Both *in vitro* and cell-based experiments confirmed these two lysine residues to be part of the FGF2 binding interface with $\alpha 1$ ¹⁰⁵. Since these cell-based experiments are part of this thesis, they will be discussed in detail in the result part, in section 4.1. The core mechanism of FGF2 secretion does not require neither the $\alpha 1$ -subunit of the Na,K-ATPase nor Tec kinase. It has been shown in a relatively recent publication how the core process exclusively depends on PI(4,5)P₂ and HSPGs¹¹⁰. In this work, this process was fully reconstituted in Giant Unilamellar Vesicles (GUVs) in an inside-out system, with heparin in the GUVs lumen. Indeed, heparin and PI(4,5)P₂ on opposite sides of the GUVs membrane were sufficient to reconstitute FGF2 translocation. Beyond these two *trans* elements, this process was dependent on *cis* elements within FGF2. These *cis* elements are three basic residues involved in the interaction with PI(4,5)P₂, which the lysine in position 127, the arginine in position 128, and the lysine in position 133¹¹¹, the latter one also involved in the interaction with heparan sulfate¹¹⁰; and two surface cysteine residues in position 77 and 95, involved in FGF2 oligomerization¹¹². FGF2 recruitment in liposomes was already shown to exclusively depend on PI(4,5)P₂, and, in that context, was also shown to be more efficient in the presence of cholesterol and sphingomyelin¹¹¹. This last finding could suggest the involvement of liquid-ordered domains in the process of FGF2 unconventional secretion, and this hypothesis has been further evaluated in cell-based assays within this study (for details, see results and discussion). The process of FGF2 translocation occurs through PI(4,5)P₂-dependent FGF2 oligomerization, a process that triggers the formation of a lipidic

membrane pore with a toroidal structure . It is still unclear at which point of the pathway FGF2 dimerize; a current hypothesis is that the first dimerization occurs between cysteine 95 residues at the α 1-subunit of the Na,K-ATPase. Indeed, as opposed to the previous hypothesis, more recent experiments (unpublished results) point at cysteine 95 to be the sole responsible residue involved in disulfide bridge formation, and higher FGF2 oligomers forming through non-covalent interactions. The current knowledge of the respective roles for cysteine residues in position 77 and 95 will be discussed in more detail in the results and discussion sections, as part of this investigation is included in this thesis. Membrane-inserted FGF2 oligomers are then resolved by membrane-proximal heparan sulfate chains on HSPGs, which retain FGF2 on cell surfaces, protecting it from proteolytic digestion and also stabilizing its interaction with high affinity FGFR^{46,95,96,103}. Interestingly, as previously mentioned, the binding pocket on FGF2 for PI(4,5)P₂, consisting of three basic residues (K127, R128, and K133), overlap with the one for HS chains¹¹⁰, resulting in a mutually exclusive interaction of FGF2 for these two *trans* elements. This competition between PI(4,5)P₂ and HSPGs for FGF2 binding is always resolved in favor of HSPGs, which, with their HS chains, have a much higher affinity interaction for FGF2 ($K_D \sim 100$ nM)⁴⁶, compared to the one of PI(4,5)P₂ ($K_D \sim 5$ μ M)^{46,111,113}. Recently, Glypican 1 (GPC1) has been found to be the dedicated HSPG to drive the unconventional secretion of FGF2¹¹⁴. GPC1 will be discussed in more detail in section 1.5, as well as its involvement in the unconventional secretion of FGF2 (it will also be discussed in the results and in the discussion sections, as part of this thesis).

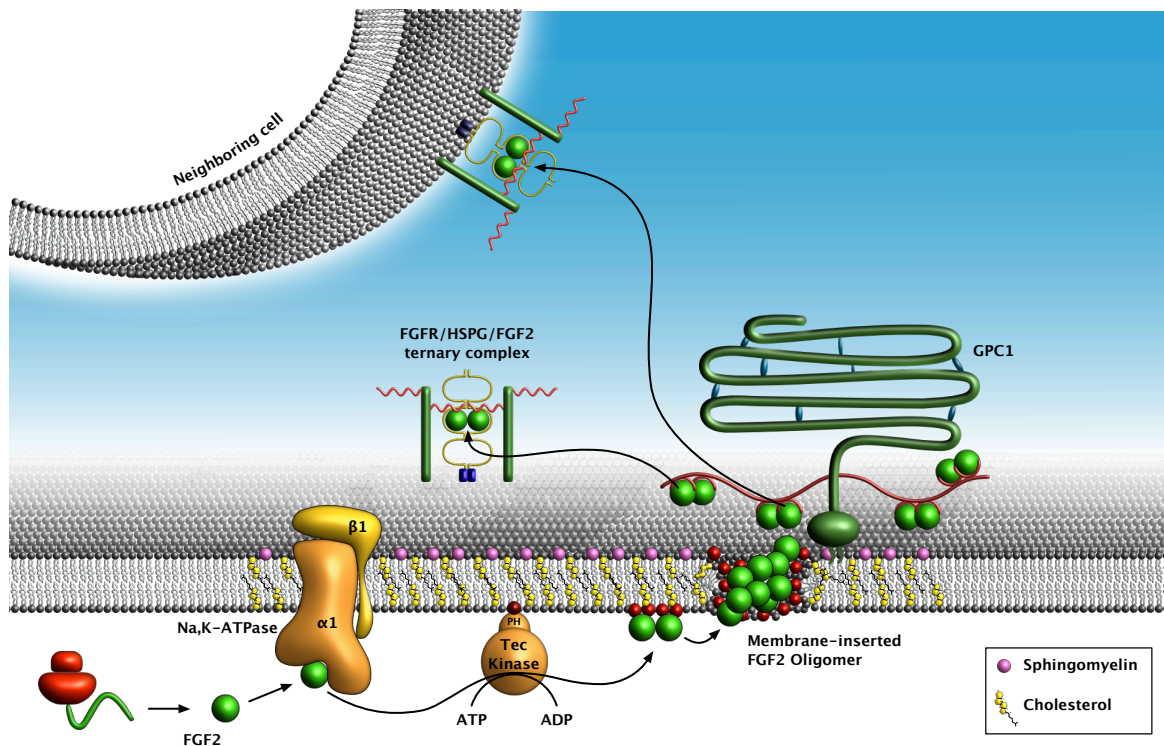


Figure 3: The Unconventional Secretory Pathway of FGF2. Fibroblast Growth Factor 2 (FGF2) follows a type I unconventional protein secretion (UPS), and, therefore, gets secreted through direct translocation across the plasma membrane. This process depends on sequential interactions of FGF2 with the $\alpha 1$ -subunit of the Na,K-ATPase, the phosphoinositide PI(4,5)P₂, and Tec kinase, which is recruited to the membrane through the interaction of its PH domain with membrane PI(3,4,5)P₃, at the inner plasma membrane leaflet. Cholesterol and spingomyelin seem to be important to organize the machinery needed for the unconventional secretion of FGF2. Membrane inserted oligomers are resolved by membrane-proximal heparan sulfate chains, which compete with PI(4,5)P₂ for interaction with FGF2. FGF2 is then trapped at cell surfaces, where it can interact with its specific receptor in an autocrine or paracrine manner. *Inspired by Lolicato and Nickel, 2022*¹⁵.

1.4 Na-K,ATPase

The vast majority of eukaryotic cells present a high concentration of K⁺ and a low concentration of Na⁺ compared to the extracellular space. These gradients are maintained through a specific and active mechanism from a transmembrane protein, the Na,K-ATPase¹¹⁶. ATP hydrolysis provides the energy needed for the active transport of Na⁺ from the inside to the outside of the cells and of K⁺ from the outside to the inside, generating the double gradient. In animal cells, this gradient is crucial as it controls the cellular volume, it allows muscle cells and neurons to be electrically excitable and favors secondary transport of sugars and amino acids. Na,K-ATPase is a member of the P-type ATPase family, which mechanism of action requires the formation of an essential phosphorylated intermediate¹¹⁷. P-type ATPases consist of one catalytic subunit α , which binds ATP at the cytosolic side, and a subunit

β , with modulatory functions. In the Na,K-ATPase, the α -subunit consist of approximately 110 kDa and it is divided into a transmembrane and a cytoplasmic part (with only small loops at the extracellular space). The cytoplasmic domain contains an actuator domain (A), a nucleotide-binding domain (N), and a phosphorylation domain (P). The β -subunit, of about 35 kDa, consist of a transmembrane helical domain and an extracellular domain¹¹⁸. Additionally, a single span membrane γ -subunit of about 7–8 kDa, also referred to as FXYP for its Pro-Phe-X-Tyr-Asp motif, has been reported in most cells studied so far, and it is thought to have modulatory effects, for example changing the affinity to Na⁺, K⁺, and ATP¹¹⁹⁻¹²³. The extracellular domain of the β -subunit has three glycosylation sites, and its glycosylation level has an effect on folding and plasma membrane localization^{124,125}.

During the catalytic cycle, a phosphate group is transferred from the ATP to the side chain of an aspartate residue of the ATPase, which provides energy for ionic transport against the concentration gradient¹²⁶. The Na,K-ATPase undergoes two conformational changes, going from a E1 to a E2 state. At the initial E1 state of its cycle, the Na,K-ATPase is bound to ATP, it is open towards the cytosol, and it has high affinity for Na⁺. Binding of all Na⁺ causes a conformational change in the transmembrane domain and, subsequently, in the N domain¹²⁷. This causes ATP hydrolysis and α subunit phosphorylation, which leads to another conformational change in the pump, allowing the three Na⁺ to get exported in the extracellular space¹²⁸. At this point, the ATPase is in the E2 state and it is opened towards the extracellular space.

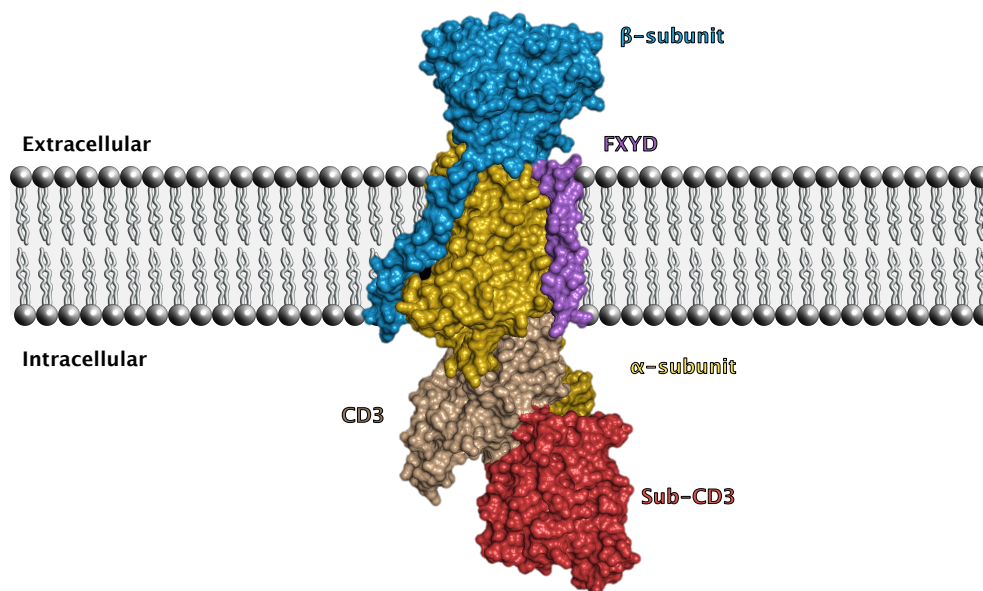


Figure 4: Schematic representation of The Na,K-ATPase. A 3D representation of the Na,K-ATPase is shown, with the different subunit highlighted in different colors. The CD3 is shown in light brown, while the subCD3 is depicted in red. Crystal structure: 3KDP.

In this state, the Na,K-ATPase has a higher affinity for K⁺ ions. After their binding, it dephosphorylates and this leads to a conformational change, which allows the two K⁺ to reach the intracellular space^{129,130}, leaving the pump open towards the cytosol and bound to ATP, ready to start a new cycle.

The Na,K-ATPase can interact with cardiotonic steroids (CTS), also known as cardiac glycosides (CG), which inhibit its activity¹³¹. The highly conserved CTS binding site occurs on the α -subunit extracellular side, specifically between the M1/M2, M3/M4 and M5/M6 loops¹³²⁻¹³⁴. CTS are steroidal drugs that are found in nature, mainly in plants from the *Digitalis* genus. Already at the end of the 18th century, it was reported in the literature that extract from these plants were used in the treatment of congestive heart failure¹³⁵. The first compounds to be isolated has been digoxin and digitoxin¹³⁶. Interestingly, in the end of the 20th century, similar compounds have been reported to be present in mammals^{137,138}, like, among others, ouabain^{139,140} and digoxin, and bufadienolides, such as bufalin and 19-norbufalin¹⁴². Binding of CTS stabilizes the ATPase in an E2 intermediate state, and prevents Na⁺ ions release from the cells. This, as a consequence, prevents Ca²⁺ release from cells, due to the indirect inhibition of the Na⁺/Ca²⁺ exchanger, which pumps Ca²⁺ ions to the extracellular space and Na⁺ ions inside the cell, following the ionic gradient. Higher cytosolic Ca²⁺ concentrations directly increase its uptake from the sarcoplasmic reticulum by the sarco-/endoplasmic reticular Ca²⁺ ATPase (SERCA)¹⁴³. Upon stimulation, high amount of Ca²⁺ get released, and this improves contractility of myocytes, overcoming congestive heart failure. Therapeutic use of CTS is however carried out at low concentrations, cause higher concentrations can lead to cardiac arrest. Beyond the effects on myocytes, treatment with CTS affects all the cellular functions connected to the Na⁺/K⁺ transmembrane gradient, like, for example (but not exclusively), cellular volume, maintenance of membrane potential, and Na⁺ symport with glucose, amino acids, nucleotides and inorganic phosphate¹⁴⁴. CTS, and in particular ouabain, have been used in research for Na,K-ATPase inhibition studies. In rodents, the inhibition of the Na,K-ATPase by CTS occurs with approximately 10³-fold higher concentrations than in other mammals. This difference is caused by the substitution of two residues, the glutamine in position 111 and the asparagine in position 122, which are present in the CTS-sensitive α 1-subunit, with arginine and aspartate, respectively¹⁴⁵.

Beyond its well-established function in pumping ions, the Na,K-ATPase has been reported to function as a scaffold for the assembly of many factors involved in signal transduction¹⁴⁶⁻¹⁴⁸, such as SRC kinase, inositol 1,4,5-triphosphate receptor (IP3R), caveolin and epidermal growth factor receptor (EGFR). This signalosome can be activated by CTS binding, which triggers a conformational change, resulting in a signal transduction cascade. The signal transduction activity of the Na,K-ATPase is not linked to its pumping activity¹⁴⁹. CTS at concentrations that only mildly affect the pumping activity, or do not affect it at all, can activate downstream signal transduction resulting in the regulation of a variety of cellular

processes, from cell proliferation¹⁵⁰ to apoptosis¹⁵¹. Low concentration of ouabain leads to an allosteric conformational change in the α -subunit, which activates adjacent SRC kinase and recruits IP₃, and phospholipase C (PLC)¹⁵². This functional microdomain allows the Na,K-ATPase to interact, with its cytosolic domain, with the ER, through the IP₃/IP₃R interaction^{153,154}. This provokes a transient increase in the intracellular levels of Ca²⁺. These oscillations in Ca²⁺ levels activate the calcium-dependent transcription factor nuclear factor- κ B (NF- κ B), which, under these conditions, activates proliferation-inducing and anti-apoptotic genes¹⁵⁵. As already mentioned, CTS binding to the Na,K-ATPase triggers activation of SRC kinase. This, in turn, can phosphorylate and, therefore, activate, EGFR, which ultimately results in the activation of the Ras-RAF-MAPK transduction cascade^{156,157}, also resulting in cell proliferation and differentiation. All of these signal transduction cascade occur in a tissue-specific manner. For example, in cardiomyocytes, the activation of Ras promotes the opening of the ATP-dependent mitochondrial potassium channel, leading to the production of reactive oxygen species (ROS)¹⁵⁸. These, in turn, activates NF- κ B, leading to cell proliferation and differentiation.

1.5 Glypican 1

FGF2 signaling occur upon activation of FGF receptors on cell surfaces^{159,160}. As mentioned before, FGF2 forms a ternary complex with high-affinity FGF receptors and HSPGs⁹⁵. It was subsequently discovered in Walter Nickel's laboratory that HSPGs not only are important players in FGF2 signaling, but they are also crucial for FGF2 export from the cells. Using a mutated form of FGF2 incapable of binding to HSPGs, they found this FGF2 version to lack the ability to get secreted¹¹¹. Similarly, wild-type FGF2 did not get secreted from cells defective in HSPGs biosynthesis¹⁶¹. These cells, CHO 745, were knock-out for xylosyl transferase, the first enzyme involved in the biosynthesis of heparan sulfate chains on the core protein of proteoglycans¹⁶². For many years, heparan sulfate chains were believed to be crucial for FGF2 export regardless of the proteoglycan they are linked to. It was only with a recent BioID screen that the existence of a dedicated HSPG started to be clear¹¹⁴. In this proteome-wide screen, GPC1 was the strongest hit, suggesting its essential role among all the others HSPGs in FGF2 secretion. Indeed, a series of biochemical assays confirmed this hypothesis, with GPC1-KO cells being defective in FGF2 export. This phenotype could not only be rescued with the overexpression of GPC1 (on GPC1-KO cells), but, under these conditions, FGF2 secretion would significantly increase compared to wild-type cells¹¹⁴. In both conditions (GPC1-KO and GPC1 overexpression), the overall content of heparan sulfate and glycosaminoglycan chains did not differ, so the observed phenotypes were directly linked to GPC1, and not to differences to total amounts of HSPGs. These evidences pointed at GPC1 being a rate-limiting factor for the unconventional secretion of FGF2. Structural and functional characteristic of GPC1 will be discussed below.

HSPGs are proteins to which one or more heparan sulfate chains, a type of glycosaminoglycan, are covalently attached. They are highly negatively charged biomolecules and can bind growth factors, cytokines, chemokines and morphogens, protecting them from proteolysis at the extracellular space¹⁶³. HSPGs are also known to cooperate with integrins to facilitate cell to cell interactions, cell to extracellular matrix attachment, and cell motility. Membrane HSPGs can act as coreceptors for a number of tyrosine kinase growth factor receptors. As previously mentioned, this is the case for the ternary complex between FGF2, high affinity FGF receptors and HSPGs⁹⁵. Membrane HSPGs consist of two major classes: syndecans and glypicans. Syndecans have a transmembrane domain, whereas glypicans are connected to the plasma membrane via a GPI-anchor. Syndecans can contain both heparan sulfate and chondroitin/dermatan sulfate chains, while glypicans only have heparan sulfate chains¹⁶³. There are six glypicans in mammals, which are divided in two subfamilies: one containing glypican-1, -2, -4, and -6; the other one containing glypican-3, and -5¹⁶⁴. Glypicans have a highly structured N-terminal core protein, containing fourteen conserved cysteine residues involved in disulfide bonds, required to stabilize the core protein structure, whereas the C-terminal contains the sequence for GPI-anchor attachment¹⁶⁵. Both subfamily members have the insertion sites for heparan sulfate chains in proximity to the C-terminus, placing them close to cell surfaces¹⁶⁴. GPI-anchored proteins partition into liquid-ordered domains, detergent-resistant membrane domains enriched in cholesterol and sphingolipids^{166,167}. These domains are thought to be involved in signaling and other cellular processes, and will be discussed in more detail in section 1.6.3. Glypicans have been reported to either stimulate or inhibit signaling activity. Considering Wnt signaling, glypicans have been proposed to facilitate and/or stabilize its interaction with the signaling receptor¹⁶⁸. The signaling of another growth factor which interacts with glypicans, Hedgehog (Hh), has been reported to get inhibited by GPC3 during development. This was due to the competition between GPC3 and Patched, the Hh receptor, for Hh binding¹⁶⁹. Glypicans can also be shed into the extracellular space through the activity of the lipase Notum. This extracellular lipase releases glypicans in the extracellular environment by cleaving the GPI anchor¹⁷⁰. Glypican shedding has been shown to play a role in the transport of growth factors like TGF- β ¹⁷¹, Wnts¹⁷⁰ and Hh¹⁷², and also of the bone morphogenic proteins (BMP)¹⁷³, leading to paracrine signaling and morphogen gradient formation. In general, selectivity for different interaction partners is achieved by the multiple combinations of modifications on heparan sulfate chains. For instance, heparin exhibit higher sulfation levels, with more than two sulfate groups per disaccharide, in contrast to typical heparan sulfates, which contain less than one sulfate group per disaccharide¹⁶³. Indeed, in Walter Nickel's group it was recently discovered how a tri-sulfated disaccharide with one N-linked and two O-linked sulfate group is enriched in GPC1 compared to GPC5 and Syndecan 4 heparan sulfate chains¹¹⁴. Co-crystallization of FGF2 with synthetic heparin showed three disaccharides like this on the binding interface¹⁷⁴, giving an explanation for the dedicated role of GPC1 in the unconventional secretion of FGF2.

1.6 Plasma membrane lipid composition

Cellular membranes have several roles, they function as barrier between compartments providing selective permeability, as physical support for biochemical reactions¹⁷⁵, as signaling molecules¹⁷⁶, as energy sources¹⁷⁷, and as protein recruitment platforms¹⁷⁸. Cellular membranes are asymmetric, having different lipid composition between the two leaflets, and they are fluid structures, with lipids and proteins being able to rapidly diffuse horizontally within the layer. All lipid molecules in the plasma membrane are amphipathic, having a hydrophilic head and hydrophobic hydrocarbon tails. Biological membranes contain three principal classes of lipids: glycerophospholipids (GPLs), sphingolipids, and cholesterol¹⁷⁵. The principal components of biological membranes are the phospholipids, which physical and chemical characteristics are responsible for membrane structures. Phospholipids differ based on their hydrophilic headgroup and on the nature of the two fatty acids (chain length, double bond number and position)¹⁷⁹(9). Based on their headgroups, we can distinguish the most common glycerophospholipids in phosphatidic acid (the simplest glycerophospholipid and only present in few amounts in cellular membranes), phosphatidyl choline (PC), phosphatidyl ethanolamine (PE), phosphatidyl serine (PS), and phosphatidyl inositol (PI). The lipid composition of the two leaflets of the plasma membrane is asymmetrical. Phosphatidylcholine and sphingomyelin are more abundant in the outer leaflet, whereas phosphatidylserine, phosphatidylethanolamine, and phosphatidyl inositol are more present in the inner leaflet¹⁸⁰. This also affects the net charge of the two leaflets, with the outer leaflet being positively charged (PC and SM are positively charged) and the inner leaflet showing a negative net charge (due to PS).

1.6.1 Cholesterol

Cholesterol is a particularly abundant lipid of eukaryotic cells, with a maximum of one molecule per molecule of phospholipid. It has a plate-like structure, and, in lipid bilayers, it is oriented in a way that its polar hydroxyl group is in proximity to the polar head of the adjacent phospholipids, whereas its hydrophobic region interacts with the hydrophobic hydrocarbon chains of the phospholipids¹⁸¹. Cholesterol molecules modulate eukaryotic plasma membrane fluidity¹⁸²; it makes lipid bilayers more rigid and less deformable, also leading to a decrease in the permeability of the bilayer to small water-soluble molecules^{183,184}. Under conditions of high rigidity of the lipid bilayer (for instance at low temperatures), however, cholesterol can also increase the fluidity, preventing the hydrocarbon chains from coming together and crystallizing. Cellular cholesterol is mainly present in the plasma membrane; here it is often found to be packed with sphingolipids and GPI-anchored proteins in liquid-ordered domains¹⁸⁵. These are domains of lipidic membranes with a lower fluidity due to a higher length and saturation of sphingolipids fatty acid chains and to the higher

cholesterol concentration¹⁸⁶ (these liquid-ordered domains will be discussed in more detail on section 1.6.3).

Cholesterol is mainly synthesized in the liver¹⁸⁷. Its synthesis is influenced by the levels of cellular cholesterol. All the carbon atoms of cholesterol derive from Acetyl CoA, through a biosynthetic pathway divided in three phases: i) the synthesis of the isopentenyl pyrophosphate; ii) the condensation of six isopentenyl pyrophosphate molecules, to form the squalene; iii) the cyclization of squalene and the conversion of the four rings product in cholesterol¹⁸⁸⁻¹⁹⁰. The first phase takes place in the cytosol, whether the other two in the ER lumen¹⁹¹. The synthesis of the isopentenyl pyrophosphate from Acetyl CoA is carried through the formation of 3-hydroxy-3-methylglutaril CoA (HMG-CoA) from Acetyl CoA and acetoacetyl CoA. HMG-CoA is then reduced to mevalonate, a reaction catalyzed by the enzyme HMG-CoA reductase, and that represents the rate limiting step of cholesterol biosynthesis. This enzyme is the target of statins, the most common cholesterol-lowering drugs used in therapy^{192,193}. HMG-CoA reductase-KO mice are not viable, as they die during the first phases of embryo development¹⁹⁴. Mevalonate is then converted to 3-isopentenyl pyrophosphate through three consecutive ATP-dependent reactions. Squalene, a thirty carbon atoms isoprenoid, is synthesized from the condensation of six isopentenyl pyrophosphate molecules. The final step of cholesterol biosynthesis starts with the cyclization of squalene. Squalene is first activated from the conversion in 2,3-oxidosqualene, in a O₂- and NADPH-dependent reaction, and then cyclized to lanosterol (30 carbon atoms), which is then converted to cholesterol through the remotion of three carbon atoms. As briefly mentioned before, statins represent the most commonly used drugs to lower cholesterol levels¹⁹². In this work, I employed mevastatin, also known as compactin or ML-236B, to study the effect of cholesterol depletion on the unconventional secretion of FGF2. This inhibitor was first isolated from the culture broth of *Penicillium citrinum*, in an attempt to discover inhibitors of sterol synthesis involving roughly 8000 strains of microorganism^{195,196}. Mevastatin is a competitive inhibitor of HMG-CoA reductase. The inhibition of this enzyme results in reduced levels of mevalonic acid and accumulation of HMG-CoA. The affinity of HMG-CoA reductase for mevastatin is about 10000-fold higher than to HMG-CoA¹⁹⁷. Mevalonate is a precursor for steroidal and non-steroidal compounds, so the inhibition of its production by mevastatin also triggers pleiotropic effects, including arrest of cell cycle and apoptosis induction^{193,198}. Nowadays, other statins are known with structural similarities to mevastatin. These are lovastatin and simvastatin, the first derived from fungal source and the latter consisting in its chemical modification, and pravastatin, chemically modified from mevastatin.

Another widely used method to manipulate cellular cholesterol levels is the utilization of Methyl- β -cyclodextrin (M β CD)^{199,200}. M β CD is a water-soluble oligosaccharide, consisting in a heptamer of α -linked D-glycopyranose units, which has a barrel-like structure, with the inside being hydrophobic and the outside hydrophilic. It can accommodate cholesterol in the

hydrophobic cavity, allowing its solubilization in aqueous solutions. M β CD has been used in several studies to deplete cellular cholesterol⁶⁵, allowing for an acute reduction, in contrast with the inhibition of cholesterol synthesis via statin treatment, in which cholesterol depletion is achieved after longer incubation times (days). M β CD is also used to enrich cellular cholesterol levels. In this case, M β CD is complexed to saturation with cholesterol prior the addition to cells, and this allows M β CD to work as cholesterol donor²⁰⁰.

One of the most widely used ways to image cholesterol is based on Filipin staining²⁰¹⁻²⁰³. Filipin is a polyene macrolide with antifungal activity which promotes membrane leakage. It was isolated from the mycelium and culture filtrates of *Streptomyces filipinensis*, from a soil sample collected in the Philippines (from which the name Filipin). Filipin is a complex mixture of four (or more) polyene amphipathic macrolides. Filipin binds to free unesterified cholesterol, whereas it cannot bind esterified cholesterol²⁰⁴. One of the disadvantages of this technique is that it requires cell fixation, which does not allow for dynamic studies in living cells. Nevertheless, it is a very useful tool which has been used to characterize type C Niemann–Pick disease, and it is still used in its diagnosis^{205,206}.

1.6.2 Sphingolipids

Phospholipids which have a sphingosine backbone are called sphingolipids. Sphingosine is an amino–alcohol with an eighteen–carbon unsaturated chain²⁰⁷. Synthesis of sphingolipids starts at the cytosolic leaflet of the ER with the condensation of palmitoyl CoA with cytosolic serine, a reaction that occurs through the enzyme serine palmitoyl transferase (SPT)²⁰⁸. This enzyme has its catalytic site facing the cytosol²⁰⁹, and produces 3–ketodihydrosphingosine, which is subsequently reduced to dihydrosphingosine (DHSph) through the action of 3–ketodihydrosphingosine reductase (KDHR) in a NADPH–dependent manner. In mammalian cells there are six ceramide synthase enzymes (CerS1–6) which catalyze acylation of DHSph and are localized to the ER with the catalytic site facing the cytosol^{210,211}. Each CerS is thought to produce different ceramide species based distinct acylCoA preferences²¹²⁻²¹⁷. Ceramides are transported from the ER to the Golgi for further modifications through the ceramide transfer protein (CERT)²¹⁸. In the N–terminal of CERT there is a PH domain that recognize PI(4)P molecules on Golgi membranes, allowing for a specific transfer to the Golgi. The generation of more complex sphingolipids occurs through the substitution of the hydroxyl group of ceramides. Complex sphingolipids can be divided in two major groups based on this substitution, sphingomyelin species (SM), and glycosphingolipids (GSLs). The simplest GSLs are the cerebroside, in which there is only one sugar molecule, glucose or galactose. Galactosylceramide is generated from UDP–galactose and ceramide through the action of Ceramide galactosyltransferase (CGT), an ER transmembrane enzyme with its catalytic site

facing the lumen of the ER²¹⁹. Similarly, glucosylceramide is synthesized from ceramide and UDP-glucose by glucosylceramide synthase (GCS), a cis-Golgi transmembrane enzyme with its catalytic site facing the cytosol²²⁰. The most complex glycolipids are the ganglioside, which can contain up to seven sugar molecules, in a branched chain²²¹. Glycolipids are always on the outer leaflet of the plasma membrane, and the sugar molecules on cells membrane can act as antigens, like in the case of the blood groups, based on the glycolipids present at the membrane of erythrocytes. Sphingomyelin represents the most abundant sphingolipid in mammalian cells. It is produced by sphingomyelin synthase (SMS), mainly at the trans-Golgi²²². There are two known SMSs, SMS1 and SMS2 (and a possible third member, SMSr), both located at the trans-Golgi with the catalytic site facing the lumen, and SMS2 also present at the plasma membrane (with the catalytic site facing the extracellular space). SMSs catalyze the formation of SM transferring the phosphocholine headgroup from PC to ceramide, producing, beyond SM, diacylglycerol (DAG)²²³⁻²²⁶.

Sphingomyelin breakdown occurs through the action of sphingomyelinase (SMase), which hydrolyzes the phosphodiester bond of SM to generate ceramide and phosphocholine. Based on localization and optimal pH activity, different SMases can be distinguished^{227,228}. Alkaline SMase is only expressed in liver and intestine, and it digests dietary SM²²⁹. Acid SMase (aSMase) is mainly present in lysosomes, where it is involved in the catabolism of SM present on endosomal membranes, and can also be secreted into the extracellular space, where SM-containing lipoproteins are abundant in the plasma^{230,231}. Genetic defects regarding aSMase cause severe lipid storage diseases, such as type A and type B Niemann Pick Disease (NPDA and NPDB, respectively)^{232,233}. NPDA is caused by a complete absence of aSMase, which results in progressive neurodegenerative disease with psychomotor retardation, lung disease, hepatosplenomegaly, all conditions that cause premature death within the first years after birth. NPDB results in a less severe disease, with the absence of neurological symptoms²³⁴. There are four neutral SMase (nSMase), encoded by four genes, that localize to the plasma membrane, with the exception of the Mitochondria associated SMase (MA-SMase)²³⁵. nSMase 2 is the best characterized nSMase and contains two palmitoyl-binding cysteine clusters, which palmitoylation is important for nSMase 2 recruitment to the membrane and its stability²³⁶.

1.6.3 Liquid-ordered domains

The existence of liquid-ordered domains in biological membranes, often referred to as lipid rafts, has for long being debated, both because of their nanoscale size, ranging from 20 to 100 nm and, therefore, below the diffraction limit of light microscopy, and for their rapid dynamics²³⁷. Already in the middle of the '70s there has been the first observations of the

effect of temperature on membrane behavior, leading to the proposal of clusters of lipids^{238,239}. In 1982, Karnovsky et al. observed multiple phases in the membrane lipid environment, and proposed the concept of lipid domains²⁴⁰. Eventually, in 1997, Kai Simons and Elina Ikonen proposed the theory of lipid rafts. In their model, these rafts are membrane domains enriched in sphingolipids and cholesterol¹⁸⁶. Because of the inverted cone-like shape of sphingolipids, their head groups occupy a larger area than their fatty acid chains. This brings to the formation of voids, which are filled by cholesterol molecules, with their cone-like shape, leading to close-packed cholesterol-sphingolipid clusters²⁴¹. These domains are insoluble in non-ionic detergents (such as Triton X-100) at 4°C, and that is why they are also called Detergent Resistant Membranes (DRMs)^{242,243}. The high lipid to protein ratio of these domains gives them a lower density compared to solubilized proteins, and this allows for isolation of DRMs by flotation on sucrose-density gradients, where they are typically isolated at the 5%–30% sucrose interface²⁴⁴. Two different kinds of liquid-ordered domains have been proposed to exist: caveolae and planar lipid rafts (also referred to as non-caveolae rafts)¹⁹¹. Caveolae are flask-shaped invaginations of the membrane, which formation is dependent on caveolin and cholesterol^{245,246}. Planar lipid rafts are flotillin-positive and are way more difficult to observe with common light microscopy techniques. Their lipid composition is similar to the one of caveolae, being both enriched in cholesterol and sphingolipids. Both kinds of domains are thought to be important for signaling molecules recruitment, as well as their spatial organization. This spatial compartmentalization favors the kinetic of signal transduction and processes that occur at the plasma membrane¹⁸⁵. Not all kind of proteins can associate with liquid-ordered domains; there are mainly three kinds of modifications that can partition a protein into liquid-ordered domains. These modifications can be GPI-anchoring of the protein to the extracellular leaflet of the plasma membrane^{167,247,248}, acylation of intracellular membrane-associated Tyrosine kinases of the Src family²⁴⁹, and palmitoylation of transmembrane proteins²⁵⁰.

1.7 Total Internal Reflection (TIRF) Microscopy

The unconventional secretion of FGF2 is a process that takes place at the plasma membrane^{46,103,251,252}. For this reason, the best way to image this process is by using Total Internal Reflection Fluorescence (TIRF) Microscopy. The purpose of TIRFM is to selectively illuminate fluorophores that are right near the adherent cell surface while minimizing fluorescence from intracellular regions²⁵³. TIRFM was developed by E.J. Ambrose, in 1956²⁵⁴, when he found a way to control the excitation scheme, so that only cell parts very close to the glass interface would be excited. He exploits total internal reflection, which occurs when light is totally reflected off a surface. If a beam of light passes through glass and then through water, which has a lower refractive index, it will bend to a larger angle. Increasing the incident angle will eventually cause the resulting angle of refraction to reach 90°. This is called critical

angle, because once it is exceeded total internal reflection is achieved and the light will not enter the second medium. At the point of total internal reflection, an evanescent wave is generated, which intensity decays exponentially with distance from the interface. The typical penetration depth of the evanescent field varies between 60 nm and 100 nm (with a maximum of 200 nm)²⁵⁵. The evanescent wave excites fluorophores near the interface and ignores anything else. Therefore, TIRFM works for samples that fluoresce and are close to the interface²⁵⁶.

There are different geometries that can be used for TIRFM. The two most common ones are prism-based and objective-based^{257,258}. Prism-based TIRF was the first method used for studying interfaces, and it has been used for long in cellular biology studies. It can be built with both an inverted or a non-inverted setup. In prism-based TIRF, a prism is used to reach the critical angle, and create the evanescent wave²⁵⁹. In objective-based TIRF (also referred to as prism-less TIRF), which was introduced after prism-based, excitation light enters the objective lens off-center, so that it can be sent at an angle to hit the glass/water interface²⁶⁰. With this method, it is easy to switch between standard epifluorescence and TIRF by simply changing the off-axis position of the beam focus at the objective's back focal plane. Furthermore, there are commercially available objective-based TIRF microscopes, which makes it much accessible to many groups compared to prism-based TIRF. Because the critical angle of glass and water must be exceeded, objective TIRF only works if the objective lens has a high numerical aperture of at least 1.34 (since water refractive index is 1.33). The fluorescent signal travels down the objective with the reflected laser light. The excitation and emission sources are separated by a dichroic mirror, allowing only the fluorescent signal to reach the detector. Both prism- and objective-based TIRF can be used for nanoscale and single molecule imaging²⁶¹.

In a recent publication, Dr. Eleni Dimou, a former PhD student from Walter Nickel's group, established two single molecule TIRF-based assay to study both recruitment at the inner plasma membrane leaflet and translocation on cell surfaces of FGF2²⁶². A schematic representation of the two TIRF assays is depicted in Figure 5. The cell lines used in these assays overexpress FGF2-GFP in a doxycycline-dependent manner. Single molecule real time TIRF recruitment assay exploits the leakiness of this system, that allows for a basal expression of FGF2-GFP in the absence of doxycycline. Under these conditions, only few amounts of the protein are expressed, and this allows to image single FGF2-GFP molecules in the vicinity of the plasma membrane. This enables to compare different conditions, such as mutant vs wild-type cells, or treated vs untreated cells, in order to quantify how these conditions affect FGF2-GFP recruitment at the inner plasma membrane leaflet of living cells. Single molecule TIRF translocation assay allows to quantify single FGF2-GFP molecules on cell surfaces.

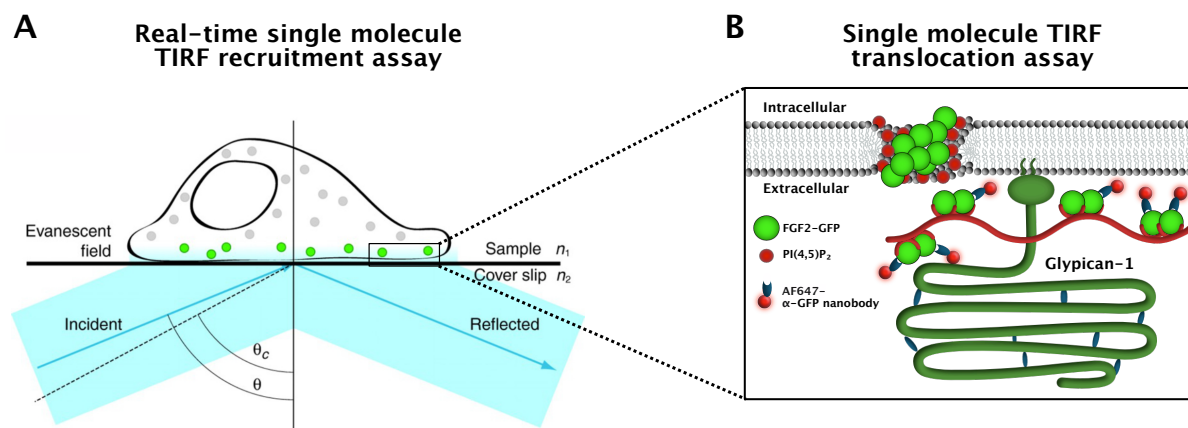


Figure 5: Single molecule TIRF assays. **A**, Schematic representation of real-time single molecule TIRF assay. FGF2-GFP single molecules recruited at the inner plasma membrane leaflet get excited, and are visible in a TIRF setup, while cytosolic FGF2-GFP molecules do not enter in the evanescent field and, therefore, do not get excited. **B**, Schematic representation of single molecule TIRF translocation assay, in which membrane-impermeable Alexa-Fluor labelled anti-GFP nanobodies are used to stain translocated FGF2-GFP particles. In this way, translocated FGF2-GFP particles are visible in the far-red channel, and it is possible to discriminate between them and intracellular FGF2-GFP particles²⁶². Adapted from Mattheyses, Simon and Rappoport, 2010²⁶³.

This is achieved through membrane-impermeable α -GFP nanobodies, which bind translocated FGF2-GFP particles and, since they couple with Alexa-Fluor 647, are visualized in a different channel than GFP, allowing to distinguish intra- and extracellular FGF2-GFP population. Under these conditions, similarly to recruitment assay, it is possible to evaluate how different conditions affect FGF2 translocation efficiency to the extracellular space. Both recruitment and translocation assay will be discussed in more detail, from a technical point of view, in the materials and methods section of this thesis.

2. Aims of the thesis

The unconventional secretory pathway of FGF2 has been studied and understood in high details in the last two decades⁴⁶. Beyond bulk measurements of FGF2 translocation from cells, the core mechanism of its membrane translocation has been recently elucidated with a fully reconstituted inside–out Giant Unilamellar Vesicles (GUVs) system¹¹⁰. While the $\alpha 1$ subunit of the Na,K–ATPase, Tec kinase, and PI(4,5)P₂ have been identified as crucial components interacting with FGF2 at the inner plasma membrane leaflet for its unconventional secretion of FGF2 from cells, the sequence of interaction with them was not fully understood at the beginning of this thesis. For this reason, the first aim of this thesis was to bring light on the sequence of interaction of FGF2 at the inner plasma membrane leaflet, before its translocation to the cell surface occurs. In order to answer this question, I employed a recently established single molecule TIRF assay²⁶², which allows to quantify single FGF2 molecules recruited at the inner plasma membrane leaflet. I used this assay in combination with variant mutant forms of FGF2 with an impaired binding to either the $\alpha 1$ subunit of the Na,K–ATPase, or to PI(4,5)P₂. This TIRF assay, which could be used to study both recruitment to the inner plasma membrane leaflet and translocation to cell surfaces, could be used to study other processes involved in the unconventional secretion of FGF2. I could collaborate in the investigation on a particular heparan sulfate proteoglycan, Glypican 1, which we found to be the rate–limiting factor for FGF2 secretion, and on a project on two FGF2 surface cysteine residues, which has been for many years thought to be both involved in intermolecular disulfide bridges formation¹¹², but that we found to have different specific roles. Finally, I studied how plasma membrane properties impact the unconventional secretion of FGF2, with a specific focus on cholesterol and sphingomyelin, both important components of liquid–ordered domains.

Jointly, the results achieved in this thesis enhanced our knowledge on the unconventional secretion of FGF2, with a better understanding of the sequence of interaction of FGF2 at the inner plasma membrane leaflet, a more specific understanding of the role of certain *cys* components on FGF2, a contribution on the importance of Glypican 1 in this process, and clear evidences on the importance of the plasma membrane lipid environment for FGF2 secretion from cells.

3. Materials and Methods

3.1 Materials

3.1.1 Consumables

Product	Supplier	Reference number
1.5 mL tubes	Sarstedt	72.690.001
10 mL pipettes	Greiner Bio-one	607180
15 mL tubes	Greiner Bio-one	188271
2 mL Amber Screw Top glass vials	Supelco	507628
2 mL tubes	Greiner Bio-one	623201
25 mL pipettes	Greiner Bio-one	760180
5 mL pipettes	Greiner Bio-one	606180
5 mL Round-Bottom Polystyrene Tubes	Falcon (Corning)	352003
5 mL Round-Bottom Polystyrene Tubes, with cell strainer	Falcon (Corning)	352235
55 mL tubes	Greiner Bio-one	227261
6-, 12-, 24-, 48-well cell culture plate	Greiner Bio-one	-
8-well glass bottom μ slides	Ibidi	80827
96-well plate, flat bottom	Greiner Bio-one	655182
Cell culture plates 60, 100, and 150 mm	Greiner Bio-one	-
Cell scraper	Serva	99004
Cryotubes CryoS	Greiner Bio-one	122263
Cuvette	Sarstedt	67.742
Exmire microsyringe	MZ-Analysentechnik	4035-11500
Glass beads 2.85-3.3 mm	Carl Roth	A557.1
Glass Pasteur pipettes	Brand	747715
Immobilon®-FL PVDF transfer membrane	Millipore	IPFL00010
LUNA™ Cell counting slides	Logos Biosystems	L12001
Nitrile gloves	Starguard	SG-C-M
NuPAGE™ 4-12% Bis-Tris gels 1mm x10 well	Invitrogen (Thermo Fischer)	NP0321
NuPAGE™ 4-12% Bis-Tris gels 1mm x15 well	Invitrogen (Thermo Fischer)	NP0323
PCR tubes	Kissler	S0141
Petri dish	Greiner Bio-one	-

Pierce™ Streptavidin UltraLink™ Resin	Thermo Fisher	53114
Pipette tips	Sarstedt	70.3030.XXX
Pipette tips (with filter)	Greiner Bio-one	–
Robust nitrile gloves	TouchNTuff	92–600
SafeSeal 1.5 mL tubes	Sarstedt	72.706
SafeSeal 2 mL tubes	Sarstedt	72.695.500
Syringe filters 0.20 µm	Whatmann GE Healthcare	10462200
Syringe filters 0.45 µm	Whatmann GE Healthcare	10462100
Syringes 10 mL	BD Plastikpak	300912
Syringes 50 mL	BD Plastikpak	300865
Vacuum filter	qpore	500022
Whatman paper 3 mm	Whatman	742118

3.1.2 Chemicals and biological reagents

Product	Supplier	Reference number
(R)–Mevalonic acid lithium salt	Sigma–Aldrich	50838
1 kb DNA ladder	NEB	N3232
100 bp DNA ladder	NEB	N3231
2–mercaptoethanol	Merck	8.05740
Acetic Acid	Sigma–Aldrich	33209
Ampicillin sodium salt	Gerbu Biotechnik	1046
Bacto Agar	Becton Dickinson	214010
Bacto Tryptone	Sigma–Aldrich	95039
Bacto Yeast extract	Gibco	80705
Boric Acid	Labochem Int. (neoLAB)	LC–5914.1
Bovine Serum Albumin (BSA) Fraction V	Carl–Roth	8076
Bovine Serum Albumin (BSA), fraction V	Carl–Roth	8076
Bromphenol blue	Serva	11447413
Calcium chloride	Sigma–Aldrich	31307
Cell Dissociation Buffer (CDB)	Gibco	13151014
Chloroform	Sigma–Aldrich	32211–M
Cholesterol	Avanti	700000P
Collagen R	Serva	47254
cOmplete EDTA–free Protease Inhibitor Cocktail	Sigma–Aldrich	54925800
DEAE–dextran	Sigma–Aldrich	78816

Materials and Methods

Delipidized serum	Bio & Sell	FCS.LFS.0100
Dimethyl sulfoxide (DMSO)	Sigma–Aldrich	D8418
Disodium hydrogen phosphate dihydrate	AppliChem	A3567,1000
DMEM high glucose	Sigma–Aldrich	D6429
DMEM low glucose	Sigma–Aldrich	D6046
Doxycycline	Clontech	564–25–0
EDTA	Honeywell	34549
Ethanol (absolute)	Sigma–Aldrich	32205–M
EZ–Link–Sulfo–NHS–SS–Biotin	Thermo Fisher Scientific	21331
FACS buffer	Becton Dickinson	342003
FACS clean	Becton Dickinson	340346
FACS rinse	Becton Dickinson	340345
Fetal Calf Serum (FCS)	Biochrom AG	S0615
Filipin complex	Sigma–Aldrich	F–9765
G418	Sigma–Aldrich	G8168
Gel Loading Dye, Purple, no SDS (6x)	NEB	B7025S
GFP Booster–AlexaFluor® 647	Chromotek (Proteintek)	gb2AF647
Glycerol	Sigma–Aldrich	15523
Glycine	Labochem Int. (neoLAB)	LC–4522.2
GW4869	Sigma–Aldrich	D1692
Heparinase III	NEB	P0737
HEPES	Sigma–Aldrich	3375
Hoechst stain	Thermo Fisher Scientific	62249
L–glutamine	Gibco	25030
Live cell imaging solution	Thermo Fisher Scientific	A14291DJ
MEM–Alpha modification	Sigma–Aldrich	M8042
Methanol	Honeywell	32213
Methyl–β–Cyclodextrin	Sigma–Aldrich	C4555
Mevastatin	Sigma–Aldrich	M2537
Milk powder	Carl–Roth	T145
Mycoplasma Removal Agent (MRA)	MP Biomedicals	3050044
Neutral Sphingomyelinase	Sigma–Aldrich	S9396
Nonidet P–40 (NP–40)	Sigma–Aldrich	492016
NuPAGE 20x MES SDS Running buffer	Invitrogen (Thermo Fisher)	NP0002
NuPAGE 20x MOPS SDS Running buffer	Invitrogen (Thermo Fisher)	NP0001
Ouabain oxtahydrate	Sigma–Aldrich	O3125
PageRuler™ prestained protein ladder	Thermo Fisher Scientific	26617
PBS	Sigma–Aldrich	D8537

Penicillin–streptomycin	Biochrom AG	P06–07050
PFA (16%)	Electron Microscopy Sciences	15710
Pierce™ Streptavidin UltraLink™ resin	Thermo Fisher Scientific	53114
Potassium chloride	Sigma–Aldrich	31248
Potassium dihydrogen phosphate	AppliChem	A3620,1000
RedSafe Nucleic Acid Staining Solution	iNtRON Biotechnology	21141
SDS	Bio–Rad	1610301
Sodium chloride	Labochem Int. (neoLAB)	LC–5932.1
Sodium hydroxide	Sigma–Aldrich	30620
Sodium–deoxycholate	Sigma–Aldrich	30970
Sphingomyelin	Avanti	860061P
Triethanolamin	Sigma–Aldrich	90278
Tris base	Carl–Roth	4855.2
Triton X–100	Sigma–Aldrich	T8787
Trypsin–EDTA (0.05%)	Gibco	25300
Tween–20	Sigma–Aldrich	P9416
Ultrapure™ Agarose	Thermo Fisher Scientific	16500500

3.1.3 Biochemical kits and Assays

Product	Supplier	Reference number
DNA Ligation kit	Takara	6022
MBS Mammalian Transfection Kit	Agilent Technologies	200388
Minute™ Plasma Membrane Protein Isolation and Cell Fractionation Kit	Invent biotechnologies	SM–005
NucleoBond Xtra Midi Plus	Macherey–Nagel	740410
NucleoSpin Plasmid Mini Prep kit	Macherey–Nagel	740588
QIAquick Gel Extraction Kit	Qiagen	28704
QIAquick PCR Purification Kit	Qiagen	28106

3.1.4 Antibodies

Antibodies	Supplier	Ref. number	WB Dilution
Mouse 3G10 (Δ HS)	Ambio	370260	1:500
Mouse monoclonal anti–FGF2	Thermo Fischer Scientific	MA1–24682	1:500

Mouse monoclonal anti-GAPDH	Thermo Fisher Scientific	AM4300	1:20000
Mouse monoclonal anti- α 1	Abcam	Ab7671	1:200
Rabbit anti-HA	Sigma Aldrich	H6908	1:500
Rabbit polyclonal anti-calnexin	Enzo	ADI-SPA-860	1:1000
Rabbit polyclonal anti-FGF2	Custom made, Pineda Antibody Service	-	1:500
Rabbit polyclonal anti-GFP	Custom made, Pineda Antibody Service	-	1:500
Rabbit polyclonal anti-tubulin	Abcam	Ab18251	1:1000
Secondary goat anti rabbit APC	Invitrogen	A-10931	1:500
Secondary goat anti-mouse AlexaFluor680	Thermo Fisher Scientific	A21057	1:10000
Secondary goat anti-rabbit IRDye 800CW	LI-COR Biosciences	926-32211	1:10000

3.1.5 Plasmids

Plasmid	Source
pRev TRE2	Nickel lab
pRev TRE2 FGF2(wt)-GFP	Nickel lab
pRev TRE2 FGF2(K54E)-GFP	Created within this thesis
pRev TRE2 FGF2(K60E)-GFP	Created within this thesis
pRev TRE2 FGF2(K54/60E)-GFP	Created within this thesis
pRev TRE2 FGF2(V76E)-GFP	Created within this thesis
pRev TRE2 FGF2(C77A)-GFP	Created within this thesis
pRev TRE2 FGF2(H58Y)-GFP	Created within this thesis
pRev TRE2 FGF2(P44G)-GFP	Created within this thesis
pRev TRE2 FGF2(P57G)-GFP	Created within this thesis
pRev TRE2 FGF2(K54/60E/C77A)-GFP	Created within this thesis
pRev TRE2 FGF2(K54/60E/C77A/H58Y)-GFP	Created within this thesis
pRev TRE2 FGF2(K54/60E/C77A/H58Y/P44/57G)-GFP	Created within this thesis
pRev TRE2 FGF2(K54/60E/C77A/H58Y/P44/57G/V76E)-GFP	Created within this thesis
pRev TRE2 FGF2(K127Q/R128Q/K133Q)-GFP	Created within this thesis
pRev TRE2 FGF2(K54E/ K127Q/R128Q/K133Q)-GFP	Created within this thesis
pRev TRE2 FGF2(K60E/ K127Q/R128Q/K133Q)-GFP	Created within this thesis
pRev TRE2 FGF2(K54/60E/ K127Q/R128Q/K133Q)-GFP	Created within this thesis
pRev TRE2 FGF2(V76E/ K127Q/R128Q/K133Q)-GFP	Created within this thesis
pRev TRE2 FGF2(C77A/ K127Q/R128Q/K133Q)-GFP	Created within this thesis

pRev TRE2 FGF2(H58Y/ K127Q/R128Q/K133Q)-GFP	Created within this thesis
pRev TRE2 FGF2(P44G/ K127Q/R128Q/K133Q)-GFP	Created within this thesis
pRev TRE2 FGF2(P57G/ K127Q/R128Q/K133Q)-GFP	Created within this thesis
pRev TRE2 FGF2(K54/60E/C77A/ K127Q/R128Q/K133Q)-GFP	Created within this thesis
pRev TRE2 FGF2(K54/60E/C77A/H58Y/ K127Q/R128Q/K133Q)-GFP	Created within this thesis
pRev TRE2 FGF2(K54/60E/C77A/H58Y/P44/57G/ K127Q/R128Q/K133Q)-GFP	Created within this thesis
pRev TRE2 FGF2(K54/60E/C77A/H58Y/P44/57G/V76E/ K127Q/R128Q/K133Q)-GFP	Created within this thesis
pRev TRE2 FGF2(C95A)-GFP	Created within this thesis
pRev TRE2 FGF2(C77/95A)-GFP	Created within this thesis
pRev TRE2 FGF2(C95A/ K127Q/R128Q/K133Q)-GFP	Created within this thesis
pRev TRE2 FGF2(C77/95A/ K127Q/R128Q/K133Q)-GFP	Created within this thesis

3.1.6 Cell Lines

Cell line	Source
HEK EcoPack 2-293	Clontech
CHO K1 MCAT TAM/CD2 (CHO K1)	Nickel lab, BZH
CHO K1 FGF2-GFP	Created within this thesis
CHO K1 GFP	Created within this thesis
CHO K1 FGF2(K54E)-GFP	Created within this thesis
CHO K1 FGF2(K60E)-GFP	Created within this thesis
CHO K1 FGF2(V76E)-GFP	Created within this thesis
CHO K1 FGF2(K54/60E)-GFP	Created within this thesis
CHO K1 FGF2(C77A)-GFP	Created within this thesis
CHO K1 FGF2(C95A)-GFP	Created within this thesis
CHO K1 FGF2(H58Y)-GFP	Created within this thesis
CHO K1 FGF2(P44G)-GFP	Created within this thesis
CHO K1 FGF2(P57G)-GFP	Created within this thesis
CHO K1 FGF2(K54/60E/C77A)-GFP	Created within this thesis
CHO K1 FGF2(K54/60E/C77A/H58Y)-GFP	Created within this thesis
CHO K1 FGF2(K54/60E/C77A/H58Y/P44/57G)-GFP	Created within this thesis
CHO K1 FGF2(K54/60E/C77A/H58Y/P44/57G/V76E)- GFP	Created within this thesis
CHO K1 FGF2(K127Q/R128Q/K133Q)-GFP	Created within this thesis

CHO K1 FGF2(K54E/ K127Q/R128Q/K133Q)-GFP	Created within this thesis
CHO K1 FGF2(K60E/ K127Q/R128Q/K133Q)-GFP	Created within this thesis
CHO K1 FGF2(V76E/ K127Q/R128Q/K133Q)-GFP	Created within this thesis
CHO K1 FGF2(K54/60E/ K127Q/R128Q/K133Q)-GFP	Created within this thesis
CHO K1 FGF2(C77A/ K127Q/R128Q/K133Q)-GFP	Created within this thesis
CHO K1 FGF2(C95A/ K127Q/R128Q/K133Q)-GFP	Created within this thesis
CHO K1 FGF2(H58Y/ K127Q/R128Q/K133Q)-GFP	Created within this thesis
CHO K1 FGF2(P44G/ K127Q/R128Q/K133Q)-GFP	Created within this thesis
CHO K1 FGF2(P57G/ K127Q/R128Q/K133Q)-GFP	Created within this thesis
CHO K1 FGF2(K54/60E/C77A/ K127Q/R128Q/K133Q)- GFP	Created within this thesis
CHO K1 FGF2(K54/60E/C77A/H58Y/ K127Q/R128Q/K133Q)-GFP	Created within this thesis
CHO K1 FGF2(K54/60E/C77A/H58Y/P44/57G/ K127Q/R128Q/K133Q)-GFP	Created within this thesis
CHO K1 FGF2(K54/60E/C77A/H58Y/P44/57G/V76E/ K127Q/R128Q/K133Q)-GFP	Created within this thesis
CHO K1 FGF2(C77/95A)-GFP	Created within this thesis
CHO K1 FGF2(C77/95A/ K127Q/R128Q/K133Q)-GFP	Created within this thesis
U2OS FGF2-GFP	Created within this thesis
U2OS GFP	Created within this thesis
CHO CD4-GFP	Nickel lab
CHO K1 FGF2-GFP + HA-GPC1 (single clones)	Created within this thesis, together with Annalena Meyer
CHO K1 FGF2-GFP +GPC1	Nickel lab

3.1.7 Equipment

Device	Supplier
Centrifuge 5404R	Eppendorf
Centrifuge 5417R	Eppendorf
FACSCalibur™ Flow Cytometer	Becton Dickinson
Gel Doc™ XR	BioRad
Heraeus Megafuge 4oR	Thermo Fischer Scientific
LSM 800 Confocal microscope	Zeiss
LUNA™ Automated Cel Counter	Logos Biosystems

Nanodrop ND-100	Thermo Fischer Scientific
Odyssey CLx Imaging system	LI-COR Biosciences
Olympus xCellence TIRF/Scanner FRAP	Olympus
PCR Thermocycler	FastGene
PCR Thermocycler primus 25	peQLab
PCR Thermocycler primus 96	peQLab
Sonication bath	Bandelin

3.1.8 Softwares

Software	Supplier
Affinity Designer	Serif Ltd.
ApE (A plasmid Editor)	M. Wayne Davis ²⁶⁴
Fiji	Schindelin, 2012 ²⁶⁵
Image Studio Lite	LI-COER Biosciences
Mendeley Reference Manager	Mendeley Ltd.
Microsoft Office 2019	Microsoft
Olympus xCellence	Olympus
Prism 5	GraphPad
SnapGene	Dotmatics
ZEN (blue edition)	Zeiss

3.2 Methods

3.2.1 Molecular Biology techniques

Preparation of calcium competent *E. coli* cells

DH5 α *Escherichia coli* cells were incubated o/n, shaking at 37°C to expand. The next morning, cell suspension was inoculated into 1000 mL LB medium into two Erlenmeyer flask (with 500mL culture each). The two flasks were incubated at 37°C, while shaking, and the growth rate was evaluated by measuring the OD₆₀₀ every 30 min. Bacteria incubation was stopped once the OD₆₀₀ reached 0.5, meaning that they reached logarithmic phase. At that point, the flasks were transferred on ice for 15 min. Bacteria were pelleted in 50 mL tubes at 4000 x g for 5 min at 4°C. Each pellet was resuspended in 10 mL ice-cold 0.1 M CaCl₂, and then centrifuged again. Each pellet was resuspended in ice-cold 0.1 M CaCl₂, 20% glycerol. Competent *E. coli* were aliquoted in 200 μ L aliquots in 1.5 mL tubes, snap frozen in liquid nitrogen and stored at -80°C.

Transformation into *E. coli*

10% DNA (v/v) was added to calcium competent DH5 α *E. coli* cells, which were previously thawed on ice. This mixture was incubated on ice for 30 min, and afterwards the bacteria were heat-shocked at 37°C for 20 sec. Subsequently, bacteria were cooled down on ice for 2 min, and 400 μ L LB medium was added to the bacteria, which were expanded for 1 h at 37°C, while shaking at 700 rpm. Afterwards, the bacteria suspension was either added into a 15 mL tube with 5 mL LB medium and specific selection marker antibiotic (ampicillin or kanamycin) and incubated o/n shaking at 37°C, to expand a single vector-containing *E. coli* clone, or plated on agar plates containing antibiotic (ampicillin or kanamycin) and incubated o/n at 37°C, for selection of vector-positive clones. In the latter case, the next day single colonies were picked and added to 15 mL tube containing 5 mL LB medium and specific selection marker antibiotic (ampicillin or kanamycin). Afterwards, plasmid DNA was isolated with a miniprep kit, which will be further discuss below.

Plasmid DNA isolation

Overnight bacteria cultures were pelleted down at 3000 x g for 10 min. at room temperature. The starting culture was either 5 mL, for Miniprep, or 150 mL, for Midiprep. Midiprep was performed to prepare enough plasmid DNA that would be subsequently used for mammalian cell transfection (which will be discussed in detail below). Plasmid isolation was performed

using the Nucleospin® Plasmid kit from Macherey–Nagel. In brief, pellets were resuspended in Resuspension Buffer A1, supplemented with RNase A, and then lysed in lysis buffer A2. The lysis reaction was performed at room temperature for 5 min., and stopped with neutralization buffer A3. Lysed *E. coli* were centrifuged at 11000 x g and supernatant was collected and transferred into Nucleospin® Plasmid column for DNA binding. After centrifugation for 1 min. at 11000 x g and discard of the flow-through, buffer A4, supplemented with ethanol, was added and the tube was centrifuged at 11000 x g for 1 min at room temperature to wash the bound DNA. DNA was then eluted with 30 µL elution buffer AE, or simply molecular grade H₂O when the DNA was subsequently meant for sequencing. Within this thesis, plasmids have been sent for sequencing either to GATC/Eurofins genomics, or to Mycosynth SeqLab. DNA concentrations were measured with the spectrophotometer Nanodrop ND-1000, measuring the absorbance at 260 nm (A_{260}). DNA solutions were stored at -20°C.

Agarose gel electrophoresis

DNA molecules were separated based on their molecular weight using agarose gel electrophoresis. Depending on the Kb of the DNA that needed to be resolved, different agarose concentrations were used. For higher Kb (> 800 bp) 1% agarose gel was used; for medium molecular weight (300 bp < x < 800 bp) 1.5% agarose; and for lower molecular weight (< 300 bp) 2% agarose. Agarose gels were prepared adding the appropriate amount of agarose in 1x TAE buffer (40 mM Tris, 20 mM acetic acid, 1 mM EDTA). Agarose was solubilized by heating in the microwave and, after cooling it down, RedSafe dye was added. This mixture was then poured into gel caster chamber, with the appropriate combs to create pockets in which DNA would be subsequently added. Agarose gels were stored at 4°C until use. For DNA analysis, DNA samples were mixed with 6x purple gel loading dye [New England BioLabs (NEB)] and loaded into agarose gel's pockets. As a molecular weight marker, it was used either the 1 Kb DNA ladder or the 100 bp DNA ladder from NEB. Electrophoresis was performed in 1x TAE buffer, applying 120 Volts for 15 min. DNA visualization was performed with the Gel Doc 200 system (Bio-Rad). Agarose gel electrophoresis was performed either to analyze DNA (e.g., for restriction analysis) or to isolate it for further applications. In the latter case, the agarose gel band containing the desired DNA was cut with a sterile scalpel and then purified with the QIAquick® Gel extraction kit (QIAGEN). In brief, the agarose gel was dissolved at 50°C in buffer QG, isopropanol was added and, after mixing the solution, everything was added to a QIAquick spin column. A centrifugation step was performed to bind DNA to the column, the flow-through was discarded and the column was centrifuged again with buffer PE, for washing. DNA was eluted in water, and subsequently used for ligation reaction (which will be further discussed below), or stored at -20°C.

Site Directed Mutagenesis (SDM)

To introduce mutations in DNA constructs, Site-directed mutagenesis was employed. Specific primers, between 22 bp and 38 bp, were self-designed, always including the specific mutation in the middle of the oligo sequence, and ending both sides with the same nucleotides (either cytosine or guanine, for a stronger binding). PCR reaction was prepared in a final volume of 50 μ L volume, with the template DNA being either pcDNA 3.1, or pRev TRE 2, containing various forms of FGF2-GFP. The PCR mixture was prepared as follows:

Template DNA	1 μL (50 ng/μL)
dNTPs	1 μ L (10 mM stock)
Forward primer	1.3 μ L (10 pmol/ μ L stock)
Reverse primer	1.3 μ L (10 pmol/ μ L stock)
High-Fidelity DNA Polymerase	1 μ L
5x HiFi buffer	10 μ L
ddH ₂ O	ad 50 μ L

PCR mixtures were then put in the Thermal cycler, for the PCR reaction to occur, with the following program:

Step	Temperature	Time	Number of cycles
Initial Denaturation	98 °C	4 min	1
Denaturation	98°C	45 sec	
Annealing	60°C	45 sec	16
Extension	72°C	3 min	
Final Extension	72°C	10 min	1
Samples cooling and storage	8°C	Infinite	

17 μ L of the PCR reaction were subsequently digested with DpnI for 1 h at 37°C. This enzymatic digestion removed parental methylated DNA (i.e., not containing the desired mutation), not affecting the demethylated newly synthesized DNA (containing the desired mutation). 3 μ L of the digested product were used to transform XL1 Blue E. coli strain (following the same procedure described for DH5 α , with the only difference of the heat shock carried for 45 sec. at 42°C). Transformed E. coli cells were plated on LB agar plates, and colonies, after expansion and plasmid DNA isolation, were checked for correct mutation insertion via DNA sequencing. Correctly mutated sequences were digested with specific restriction enzymes and inserted in the final vector pRev TRE 2, for stable mammalian cell lines preparation (this procedure will be discussed more in detail below).

Restriction enzyme digestion was performed in 20 μ L, in 1x CutSmart NEB buffer, with the appropriate restriction enzymes, for 1 h at 37°C. Furthermore, the vector was treated with alkaline phosphatase for 30 min at 37 °C, to remove the 5' phosphate group and avoid self-

closure of the vector. Insert was not dephosphorylated, to allow ligation with the digested and dephosphorylated vector. Following restriction enzyme digestion, vector and insert were purified with preparative agarose gel electrophoretic run, as described above. The resulting DNAs were used in to perform ligation reaction, that will be described below.

DNA Ligation

Ligation reactions were performed using an insert:vector ratio of 2:1. 50 ng of vector were used for the ligation. To calculate the ng of insert needed, the following proportion was employed:

$$50 \text{ (ng of vector)} : \text{vector bp} = x \text{ (ng of insert)} : \text{insert bp}$$

The ng of insert resulting from this proportion were then multiplied times 2, to reach the final 2:1 ratio. Ligation was performed employing the Takara DNA ligation kit, for 30 min at 16°C. Beyond this ligation mixture, a mixture without insert was always prepared, as control for vector self-ligation. Ligation products were transformed into competent *E. coli* DH5α cells (as described above).

3.2.2 Cell Biology techniques

Cell Maintenance

Chinese Hamster Ovary (CHO) and CHO K1 cells were cultured in Minimal Essential Medium Eagle (α-MEM), whereas Human Embryonic Kidney (HEK) EcoPack 2-293 and U2OS cells were cultured in Dulbecco's Modified Eagles Medium (DMEM). Both mediums were supplemented with 10% heat inactivated Fetal Calf Serum (FCS), 100 U/mL penicillin, and 100 µg/mL streptomycin. α-MEM was further supplemented with 2 mM glutamine. Cell lines were grown at 37 °C, in the presence of 5 % CO₂, and with 95 % humidity. HEK cells were cultivated in collagen-coated dishes, prepared adding to the dishes a sterile water-based collagen solution containing 0.02 % Collagen R (Serva). The dishes were left drying under a laminar flow hood. Passages for CHO and CHO K1 cells were made every 2-3 days, whereas for HEK and U2OS cells were made every 2-5 days. CHO, CHO K1 and U2OS were expressing their constructs under the control of doxycycline, that was generally added at a concentration of 1 µg/mL 17-24 h prior the experiments (unless otherwise stated) to induce protein expression. To perform single molecule real-time TIRF recruitment assay, doxycycline was not added to achieve single molecule detection (exploiting the leakiness of the system, that allows for a low rate of expression even in the absence of doxycycline). Single molecule TIRF Translocation experiments with CHO cells overexpressing CD4-GFP in a doxycycline-dependent manner

were also performed in the absence of doxycycline, for the same reason. All the other single molecule TIRF translocation experiments involving FGF2–GFP, as well as Biotinylation experiment, were performed in the presence of doxycycline.

Freezing and thawing of mammalian cells

Thawing of cells were performed as follows. Cryotubes were taken from liquid nitrogen tank, let stand for about a minute at room temperature and then quickly thawed in warm water. Thawed cells were poured into 50 mL tubes containing 7 mL of appropriate medium, and centrifuged for 3 min at 1000 rpm. Supernatant was discarded and pellet resuspended in 10 mL of growth medium, and then transferred into 10 cm dish. A small aliquot of cells was transferred into a 6–well plate, in order to start the treatment with Mycoplasma Removal Agent (MRA), that lasts for a week. For freezing cells, freezing medium was prepared including 40% growth medium, 40% FCS, and 20% DMSO. This freezing medium was filtered sterile and refrigerated. Meanwhile, confluent cells were detached from a 10 cm dish with trypsin and pelleted down in a 15 mL tube. Cells were then resuspended in growth medium and, per each vial, 750 μ L of the cell suspension were transferred, together with 750 μ L of freezing medium, reaching a final DMSO concentration of 10%. Cryovials were put at -80°C for a few days, and then transferred into a liquid nitrogen tank for longer storage.

Making Stable cell lines

Stable cell lines were generated using a retroviral transduction system, based on Moloney Murine Leukemia Virus (MMLV). Recombinant virus particles were generated in HEK EcoPack 2–293 cells, containing in their genome the retroviral packaging proteins pVPack–GP and pVPack–eco, after transfection with the pRev TRE 2 vector, containing a TET–Responsive Element. HEK cells transfection and retrovirus production were performed using the MBS Mammalian Transfection Kit (Agilent Technologies). HEK cells were seeded on collagen–coated dishes and let grow until ~ 60 – 70% confluency. On the day of transfection, 9 μ g of DNA in 450 μ L of sterile water were mixed with 50 μ L Solution I and 500 μ L Solution II, and incubated for 20–30 min at room temperature. Meanwhile, HEK cells medium was substituted with medium containing MBS (Modified Bovine Serum) and 25 μ M chloroquine, and subsequently the DNA mixture was added to them in a drop–wise fashion. Following 3 h incubation, the medium was substituted with growth medium containing 25 μ M chloroquine, and after a further 6–7 h incubation, medium was again substituted with normal growth medium. 72 h after transfection, HEK cells supernatant, containing retroviral particles, was collected and filtered through a 0.45 μ m filter, and subsequently added to target cells for transduction. CHO K1

and U2OS cells, constitutively expressing the murine cationic amino acid transporter (MCAT-1) and rtTA2-M2, a Tet-ON transactivator, were the targets of retroviral transduction.

Stable cell line pools were sorted based on GFP or HA expression levels using a FACS approach. Cells were subjected to three subsequent FACS sorting, the first and the last with addition of doxycycline to select positive cells expressing the protein of interest, and the second in the absence of doxycycline, to eliminate cells that express high protein levels even in the absence of doxycycline. Cell lines overexpressing untagged proteins were subjected to antibiotic selection, starting 72 h after transduction.

Ouabain treatment

Ouabain, resuspended in DMSO, was used at different concentrations on a U2OS cell line stably expressing FGF2-GFP in a doxycycline-dependent manner. For FGF2-GFP recruitment analysis, ouabain treatment was conducted for 6 h in culture conditions, in the absence of doxycycline. Translocation analysis was conducted in the presence of doxycycline, and, prior the addition of ouabain, cells were washed with 500 µg/mL heparin, to wash previously translocated FGF2-GFP particles. Ouabain treatment was then conducted for 6 h in culture conditions. For both analyses, ouabain treatment was performed with increasing concentrations of ouabain of 25 µM, 50 µM, and 50 µM. Furthermore, the same amount of DMSO used to deliver the different ouabain concentrations was added to the mock condition. Single molecule TIRF recruitment and translocation assay were then conducted as described in the dedicated section.

MβCD:cholesterol complexes treatment

Cholesterol, dissolved in chloroform at 10 mg/mL, was dried under a nitrogen stream and, afterwards, under vacuum at room temperature in Amber glass tubes. Methyl-β-Cyclodextrin (MβCD), solubilized in Live Cell Imaging Solution (Thermo Fisher Scientific) at 200 mM was added to the cholesterol lipid film, with a molar ratio of MβCD to cholesterol of 10 to 1. The mixture was sonicated and vortexed at room temperature, warming it up at 37°C between every vortex/sonication cycles, for 1 h or until complete dissolution of the cholesterol lipid film. 100x single use aliquots were stored at -20 °C. Cells (either CHO K1 or U2OS, both stably expressing FGF2-GFP in a doxycycline-dependent manner) were treated with Cholesterol:Methyl-β-Cyclodextrin complexes (with a final cholesterol concentration of 0.2 mM) for 1 h in culture conditions, in Live Cell Imaging Solution.

Mevastatin treatment

Cells (either CHO K1 or U2OS, both stably expressing FGF2–GFP in a doxycycline–dependent manner) were seeded in normal growth medium 24 h before the addition of mevastatin, which was used at a final concentration of 5 μ M, and was added to cells together with 50 μ M mevalonate in the presence of de–lipidized serum. This treatment was conducted for 24 h in culture conditions. The mock condition was added with the same volume of ethanol, used to deliver mevastatin to cells at a 5 μ M concentration. Subsequent real–time single molecule TIRF recruitment assay, single molecule TIRF translocation assay, mass spectrometry sample preparation, and Filipin staining, were conducted as described in the respective sections.

Sphingomyelinase treatment

Sphingomyelinase (SMase) treatment was conducted on a stable CHO K1 cell line overexpressing FGF2–GFP in a doxycycline–dependent manner. Cells were treated with increasing concentrations of SMase: 0.01 U/mL, 0.05 U/mL, 0.1 U/mL, 0.3 U/mL, and 0.5 U/mL. SMase treatment was conducted for 4 h in culture conditions. the enzyme was delivered in 50 mM Tris, 50% glycerol. The mock condition was added with the same volume of 50 mM Tris, 50% glycerol used for the different enzyme concentrations. Subsequent analyses, such as cell surface biotinylation assay, real–time single molecule TIRF recruitment assay, single molecule TIRF translocation assay, and mass spectrometry sample preparation, were conducted as described in the respective sections.

M β CD:sphingomyelin complexes treatment

Sphingomyelin, dissolved in chloroform at 10 mg/mL, was dried under a nitrogen stream and, afterwards, under vacuum at room temperature in Amber glass tubes. Methyl– β –Cyclodextrin (M β CD), solubilized in Live Cell Imaging Solution (Thermo Fisher Scientific) at 200 mM was added to the sphingomyelin lipid film, with a molar ratio of M β CD to sphingomyelin of 10 to 1. The mixture was sonicated and vortexed at room temperature, warming it up at 37°C between every vortex/sonication cycles, for 2 h or until complete dissolution of the sphingomyelin lipid film. 100x single use aliquots were stored at –20 °C. Cells were treated with sphingomyelin:Methyl– β –Cyclodextrin complexes (with a final sphingomyelin concentration of 0.2 mM) for 1 h in culture conditions, in Live Cell Imaging Solution.

3.2.3 Biochemical techniques

Whole Cell Lysate

Whole cell lysates were prepared starting from 6-well plates, with and without doxycycline, to check for doxycycline-dependent expression of the protein of interest. Cells were detached in 1 mM EDTA (prepared in PBS), and collected by centrifugation for 5–10 min at 500 x g. pellets were lysed in RIPA buffer containing protease inhibitors (Roche) on ice for 30 min in 1.5 mL tubes. Afterwards, tubes were centrifuged for 10 min at 20000 x g, to remove cell debris, and supernatant was collected in a fresh 1.5 mL tube, where it was mixed with 4x SDS sample buffer. Samples were boiled for 10 min at 95°C, cooled down for about a minute on ice and spined down. Boiled samples were either directly loaded on SDS-PAGE for western blot analysis, or stored at -20°C until use.

Western blotting analysis

SDS-Poli-Acrylamide Gel Electrophoresis (SDS-PAGE) was performed to separate proteins based on their molecular weight. Within this thesis, NuPAGE Bis-Tris gels were employed, with a 4–12% gradient polyacrylamide concentration, containing either 10, 15, or 17 wells. SDS-PAGE was performed using NuPAGE MES or MOPS SDS Running Buffer, at 200 V for 40 or 55 min, respectively. A Pre-stained PageRuler (Thermofisher) protein ladder was used as a molecular weight marker. Following SDS-PAGE, western blot was performed to transfer size separated proteins from the polyacrylamide gel to a PVDF membrane. Western blot was performed for 1 h at 100 V, in blot buffer (40 mM glycine, 25 mM Tris base, and 20% methanol, final pH 8.4). PVDF membrane was activated in methanol for about a minute, and then put on top of the gel containing the proteins. Gel and membrane were placed in the middle of two layers of Whatman paper and sponges, and then everything was inserted into the gel chamber, together with an ice block to prevent overheating. After one hour, PVDF membrane were blocked in PBS containing 5% milk for 1 h at room temperature, or overnight in the cold room. After two washing steps in PBS supplemented with 0.05% Tween20 (PBS-T), a primary antibody solution prepared in PBS-T, with 2% BSA and 0.02% Na-azide, was added to the membrane and incubated for 1 h at room temperature, or overnight in the cold room. Following primary antibody staining, four washing steps with PBS-T were performed and secondary antibody was added, in PBS-T with 2% BSA and Na-azide, for 30 min at room temperature. Prior imaging, 4 washing steps were performed with PBS-T and one with PBS. Membranes were imaged with the LI-COR Odyssey CLx imaging system and analyzed with Image Studio Lite Software (Version 5.0.21, LI-COR Biosciences). Primary antibody solutions were stored either at 4°C or, for longer time storage, at -20°C, whereas secondary antibody solutions were stored at 4°C. Both primary and secondary solutions were used for a maximum of 7 times.

Cell Surface Biotinylation Assay

Cell Surface Biotinylation Assay was used to quantify secretion efficiency of proteins at cells surfaces. After protein expression was induced by doxycycline for ~18 h, surface proteins were biotinylated with a membrane impermeable biotinylation reagent, which reacts with protein's primary amines. This reagent was dissolved in a basic biotinylation buffer and, after cells were washed with PBS calcium/magnesium, they were incubated for 30 minutes on ice with this biotinylation reagent. Subsequently, cells were washed once with a glycine-based quenching buffer, and then incubated with the same quenching buffer for 20 minutes on ice. Afterwards, cells were washed twice with PBS and incubated for 10 min at 37°C with a Nonidet P-40-based lysis buffer (1% Nonidet P-40, 50 mM Tris/HCl pH 7.5, 62.5 mM EDTA pH 8, 0.4% Na-deoxycholate), supplemented with Protease inhibitors (Roche). Cells were then scraped with 1 mL tips and collected in 1.5 mL tubes. Lysates were then sonicated for 3 min in a sonication bath and subsequently incubated for 15 min at room temperature, vortexing every 5 minutes to dissolve proteins. Cell lysates were then centrifuged at high speed (13000 rpm) for 10 min. An aliquot of supernatant, 5%, was taken and boiled at 95 °C, after addition of SDS sample buffer, as input. The remaining supernatant was incubated for 1 h at room temperature with streptavidin beads. Beads were then spined down at 3000 x g for 1 min, and washed four times with washing buffer, consisting of lysis buffer supplemented with 0.5 M NaCl. In the last three washing steps, lysis buffer contained only 0.1% NP-40, instead of 1%. Biotinylated proteins were then eluted from beads in SDS sample buffer via 95°C boiling. Samples were then analyzed via western blotting. For this assay, in the western blotting analysis, the membranes were stained against GFP, employing an α -GFP antibody, to detect FGF2-GFP (α -GFP antibody was used instead of α -FGF2, since in this thesis several FGF2 mutants have been employed, and this could have changed the affinity of such mutants for the α -FGF2 antibody), and against GAPDH, both as a loading control and, most importantly, to check for cellular integrity. GAPDH is in fact an intracellular protein, and its presence in the eluate (i.e., its contact with biotin), would mean a leakiness of the cells during the assay, which would impact the quantification of surface FGF2-GFP, also potentially taking into account a part of intracellular protein.

Heparinase III digest

HSPGs levels were quantified via western blot analysis, following Heparinase III digestion. Cells were seeded either on 10 cm dishes or 6-well plates, 24 h prior heparinase III digestion. Cells were detached with 1 mM EDTA (in PBS) and pelleted at 500 x g for 7 min. Cell pellets were resuspended in heparinase buffer solution (NEB). 0.5 μ L Heparinase III were added every 100 μ L solution. Cells were incubated with this solution for 6 h at 30°C, shaking them at 600 rpm,

and resuspending them every 30 to 60 min. Afterwards, cells were pelleted at 500 x g for 7 min and lysed in RIPA buffer, supplemented with a protease inhibitor cocktail, for 30 min on ice. Western blot analysis was conducted against cleaved HS chains on HSPGs with the 3G10 antibody, and tubulin, as loading control.

FACS assay

CHO K1 cells stably expressing HA-GPC1 and overexpressing FGF2-GFP in a doxycycline-dependent manner, were seeded on 12-well plates, detached with 1 mM EDTA (in PBS) and pelleted at 500 x g for 7 min. Cells were then stained in tubes against HA-tag for 1 hour at room temperature. Following 3 washing steps, cells were incubated with an APC-conjugated secondary antibody. Fluorescence was detected with BD FACSCalibur™ Flow Cytometer. Fluorescence coming from each single clone was normalized to the average of all clones analyzed, which was set to 100%.

Plasma membrane fractionation preparation for lipid mass spectrometry

Following either cholesterol or sphingomyelin manipulation in cells (either enrichment or depletion), performed as described in this section, CHO K1 plasma membrane fractions were isolated using the Minute™ Plasma Membrane Protein Isolation and Cell Fractionation Kit (Invent Biotechnologies), following the manufacturer's instructions. In brief, 24 h before treatment, cells were seeded in 15 cm dishes (Thermo scientific). Following the respective treatment, cells were detached with 1 mM EDTA (in PBS) and pelleted at 500 x g for 7 min. Pellets were rinsed with 1 mL cold PBS and, following another centrifugation step at 500 x g for 7 min, supernatant was removed completely. Cellular pellets were resuspended in 500 μ L buffer A, incubated for 5 to 10 min on ice, and vortexed for 10 to 30 sec. A 10% portion was taken at this point as input, to compare it with the respective plasma membrane fraction in following analysis. Cell suspensions were then transferred to the filter cartridge and centrifuged at 16000 x g for 30 sec. Pellets were resuspended and added to the same filter, before performing another centrifugation step at 16000 x g for 30 sec. The resulting pellets were resuspended by vortexing for 10 sec and suspensions were centrifuged at 700 x g for 1 min. Supernatants were then transferred to 1.5 mL tubes and centrifuged at 16000 x g for 15 min at 4°C. The resulting pellets were resuspended in 200 μ L buffer B by vortexing, until complete resuspension, and centrifuged at 7800 x g for 20 min. The supernatants resulting from this centrifugation step were transferred into 2 mL tubes and, after that, 1.6 mL cold PBS was added to them. The resulting suspensions were centrifuged at 16000 x g for 20 min and supernatant was removed. The resulting pellets contains purified plasma membrane fractions. Plasma membrane fractions and input were analyzed both via western blot and lipid

mass spectrometry. The western blot analysis was conducted against a plasma membrane marker (the α -1 subunit of the Na,K-ATPase) to check for plasma membrane enrichment, and an ER marker (calnexin) to check for ER contamination of the plasma membrane fractions. The samples were sent to the lipidomics facility of Prof. Dr. Britta Brügger, at the BZH, to perform lipid mass spectrometry. Beyond a further validation for successful plasma membrane enrichment, looking for cholesterol enrichment in the plasma membrane fraction compared to the input, lipid mass spec was performed to validate either cholesterol or sphingomyelin manipulation in cells, comparing mock and treated conditions.

3.2.4 Microscopy techniques

Single-molecule TIRF microscopy

Single molecule TIRF microscopy was performed as described previously²⁶². For both assays, real-time single molecule TIRF recruitment assay, and single molecule TIRF translocation assay, it was employed an Olympus IX81 xCellence inverted TIRF microscope equipped with an Olympus PLAPO $\times 100/1.45$ Oil DIC objective lens and a Hamamatsu ImagEM Enhanced (C9100-13) camera. Images were exported in the Tagged Image File Format (TIFF) and analyzed with Fiji²⁶⁵.

Cell lines used in real-time single molecule TIRF recruitment assay were either CHO K1 or U2OS, expressing either FGF2-GFP, or only GFP, in a doxycycline-dependent manner. Cells were seeded on 8-well, glass bottom μ -slide plates (ibidi), 24 h before imaging. This assay was always performed in the absence of doxycycline, exploiting the leakiness of the doxycycline-dependent system, that allows for low levels of protein synthesis. This limited amount of protein was suitable for single molecule detection of FGF2-GFP. Cells were washed two times with Live Cell Imaging Solution (Thermo Fisher Scientific) before imaging. An Olympus 488 nm, 100 mW diode laser was used to excite GFP fluorescence in TIRF mode. For widefield fluorescence, GFP was excited with an MT 20 illumination system. Widefield images were taken to select frames of cells. TIRF images were acquired as time-lapse videos, analyzed to quantify FGF2-GFP recruitment efficiency at the inner plasma membrane leaflet. Normalization was performed taking into account both cell surface area (μm^2) and FGF2-GFP (or GFP) expression level. FGF2-GFP (or GFP) expression level was quantified, for each cell, at the first frame of TIRF time-lapse videos. The Fiji plugin TrackMate²⁶⁶, with its Log G detector, was employed to identify and quantify single FGF2-GFP, or GFP particles, using a blob diameter of 0.7 μm , and a threshold adjusted for each experiment, according to the specific signal to noise ratio (but always kept constant, within the same experiment, for the different conditions analyzed).

Cell lines used in single molecule TIRF translocation assay were either CHO K1, CHO, or U2OS cells, expressing either FGF2-GFP, CD4-GFP, or only GFP, in a doxycycline-dependent manner. Cell lines overexpressing other proteins on top of FGF2-GFP, like GPC1 or HA-GPC1, have also been used in this study. Cells were seeded on 8-well, glass bottom μ -slide plates (ibidi), 24 h before imaging. This assay was usually performed after doxycycline-induced protein expression. In two cases, doxycycline was not used: in all the experiments performed with CHO CD4-GFP, since, as membrane protein, the low expression levels achieved without doxycycline were enough for single molecule detection, whereas doxycycline-induced expression would cause a too high level of protein at the membrane, and the experiments performed with GPC1 and HA-GPC1 overexpressing cells, under conditions of low FGF2-GFP expression levels. Prior imaging, cells were washed three times with Live Cell Imaging Solution (Thermo Fisher Scientific), and incubated with membrane impermeable Alexa-Fluor-labelled anti-GFP nanobodies for 30 min on ice. Cells were subsequently washed three times with PBS and fixed with 4% PFA for 20 min at room temperature. Cells were washed three times with PBS and either directly imaged, or stored at 4°C (for a maximum of 18 h) before imaging. An Olympus 649 nm, 140 mW diode laser was used to excite Alexa-Fluor 647-labeled anti-GFP nanobodies in TIRF mode. For widefield fluorescence, GFP was excited with either a MT 20 illumination system, or with an Olympus 488 nm, 100 mW diode laser. Widefield images were taken to select frames of cells. TIRF images of translocated FGF2-GFP particles (detected via membrane impermeable Alexa-Fluor-labelled anti-GFP nanobodies) were analyzed to quantify FGF2-GFP translocation efficiency from cells. Normalization was performed taking into account cell surface area (μm^2). The Fiji plugin TrackMate²⁶⁶, with its Log G detector, was employed to identify and quantify single nanobody particles (bound to either FGF2-GFP, CD4-GFP or GFP), using a blob diameter of 0.6 μm , and a threshold adjusted for each experiment, according to the specific signal to noise ratio (but always kept constant, within the same experiment, for the different conditions analyzed). In each experiment, all the conditions were normalized to wild-type cells (for mutant FGF2-GFP analysis or GPC1/HA-GPC1 overexpressing cells), or to the mock condition (for the various treatment used in this work), which were set to 1.

Filipin staining

Cellular cholesterol levels were quantified by confocal imaging following filipin (Sigma) staining. CHO K1 and U2OS cell lines stably expressing FGF2-GFP in a doxycycline dependent manner were seeded in 8-well, glass bottom, μ -slide plates (ibidi), 24 h prior imaging. Cells were incubated for either 1 h in culture conditions with cholesterol:Methyl- β -Cyclodextrin complexes, to evaluate cholesterol enrichment following this treatment, or for 24 h with 5 μM mevastatin and 50 μM mevalonate, in the presence of de-lipidized serum, in culture conditions, to evaluate cholesterol depletion following this treatment. Before imaging, cells

were rinsed three times with PBS and fixed with 3% PFA for 1 h at room temperature. Following 3 washing steps with PBS, PFA was quenched via 10 min incubation in PBS containing 1.5 mg glycine at room temperature. Filipin was first prepared as a stock solution (25 mg/mL in DMSO) and subsequently diluted in PBS, supplemented with 10% FCS, to reach a working solution of 50 µg/mL. This filipin working solution was used to stain cells for 2 h at room temperature. Following 3 washing steps in PBS, cells were imaged with a confocal laser scanning microscope (Zeiss LSM800) with a 63× oil objective.

3.2.5 Statistical analysis

Statistical analyses were performed using GraphPad Prism, either version 5 or 9. Based on the number of conditions for each experiment, a different statistical test was applied. An unpaired, two-tailed t-test was performed to compare two conditions. For more than two conditions, a one-way ANOVA test, combined with a Tukey's post hoc test, was performed. Within this thesis, data are shown as mean ± SD, with statistical significance, calculated with the stated test, indicated as follows: *ns* $p > 0.05$, * $p \leq 0.05$, ** $p \leq 0.01$, *** $p \leq 0.001$, **** $p \leq 0.0001$

4. Results

4.1 The $\alpha 1$ subunit of the Na,K-ATPase is the first physical contact of FGF2 at the inner plasma membrane leaflet

In the last few years, the unconventional secretory pathway of FGF2 gained deeper understanding⁴⁶. In a genome-wide RNAi screen designed to discover new proteins involved in the unconventional secretory pathway of FGF2, down regulation of the $\alpha 1$ subunit of the Na,K-ATPase led to a strong inhibition of FGF2 secretion from cells¹⁰⁴. Recently, a subdomain in the third cytoplasmic loop of the $\alpha 1$ subunit of the Na,K-ATPase ($\alpha 1$ -subCD3) has been identified as a minimal binding partner of FGF2¹⁰⁵. This subdomain is a globular domain of about 20 kDa in size and this allowed for solution NMR spectroscopy to map the binding interface of $\alpha 1$ -subCD3 on FGF2. This led to the identification of two lysine residues in position 54 and 60 on the molecular surface of FGF2, which were considered to potentially interact with $\alpha 1$ -subCD3¹⁰⁵. In addition to these lysine residues, a number of residues in the vicinity of this pocket have been taken into account for a possible interaction with $\alpha 1$ -subCD3. These included the valine residue in position 76, cysteine in position 77, histidine in position 58 and two proline residues in position 44 and 57. I then generated vectors expressing FGF2-GFP, containing different combinations of mutations on these sites, via site-directed mutagenesis on FGF2-GFP wild-type (for details, see materials and methods). The final vectors were validated via DNA sequencing and, subsequently, sub-cloned in pRev TRE-2, to allow for HEK EcoPack 2-293 cells transfection and virus production, and therefore for target cells transduction (for details, see materials and methods). The final constructs are indicated in table 1. Before cell transfection, final pRev TRE-2 vectors were sequenced and positive DNA sequenced vectors were amplified via midi-prep. I then generated stable CHO-K1 cell lines by retroviral transduction which express these constructs in a doxycycline-dependent manner. I validated these cell lines for doxycycline-dependent protein expression via whole cell lysate with and without doxycycline. All of these cell lines expressed adequate amounts of the respective FGF2-GFP form in response to doxycycline, with the exception of mutant forms including 6 or more substitutions in the FGF2 sequence (K54/60E/C77A/H58Y/P44/57G and K54/60E/C77A/H58Y/P44/57G/V76E).

Vector	Construct	Mutation
pRev TRE2	FGF2-GFP	Wild-type
pRev TRE2	FGF2-GFP	K54E
pRev TRE2	FGF2-GFP	K60E
pRev TRE2	FGF2-GFP	V76E
pRev TRE2	FGF2-GFP	C77A
pRev TRE2	FGF2-GFP	H58Y

Results

pRev TRE2	FGF2-GFP	P44G
pRev TRE2	FGF2-GFP	P57G
pRev TRE2	FGF2-GFP	K54/60E
pRev TRE2	FGF2-GFP	K54/60E/C77A
pRev TRE2	FGF2-GFP	K54/60E/C77A/H58Y
pRev TRE2	FGF2-GFP	K54/60E/C77A/H58Y/P44/57G
pRev TRE2	FGF2-GFP	K54/60E/C77A/H58Y/P44/57G/V76E
pRev TRE2	FGF2-GFP	K127Q/R128Q/K133Q
pRev TRE2	FGF2-GFP	K54E/K127Q/R128Q/K133Q
pRev TRE2	FGF2-GFP	K60E/K127Q/R128Q/K133Q
pRev TRE2	FGF2-GFP	V76E/K127Q/R128Q/K133Q
pRev TRE2	FGF2-GFP	C77A/K127Q/R128Q/K133Q
pRev TRE2	FGF2-GFP	H58Y/K127Q/R128Q/K133Q
pRev TRE2	FGF2-GFP	P44G/K127Q/R128Q/K133Q
pRev TRE2	FGF2-GFP	P57G/K127Q/R128Q/K133Q
pRev TRE2	FGF2-GFP	K54/60E/K127Q/R128Q/K133Q
pRev TRE2	FGF2-GFP	K54/60E/C77A/ K127Q/R128Q/K133Q
pRev TRE2	FGF2-GFP	K54/60E/C77A/H58Y/ K127Q/R128Q/K133Q
pRev TRE2	FGF2-GFP	K54/60E/C77A/H58Y/P44/57G/ K127Q/R128Q/K133Q
pRev TRE2	FGF2-GFP	K54/60E/C77A/H58Y/P44/57G/V76E/ K127Q/R128Q/K133Q

Table 1: variant forms of FGF2-GFP carrying mutations that could possibly have an impact with its interaction with the $\alpha 1$ -subunit of the Na,K-ATPase.

In panel A of figure 6, all the mutant forms of FGF2 are depicted showing their secretion efficiency via cell surface biotinylation assay^{105,112,267}. Considering single mutant forms of FGF2-GFP, single substitution of lysine 60 by glutamate and cysteine 77 by alanine seemed to have the strongest phenotype, with a 27% and a 36% reduction in secretion efficiency compared with wild-type cells, respectively (Fig. 5, panel A).

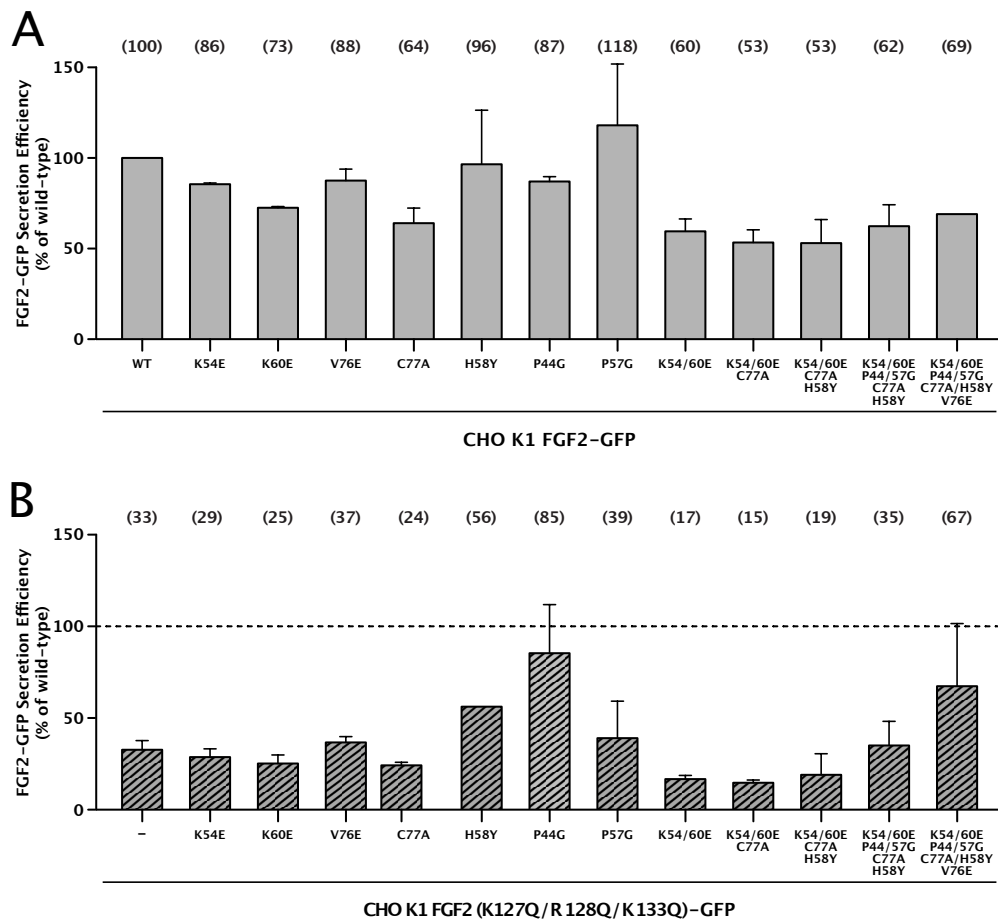


Fig. 6: Quantification of cell surface biotinylation assay for all the mutant form of FGF2-GFP generated to study the interaction with the α 1-subunit of the Na,K-ATPase. A, Secretion efficiency of FGF2-GFP variant forms carrying single substitutions of residues possibly involved in the interaction with the α 1-subunit of the Na,K-ATPase. Beyond the wild-type (WT) form of FGF2-GFP, the versions included were: K54E, K60E, V76E, C77A, H58Y, P44G, P57G, K54/60E, K54/60E/C77A, K54/60E/C77A/H58Y, K54/60E/C77A/H58Y/P44/57G, K54/60E/C77A/H58Y/P44/57G/V76E. B, Secretion efficiency of the same set of FGF2-GFP mutants shown in panel A, in combination with substitution of K127, R128, and K133 with Q [a mutant form of FGF2-GFP that cannot bind PI(4,5)P₂].

The combination of mutations of the two lysine residues led to a 40% decrease in secretion efficiency, and when cysteine 77 was replaced by alanine on top of that, secretion efficiency dropped by 47% (Fig. 6, panel A). I also combined these substitutions with mutations in the PI(4,5)P₂ binding pocket on FGF2, consisting of three basic residues on its surface (K127, R128, K133)^{110,268}. This mutant form of FGF2 was already shown to be defective for FGF2 secretion from cells^{112,268}. In this set of experiments, substitution of these three basic residues with glutamines affected FGF2-GFP secretion efficiency by 67% (Fig. 6, panel B). Consistently with the previous sets of mutants, again the most interesting substitutions seemed to be the

ones involving the two lysine residues (K54/60E), showing an 83% reduction of FGF2–GFP secretion efficiency compared with wild-type cells (Fig. 6, panel B).

For this reason, in a subsequent set of experiments, I only focused on the subset of mutants showing the strongest phenotype in terms of secretion efficiency (Fig. 7).

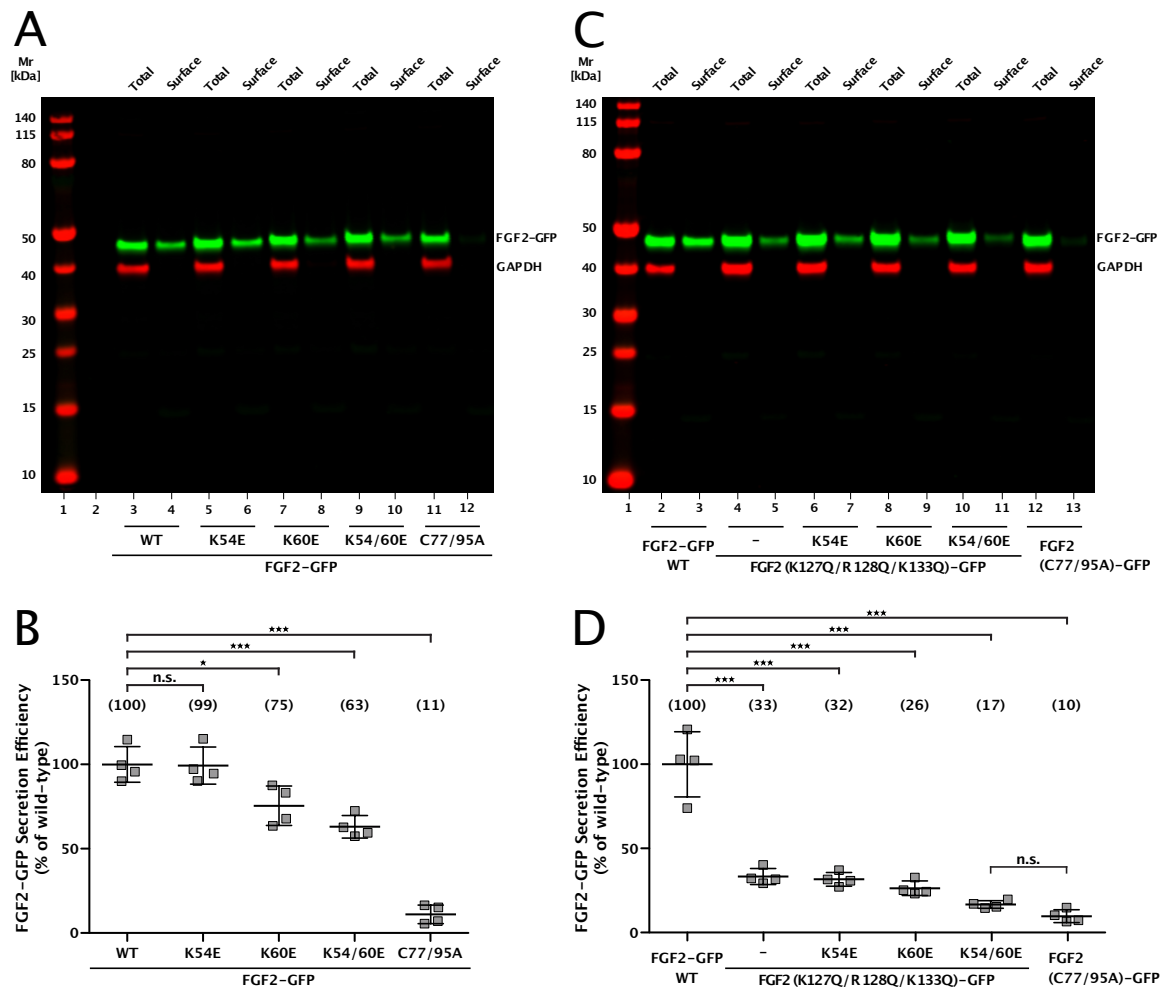


Fig. 7: the α 1-subunit of the Na,K-ATPase facilitate efficient secretion efficiency of FGF2 from cells. **A**, Representative western blot analysis of cell surface biotinylation experiments, conducted on stable CHO K1 cell lines overexpressing various mutant forms of FGF2–GFP in a doxycycline-dependent manner. Beyond wild-type FGF2–GFP, the mutant forms of FGF2–GFP were K54E, K60E, and K54/60E, as binding mutant of the α 1-subunit of the Na,K-ATPase, and C77/95A as a negative control of secretion (being the mutant with the strongest secretion phenotype so far known in the literature). Western blot analysis was conducted against GFP (to detect FGF2–GFP) and GAPDH (to check for cellular integrity during the assay, as well as a loading control). Total cell lysates and surface proteins eluted from streptavidin beads were analyzed. **B**, Quantification of cell surface biotinylation assay for cell lines shown in panel A. Data are shown as mean \pm SD (n = 4). Statistical analysis was based on a one-way ANOVA test ($n.s.$ > 0.05, * p \leq 0.05, *** p \leq 0.001). **C**, Representative western blot analysis of cell surface biotinylation experiments, conducted for stable CHO K1 cell lines overexpressing, beyond wild-type FGF2–GFP, the same mutant forms shown in panel A, in combination with mutations of the PI(4,5)P₂ binding pocket (K127Q/R128Q/K133Q). **D**, Quantification of cell surface biotinylation assay for cell lines shown in panel C. Data are shown as mean \pm SD (n = 4). Statistical analysis was based on a one-way ANOVA test (*** p \leq 0.001).

These included mutations of lysine residues in position 54 and 60, substituted with glutamates (Fig. 7, panel A), and the combinations of these with mutations in the PI(4,5)P₂ binding pocket (Fig. 7, panel C). In this set of experiments, single substitution of lysine 60 by glutamate caused a significant 25% reduction of secretion efficiency, whereas replacement of lysine 54 by glutamate did not cause any significant phenotype (Fig. 7, panel B). Nevertheless, combination of both substitutions significantly reduced secretion efficiency by 37%, showing a stronger phenotype compared to single substitution of lysine 60. Interestingly, combination of K54/60E and K127Q/R128Q/K133Q substitutions caused an impairment of FGF2 transport to the cell surface with less than 20% efficiency compared to the wild-type form of FGF2-GFP (Fig. 7, panel D). This phenotype did not differ significantly from the one observed for a mutant form of FGF2-GFP that lacks two cysteine residues (C77A/C95A) required for FGF2 oligomerization and the formation of membrane translocation intermediates, the so far most severely affected FGF2 secretion mutant known in the literature¹¹².

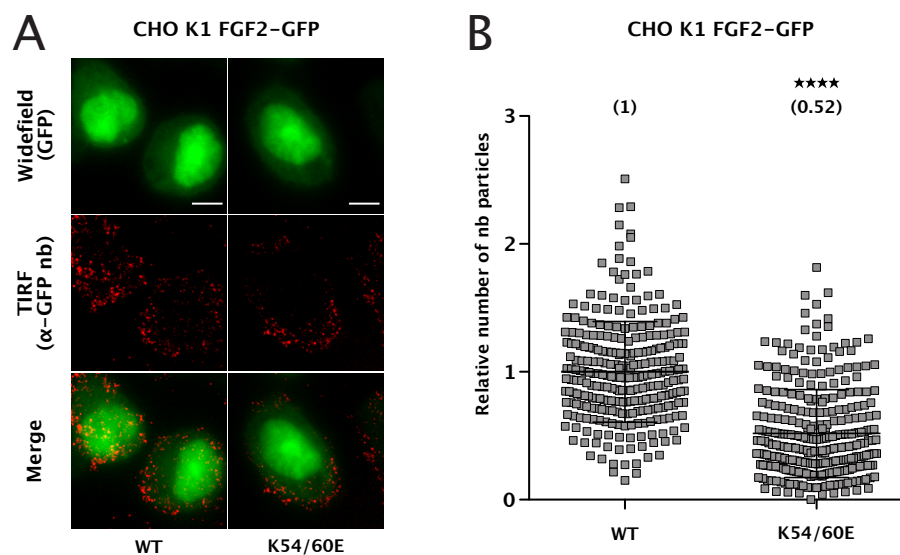


Fig. 8: FGF2-GFP translocation efficiency from cells is facilitated by the α 1-subunit of the Na,K-ATPase. **A**, Representative images of single molecule TIRF translocation assay conducted on stable CHO K1 expressing either wild-type (WT) or K54/60E FGF2-GFP, in a doxycycline-dependent manner. Images are shown as widefield, for the overall FGF2-GFP expression levels, TIRF, for translocated FGF2-GFP particles detected via membrane impermeable anti-GFP nanobodies labeled with Alexa-Fluor 647, and merge of the two channels (Scale bar = 6 μ m). **B**, Quantification of single molecule TIRF translocation assay for the cell lines shown in panel A, with the mock condition set to 1. Mean values are shown in brackets. Data are shown as mean \pm SD ($n = 4$). Statistical analysis was based on an unpaired, two-tailed t-test (**** $p \leq 0.0001$).

As a further validation of the secretion phenotype detected in biotinylation assay with these cell lines, I employed Total Internal Reflection Fluorescence (TIRF) microscopy, which allows to selectively excite fluorophores near the adherent cell surface, while minimizing

fluorescence from intracellular regions. To detect FGF2-GFP translocation efficiency, I conducted single molecule TIRF translocation assay²⁶². In particular, I focused on the K54/60E form of FGF2-GFP (Fig. 8). In this assay, the secretion efficiency of K54/60E was reduced by almost 50% compared to wild-type FGF2-GFP, similarly to the phenotype I observed in biotinylation assay (Fig. 7).

After showing an effect for the $\alpha 1$ subunit of the Na,K-ATPase on FGF2 secretion in living cells, the next thing to test was whether it had an effect on FGF2 recruitment to the plasma membrane as well. In order to answer this question, I employed single molecule TIRF recruitment assay, a previously established approach to quantify FGF2-GFP recruitment efficiency at the inner plasma membrane leaflet of living cells^{105,262}. With this assay, substitution of the lysine in position 54 with glutamate significantly reduced recruitment efficiency of FGF2-GFP by 20% when compared to wild-type cells, while single substitution of K60 did not significantly reduce FGF2-GFP recruitment efficiency, even though the average number of FGF2-GFP particles found at the inner leaflet was below compared to the average of wild-type cells (Fig. 9, panel A). Furthermore, I found that when the two lysine residues were simultaneously replaced by glutamates, FGF2-GFP recruitment efficiency was reduced by 30% (Fig. 9, panel A). This phenotype is even more striking after GFP background subtraction (Fig. 9, panel C), where the FGF2-GFP form with an impaired interaction with $\alpha 1$ showed a reduction of about 50% compared to wild-type cells. By contrast, mutations restricted to the PI(4,5)P₂ binding site in FGF2 alone did not affect FGF2-GFP recruitment at the inner plasma membrane leaflet (Fig. 9, panels B and C). In addition, the combination of K54/60E and K127Q/R128Q/K133Q substitutions caused a similar phenotype compared to the one observed for K54/60E alone (Fig. 9, panels B and C).

All together, these data suggest that the interaction of FGF2 with PI(4,5)P₂ is essential for its secretion, but it is not needed for an efficient recruitment at the inner plasma membrane leaflet. Instead, the interaction of FGF2 with the $\alpha 1$ subunit of the Na,K-ATPase is required for its efficient recruitment at the inner leaflet of the plasma membrane and, subsequently, for its secretion from cells. With this we can conclude that the physical contact of FGF2 with the $\alpha 1$ subunit of the Na,K-ATPase precedes the interaction of FGF2 with PI(4,5)P₂.

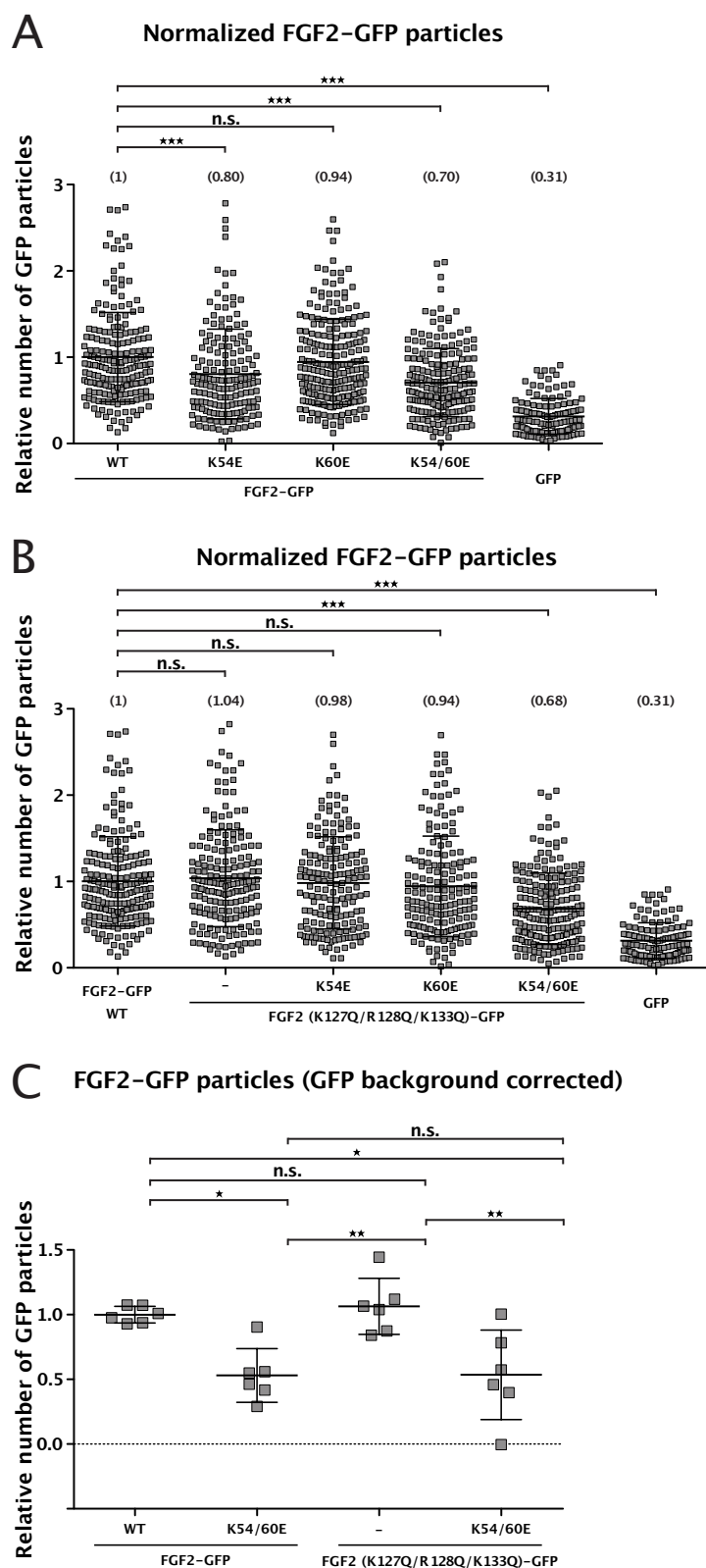


Fig. 9: The $\alpha 1$ -subunit of the Na,K-ATPase is the first physical contact of FGF2 at the inner plasma membrane leaflet, and its interaction with FGF2-GFP precedes the one with PI(4,5)P₂. **A**, Single molecule real time TIRF recruitment assay conducted on stable CHO K1 cell lines overexpressing various mutant forms of FGF2-GFP in a doxycycline-dependent manner. Beyond wild-type (WT) FGF2-GFP, the mutant forms were K54E, K60E, and K54/60E. A GFP-expressing cell line was also included in the assay, as negative control. Recruitment efficiency of FGF2-GFP WT was set to 1. Mean values for each cell line are shown in brackets. Data are shown as mean \pm SD ($n = 4$). Statistical analysis was based on a one-way ANOVA test ($n.s.p > 0.05$, $***p \leq 0.001$). **B**, Single molecule real time TIRF recruitment assay conducted on stable CHO K1 cell lines overexpressing various mutant forms of FGF2-GFP in a doxycycline-dependent manner. Beyond wild-type (WT) FGF2-GFP, the mutant forms of FGF2-GFP were K127Q/R128Q/K133Q, K54E/K127Q/R128Q/K133Q, K60E/K127Q/R128Q/K133Q, and K54/60E/K127Q/R128Q/K133Q. A GFP-expressing cell line was also included in the assay, as negative control. Recruitment efficiency of FGF2-GFP WT was set to 1. Mean values for each cell line are shown in brackets. Data are shown as mean \pm SD ($n = 4$). Statistical analysis was based on a one-way ANOVA test ($n.s.p > 0.05$, $***p \leq 0.001$). **C**, Mutant forms of FGF2-GFP carrying substitutions of K54 and K60, either on a wild-type or on a K127Q/R128Q/K133Q background, together with FGF2-GFP WT and K127Q/R128Q/K133Q, were compared after GFP background subtraction. GFP background corrected recruitment efficiency of FGF2-GFP WT was set to 1. Mean values for each cell line are shown in

brackets. Data are shown as mean \pm SD ($n = 6$). Statistical analysis was based on a one-way ANOVA test ($n.s.p > 0.05$, $*p \leq 0.05$, $**p \leq 0.01$).

4.1.1 Ouabain-dependent inhibition of the Na,K-ATPase have an impact on the unconventional secretion of FGF2

In previous experiments performed by other labs, ouabain, an inhibitor of the Na,K-ATPase, was found to interfere with FGF2 secretion from cells^{109,269}. More recently, in a work from our lab, employing Proximity Ligation Assay (PLA), ouabain treatment reduced proximity between FGF2 and the $\alpha 1$ subunit of the Na,K-ATPase in HeLa cells¹⁰⁵. In an attempt to study this process in more detail, I treated U2OS cell lines expressing FGF2-GFP with increasing concentrations of ouabain. In this case, I made use of a human cell line (U2OS) instead of CHO K1 cell line (Chinese hamster ovary), since it has been shown that rodents are resistant to ouabain²⁷⁰. Treating cells with ouabain for 6 hours resulted in a concentration-dependent reduction of FGF2-GFP translocation to cell surfaces (Fig. 10, panel A). Already at 25 μM ouabain, secretion efficiency significantly dropped to 78%. Increasing ouabain concentrations strengthen the phenotype to 61% secretion efficiency at 50 μM and to 38% secretion efficiency at 100 μM (Fig. 10, panel B).

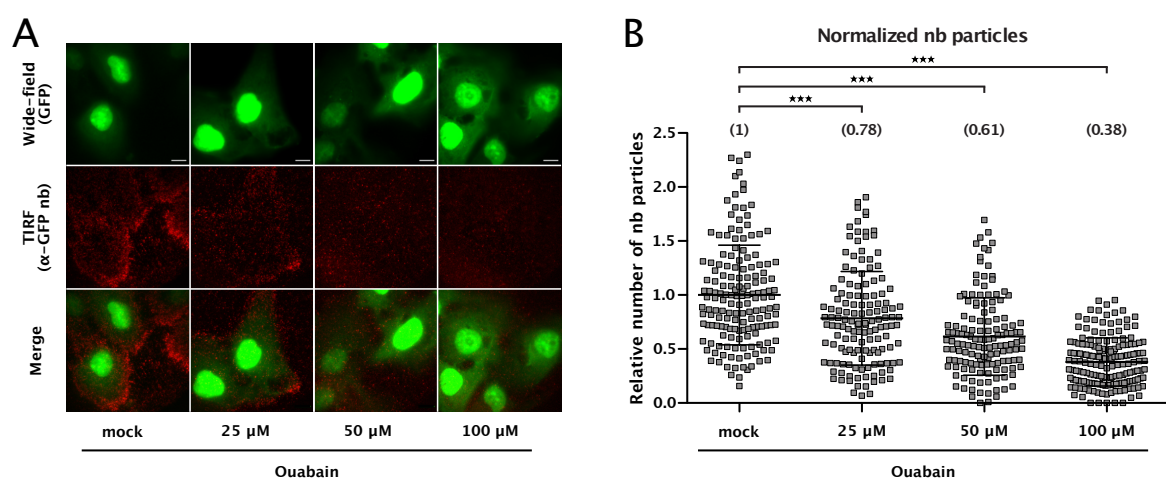


Fig. 10: Ouabain-dependent inhibition of the Na,K-ATPase impairs FGF2-GFP secretion from cells in a concentration-dependent manner. **A**, Representative images of TIRF translocation assay conducted on a stable U2OS cell line overexpressing FGF2-GFP in a doxycycline-dependent manner. Images are shown as widefield, for the overall FGF2-GFP expression levels, TIRF, for translocated FGF2-GFP particles detected via membrane impermeable anti-GFP nanobodies labeled with Alexa-Fluor 647, and merge of the two channels (Scale bar = 6 μm). They represent untreated cells (with DMSO added as mock, at the same concentration used for the ouabain treatment), as well as cells treated with increasing concentrations of ouabain: 25 μM , 50 μM , and 100 μM . Ouabain treatment was conducted for 6 h in culture conditions, after washing with 500 μM heparin, to remove previously translocated FGF2-GFP particles. **B**, Quantification of single molecule TIRF translocation assay for the conditions shown in panel A, with the mock condition set to 1. Mean values are shown in brackets. Data are shown as mean \pm SD ($n = 4$). Statistical analysis was based on a one-way ANOVA test (** $p \leq 0.001$).

Although for translocation efficiency I found a clear dose-dependent effect for ouabain, the same cannot be said about recruitment efficiency of FGF2-GFP at the inner plasma membrane leaflet. When I checked for the same concentrations of ouabain used in the previous assay, all of them reduced recruitment efficiency of FGF2-GFP, but not in a concentration-dependent manner, showing a similar phenotype between 64% and 83% recruitment efficiency, compared to the mock condition (Fig. 11, panel B). For this reason, checking lower ouabain concentrations would be something to try in the future.

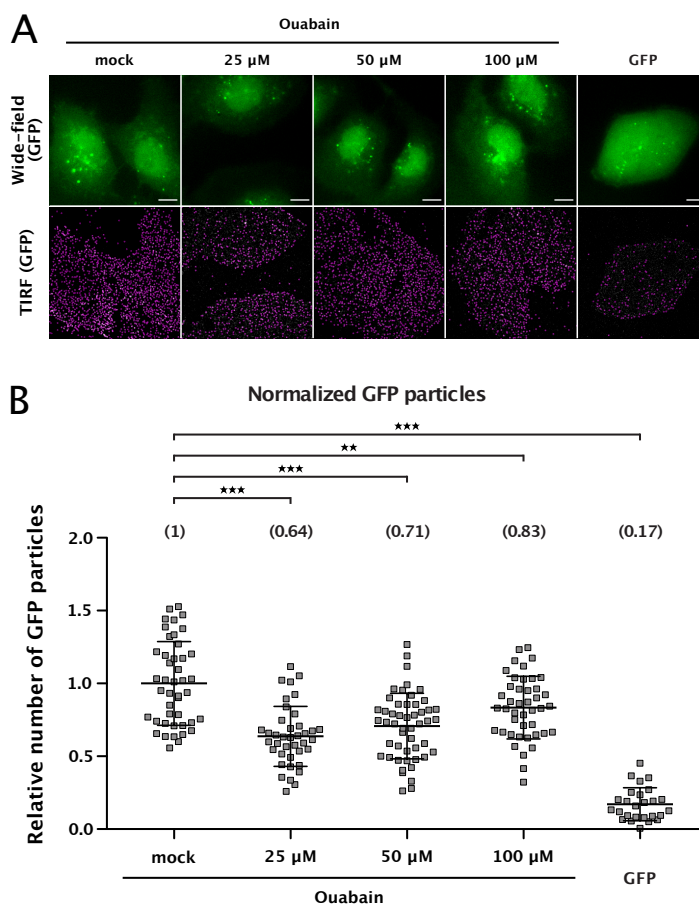


Fig. 11: Ouabain-dependent inhibition of the Na,K-ATPase impairs FGF2-GFP recruitment at the inner plasma membrane leaflet of cells. **A**, Representative images of real-time single molecule TIRF recruitment assay conducted on a stable U2OS cell line overexpressing FGF2-GFP in a doxycycline-dependent manner. Images are shown as widefield, for the overall FGF2-GFP expression levels, and TIRF, for FGF2-GFP particles recruited to the inner plasma membrane leaflet (Scale bar = 6 μ m). They represent untreated cells (with DMSO added as mock, at the same concentration used for the ouabain treatment), as well as cells treated with increasing concentrations of ouabain: 25 μ M, 50 μ M, and 100 μ M. Ouabain treatment was conducted for 6 h in culture conditions, after washing with 500 μ M heparin, to remove previously translocated FGF2-GFP particles. **B**, Quantification of real-time single molecule TIRF recruitment assay for the conditions shown in panel A, with the mock condition set to 1. Mean values are shown in brackets. Data are shown as mean \pm SD (n = 3). Statistical analysis was based on a one-way ANOVA test (**p \leq 0.01, ***p \leq 0.001).

4.2 The role of cysteine 77 and 95 on the unconventional secretory pathway of FGF2

Two cysteine residues on the surface of FGF2, cysteine 77 and cysteine 95, have been shown to be crucial for FGF2 oligomerization and for its subsequent secretion from cells¹¹². I then focused on the single contribution of the two residues in the process of FGF2 unconventional secretion. In a first set of experiments, I tested secretion efficiency of cell lines expressing alanine residues in substitution of cysteine residues, including single mutations (C77A and C95A) and double mutation (C77/95A). I first tested these cell lines employing cell surface biotinylation assay^{105,112,267}. The double cysteine mutant, C77/95A, has already been shown to have the strongest phenotype in this assay¹¹².

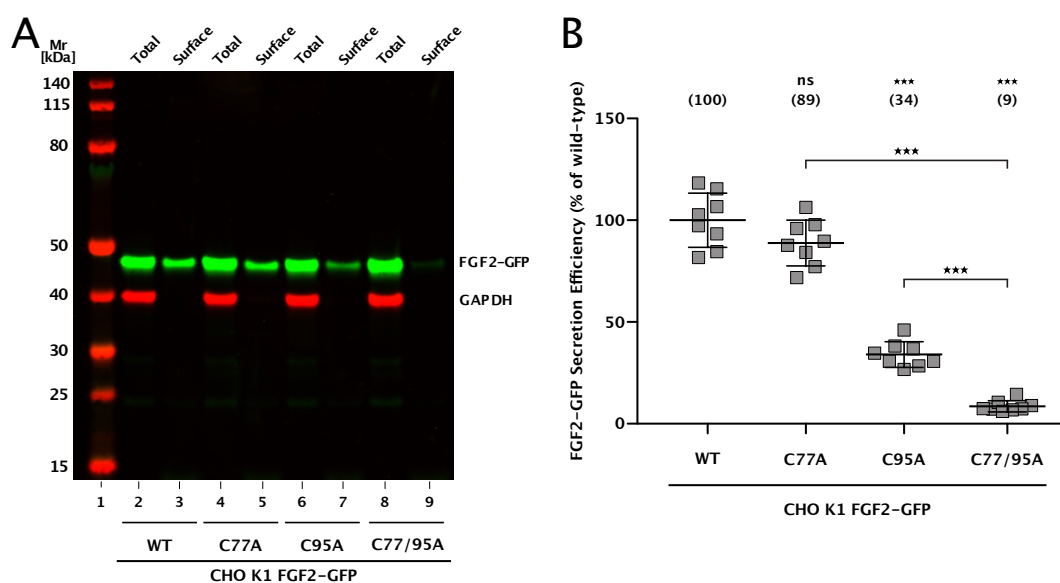


Fig. 12: Cysteine residues in position 77 and 95 of FGF2 play a role in its unconventional secretion from cells.

A, Representative western blot analysis of cell surface biotinylation experiments, conducted on stable CHO K1 cell lines overexpressing various mutant forms of FGF2-GFP in a doxycycline-dependent manner. Beyond wild-type FGF2-GFP, the mutant forms of FGF2-GFP were C77A, C95A, and C77/95A. Western blot analysis was conducted against GFP (to detect FGF2-GFP) and GAPDH (to check for cellular integrity during the assay, as well as a loading control). Total cell lysates and surface proteins eluted from streptavidin beads were analyzed. **B**, Quantification of cell surface biotinylation assay for cell lines shown in panel A, secretion efficiency of FGF2-GFP wild-type (WT) was set to 100%. Mean values for each cell line are shown in brackets. Data are shown as mean \pm SD ($n = 4$). Statistical analysis was based on a one-way ANOVA test ($nsp > 0.05$, $***p \leq 0.001$).

In this set of experiments, I reproduced this phenotype, detecting a 9% secretion phenotype, when compared to wild type cell line (Fig. 12). As for the single contribution of C77 and C95, the substitution of the first one to alanine reduced FGF2-GFP secretion efficiency by 11% compared to wild-type cells, even though not significantly (Fig. 12). Substitution of cysteine in position 95 to alanine significantly reduced FGF2-GFP secretion efficiency by 66% compared

to wild-type cells (Fig. 12). As already mentioned before, double substitution of both cysteine residues dropped secretion efficiency by 91%, not only significantly below wild-type cells, but also when compared to cells expressing either C77A or C95A forms of FGF2-GFP (Fig. 12).

I also tested secretion efficiency by means of single molecule TIRF translocation assay²⁶². With this assay, in our laboratory it has already been shown that the double cysteine mutant form of FGF2-GFP (C77/95A) did not reproduce the phenotype detectable with biotinylation assay (unpublished results). In this set of experiments, both single mutant forms of FGF2-GFP (C77A and C95A) and the double cysteine mutant (C77/95A) significantly reduced secretion efficiency of FGF2-GFP from cells when compared to the wild-type form (Fig. 13). As already mentioned, it was previously shown that the double cysteine mutant did not reproduce the phenotype observed in biotinylation assay; in this case, this mutant form of FGF2-GFP significantly dropped its secretion efficiency by 38% (Fig. 13, panel B), showing a much weaker phenotype compared to the one found in biotinylation assay (Fig. 12). Single substitution of cysteine 77 to alanine reduced secretion efficiency by 24% and the C95A mutant form of FGF2-GFP showed a secretion phenotype reduced by 61% compared to wild-type cells (Fig. 13, panel B).

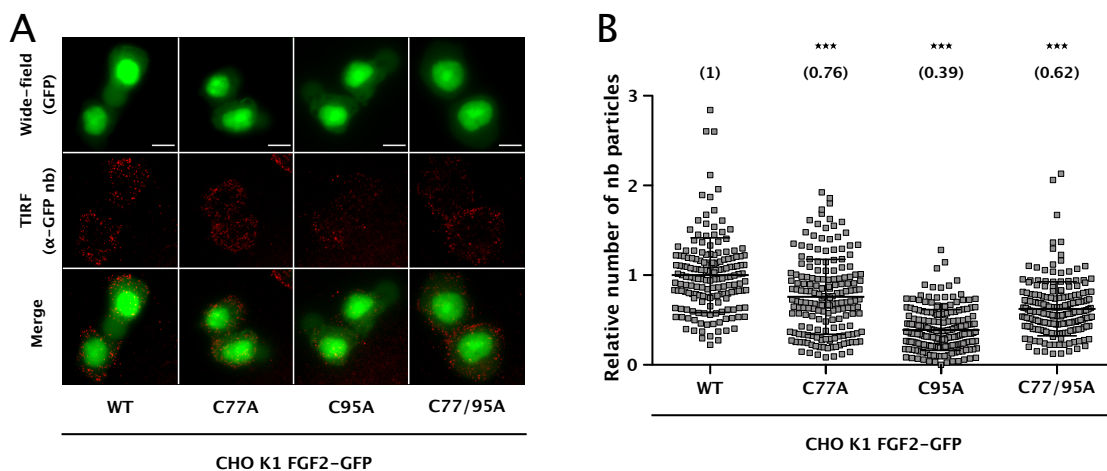


Fig. 13: FGF2-GFP translocation from cells is affected by cysteine residues in position 77 and 95 of FGF2. **A**, Representative images of TIRF translocation assay conducted on stable CHO K1 cell lines overexpressing various mutant forms of FGF2-GFP in a doxycycline-dependent manner. Beyond wild-type FGF2-GFP, the mutant forms of FGF2-GFP were C77A, C95A, and C77/95A. Images are shown as widefield, for the overall FGF2-GFP expression levels, TIRF, for translocated FGF2-GFP particles detected via membrane impermeable anti-GFP nanobodies labeled with Alexa-Fluor 647, and merge of the two channels (Scale Bar = 6 μ m). **B**, Quantification of single molecule TIRF translocation assay for the cell lines shown in panel A, with FGF2-GFP wild-type (WT) set to 1. Mean values are shown in brackets. Data are shown as mean \pm SD ($n = 4$). Statistical analysis was based on a one-way ANOVA test ($***p \leq 0.001$).

To study how substitutions of these cysteine residue have an impact on FGF2-GFP recruitment efficiency to the inner plasma membrane leaflet, I made use of real time single molecule TIRF microscopy^{105,262} (Fig. 14). Single substitution of cysteine 77 to alanine caused a significant reduction of 17% compared to the wild-type cell line (Fig. 14, panel B). When cysteine 95 was replaced by alanine, recruitment efficiency of FGF2-GFP to the inner leaflet dropped by 33% (Fig. 14, panel B). The same phenotype was observed for cells with the double cysteine mutant form (C77/95A) of FGF2-GFP (Fig. 14, panel B). In this assay, the background observed in the GFP cell line is always relatively high^{105,262}.

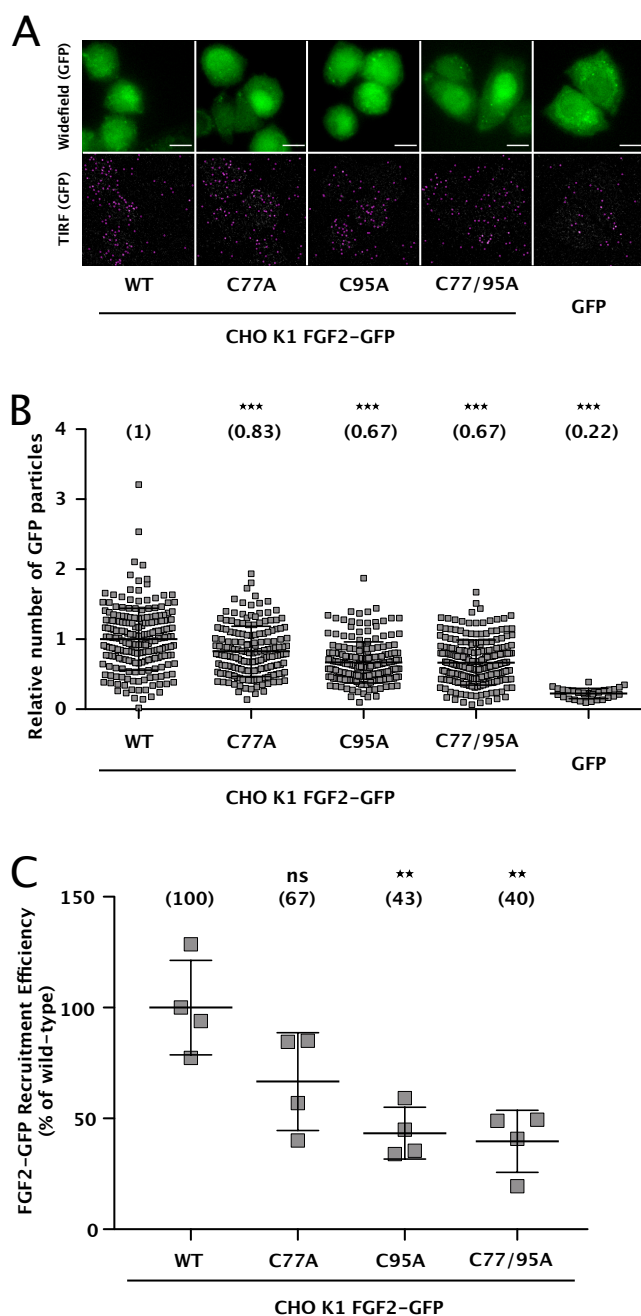


Fig. 14: FGF2-GFP recruitment from cells is affected by cysteine residues in position 77 and 95 of FGF2. **A**, Representative images of TIRF recruitment assay conducted on stable CHO K1 cell lines overexpressing various mutant forms of FGF2-GFP in a doxycycline-dependent manner. Beyond wild-type FGF2-GFP, the mutant forms of FGF2-GFP were C77A, C95A, and C77/95A. A GFP-expressing cell line was also included in the assay, as negative control. Images are shown as widefield, for the overall FGF2-GFP (or GFP) expression levels, and TIRF, for FGF2-GFP particles recruited to the inner plasma membrane leaflet. **B**, Quantification of real-time single molecule TIRF recruitment assay for the cell lines shown in panel A, with FGF2-GFP wild-type (WT) set to 1. Mean values are shown in brackets. Data are shown as mean \pm SD ($n = 4$). Statistical analysis was based on a one-way ANOVA test ($***p \leq 0.001$). **C**, All the four variant forms of FGF2-GFP shown in panel A and B (WT, C77A, C95A, C77/95A), were compared after GFP background subtraction. GFP background corrected recruitment efficiency of FGF2-GFP WT was set to 100. Mean values for each cell line are shown in brackets. Data are shown as mean \pm SD ($n = 4$). Statistical analysis was based on a one-way ANOVA test ($^{ns}p > 0.05$, $^{**}p \leq 0.01$).

For this reason, when comparing different cell lines like in this case, I remove this background from the different FGF2–GFP cells lines being investigated for their recruitment efficiency (for details, see methods). In this set of experiments, GFP background subtraction revealed a significant reduction by 60% for double cysteine mutant cells (C77/95A) compared to wild-type cells (Fig. 14, panel C). Single substitution of cysteine 95 caused a significant reduction of recruitment efficiency by 57 % and single substitution of cysteine 77 to alanine dropped recruitment efficiency by 33% (Fig. 14, panel C).

4.3 Glypican 1 is a rate limiting factor of FGF2 secretion from cells

Beyond *cys* elements of FGF2, I also focused on *trans* element appertaining to its secretion machinery. This project started a few years ago with a Bio ID screen performed by Eleni Dimou, Matthias Gerstner and Severina Klaus, in which the strongest hit for FGF2 was Glypican 1 (GPC1)²⁶⁷. Following this result, other PhD students from our laboratory focused on a detailed analysis of GPC1, and this was shown to be critical for FGF2 secretion²⁶⁷. My contribution to this project involved checking FGF2–GFP secretion efficiency via single molecule TIRF microscopy in the context of GPC1 overexpression at different FGF2–GFP expression levels. This was achieved changing the culture conditions of the cells, having them either with or without doxycycline. In the first case, FGF2–GFP is expressed at high levels, in the second one, only few amounts of protein are expressed, due to the leakiness of the doxycycline-dependent expression system. This last condition usually does not make it feasible to quantify secreted FGF2–GFP particles, but the combination of high resolution TIRF microscopy and increased secretion efficiency of cell lines overexpressing GPC1, allowed to study FGF2–GFP secretion efficiency even at low expression levels. Under conditions of high expression levels, FGF2–GFP secretion efficiency raised by about 50% in CHO K1 cells overexpressing GPC1 compared to wild-type CHO K1 cells (Fig. 15, panel B). The experiments performed at low FGF2–GFP expression levels (Fig. 15, panel D) showed an increase of its secretion efficiency four times higher compared to wild-type cells not overexpressing GPC1. Since these cells are pools, they showed a big variety in terms of FGF2–GFP secretion efficiency. This was probably due to the different amount of GPC1 being expressed in different cells. Intriguingly, single cells showed more than 30-fold increase of FGF2–GFP particles on their surface compared to the average of wild-type cells (Fig. 15, panel D).

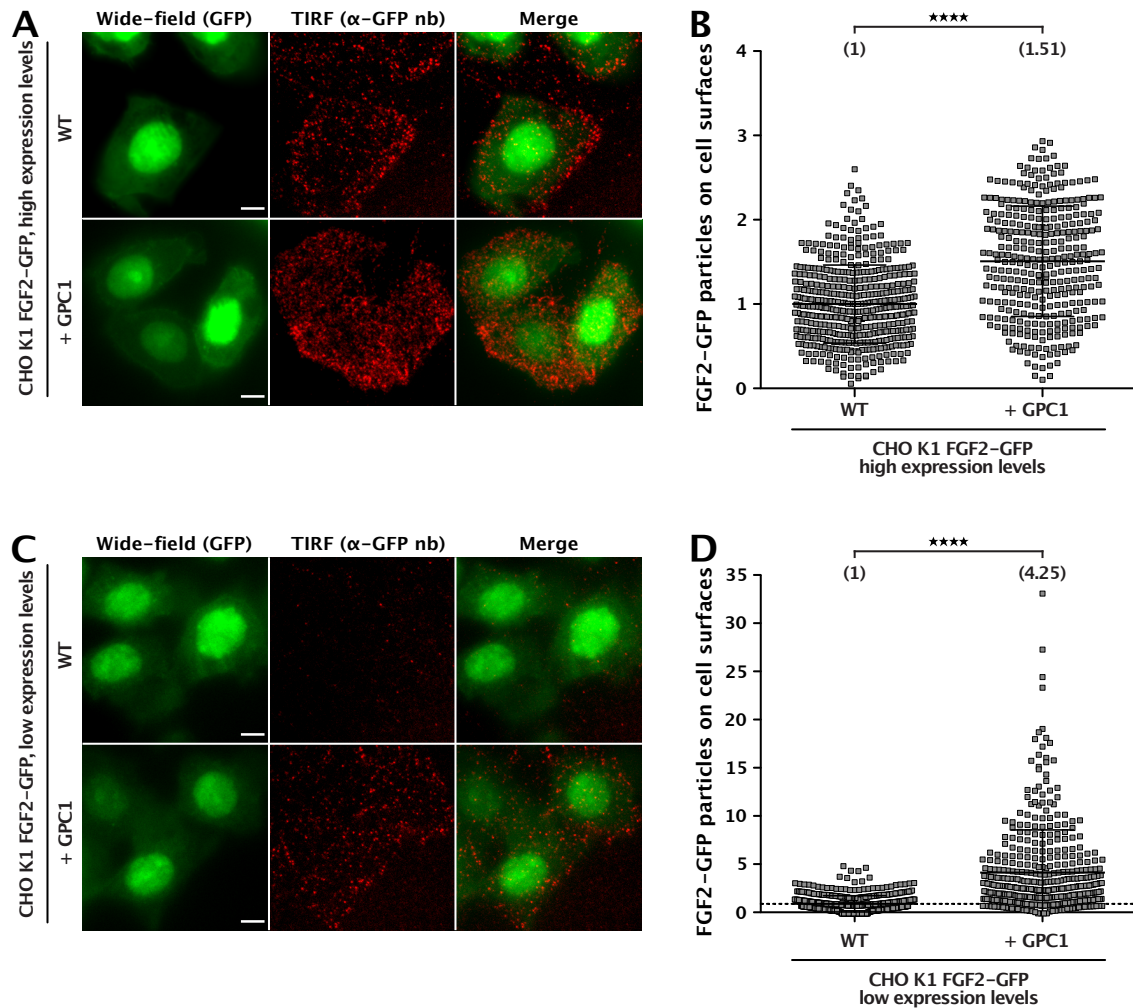


Fig. 15: Glypican-1 (GPC1) is the rate limiting factor for the unconventional secretion of FGF2. **A**, Representative images of single molecule TIRF translocation assay conducted on stable CHO K1 overexpressing either only FGF2-GFP in a doxycycline-dependent manner, or, in addition to FGF2-GFP, GPC1. These experiments were conducted in the presence of doxycycline and, therefore, at high FGF2-GFP expression levels. Images are shown as widefield, for the overall FGF2-GFP expression levels, TIRF, for translocated FGF2-GFP particles detected via membrane impermeable anti-GFP nanobodies labeled with Alexa-Fluor 647, and merge of the two channels. **B**, Quantification of single molecule TIRF translocation assay for the conditions shown in panel **A**. Data are shown as mean \pm SD ($n = 4$). Statistical analysis was based on an unpaired, two-tailed t-test (**** $p \leq 0.0001$). **C**, Representative images of single molecule TIRF translocation assay conducted on same cell lines shown in panel **A**, but in the absence of doxycycline and, therefore, at low FGF2-GFP expression levels. **D**, Quantification of single molecule TIRF translocation assay for the conditions shown in panel **C**. Data are shown as mean \pm SD ($n = 4$). Statistical analysis was based on an unpaired, two-tailed t-test (**** $p \leq 0.0001$).

To challenge this hypothesis, together with Annalena Meyer, another Ph.D. student from our lab, I sorted GPC1 overexpressing cells for different levels of GPC1. More precisely, we used HA-tagged GPC1 to allow for antibody staining. After this sorting procedure, we focused on characterizing these 9 single clones for HA-GPC1 expression levels using two independent techniques. The quantification of HA-GPC1 levels was mainly performed by Annalena Meyer,

while I focused on quantifying FGF2–GFP secretion efficiency in these different clones using TIRF microscopy. In brief, quantification of HA–GPC1 levels was achieved with two independent assays: western blotting and FACS analysis. In order to detect HA–GPC1 via western blot, she digested it with heparinase III, which removes the heparan sulfate chains and frees the attaching site, which is recognized by the 3G10 antibody. As an independent technique, she stained cells with anti–HA antibody and then looked at their respective fluorescence via FACS. As reported in Fig. 16 (panel B and C), both assays showed similar results for these clones in terms of HA–GPC1 expression levels, with three clones (B9, H4' and H11) expressing higher amounts compared to the average of all the analyzed clones. Regarding FGF2–GFP secretion efficiency, I incubated cells without doxycycline to check for secretion efficiency at low FGF2–GFP expression levels.

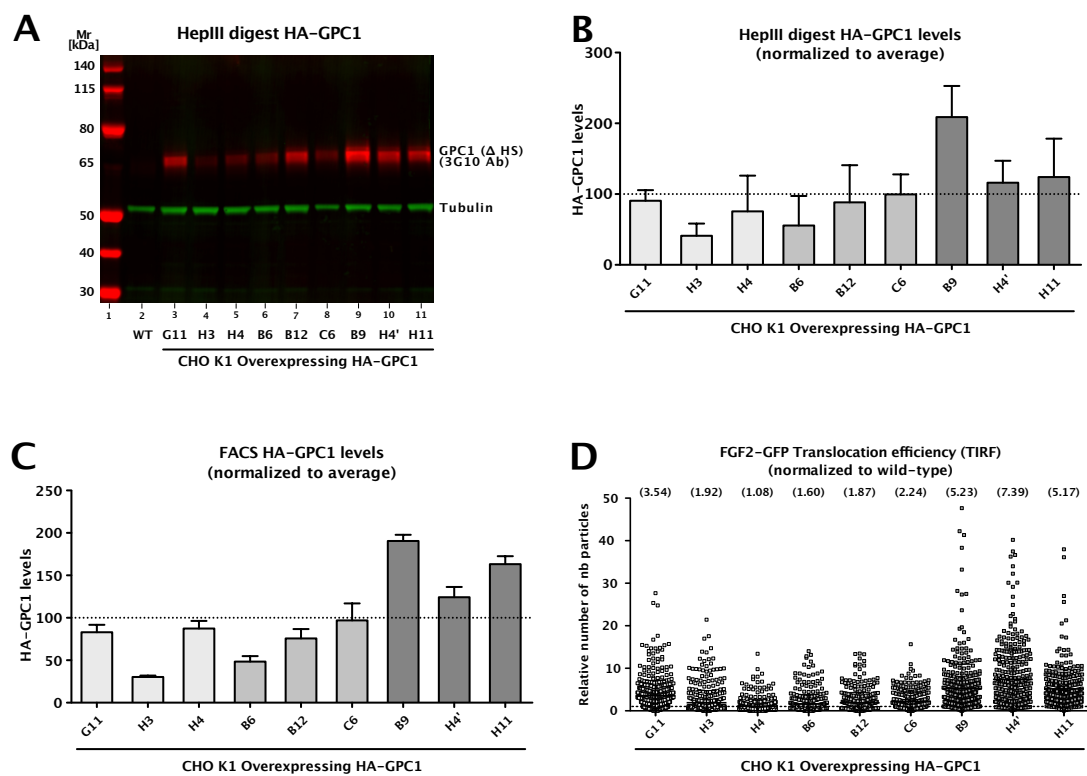


Fig. 16: FGF2–GFP translocation efficiency correlates with HA–GPC1 expression levels. **A**, Representative western blot analysis following Heparinase III digest on CHO K1 cells overexpressing FGF2–GFP in a doxycycline–dependent manner, and constitutively overexpressing HA–GPC1. These cells are single clones. Heparinase III digest have been performed to remove heparan sulfate chains from HSPGs and make use of the 3G10 antibody, which recognized HS chains attachment sites on the core protein. Tubulin was used as a loading control. **B**, Quantification of the western blot analysis shown in panel **A**. Data are shown as mean \pm SD ($n = 4$). Values have been normalized to the average of all single clones, which was set to 100%. **C**, FACS analysis performed to quantify the expression levels of HA–GPC1 for the single clones shown in panels **A** and **B**. FACS has been performed using a primary antibody directed against the HA–tag, and a fluorescently labeled secondary antibody. Data are shown as mean \pm SD ($n = 4$). Values have been normalized to the average of all single clones, which was set to 100%. **D**, Single molecule TIRF translocation assay, conducted on the single clones shown in panels **A**, **B**, and **C**. Data are shown as mean \pm SD ($n = 4$). Values have been normalized to the wild–type (not shown), which was set to 1.

After performing TIRF translocation assay on all clones, I quantified secretion efficiency and normalized it to wild-type cells not overexpressing GPC1. While most of the clones did not show high differences between each other, the three clones having higher amounts of HA-GPC1 (B9, H4' and H11) clearly had an increase FGF2-GFP secretion efficiency, with an average of FGF2-GFP particles on cell surfaces more than 5 times higher compared to the average of particles on the surface of wild-type cells (Fig. 16, panel D). B9 and H11 single clones showed an average of 5.23 and 5.17 times higher compared to the average FGF2-GFP particles found on wild-type cells surfaces, respectively; H4' cells increased their secretion efficiency 7.39 times more compared to wild-type cells.

4.4 The importance of plasma membrane lipid composition on the unconventional secretion of FGF2

4.4.1 The role of cholesterol in the unconventional secretory pathway of FGF2

In earlier investigations from our group, FGF2 has been shown to interact with PI(4,5)P₂ in a more efficient way when the interaction was taking place in a plasma membrane like lipid environment¹¹¹. In particular, cholesterol and sphingomyelin (SM) were shown to have a pivotal role in the FGF2-PI(4,5)P₂ interaction. The aim of this project was to investigate this effect in living cells employing single molecule TIRF microscopy. In particular, I conducted these experiments in two different cell lines, CHO K1 and U2OS, both expressing FGF2-GFP under doxycycline control. To increase cellular cholesterol levels, I prepared cholesterol:Methyl- β -Cyclodextrin complexes in imaging solution and used them to treat cells for 1 hour at 37°C²⁰⁰. I monitored cholesterol levels in treated and untreated cells with two independent methods: Filipin staining and lipid mass spectrometry. Filipin is used to stain cholesterol in cellular membranes^{201,271}. Based on confocal microscopy, I quantified the mean intensity of the two conditions, and then normalized to the untreated condition, set to 1. CHO K1 cells showed a significant increase of cholesterol levels of 56%, when treated with cholesterol:M β CD complexes (Fig. 17, panel B). Similarly, U2OS cells significantly increased their cholesterol levels, based on filipin staining, by 48% (Fig. 17, panel D).

To further validate this method, I prepared membrane fractions of CHO K1 cells, in order to analyze their cholesterol levels via lipid mass spectrometry. I enriched membrane fractions using the Minute™ Plasma Membrane Protein Isolation and Cell Fractionation Kit (Invent Biotechnologies). In parallel to lipid mass spec, I performed western blot analysis on 2% of the input (whole cell lysate) and 50% of the membrane fraction. Western blot analysis allowed to check for plasma membrane enrichment and contamination of the membrane fractions.

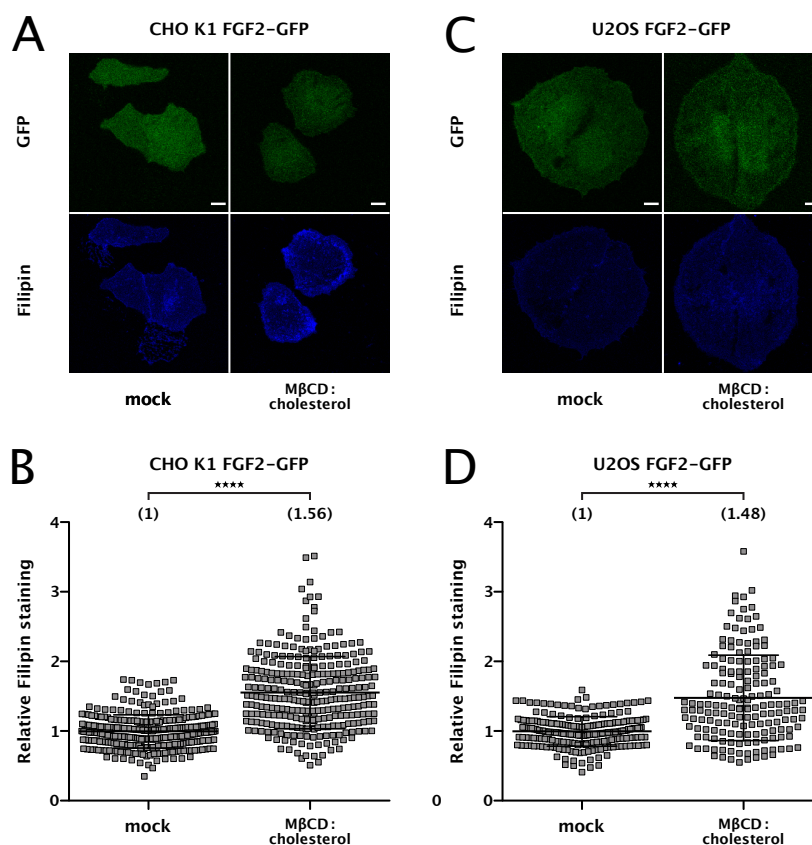


Fig. 17: Treating cells with cholesterol:Methyl- β -Cyclodextrin complexes enhances their cholesterol levels, based on Filipin staining. **A**, Representative confocal images following Filipin staining on stable CHO K1 cells overexpressing FGF2-GFP in a doxycycline-dependent manner. Images represent untreated cells, as well as cells treated with Cholesterol:Methyl- β -Cyclodextrin (1:10 molar ratio) complexes for 1 h in culture conditions. Filipin staining was performed on cells to visualize cholesterol. For each condition, GFP (to visualize FGF2-GFP) and filipin (to detect cholesterol) fluorescence are shown (Scale bar = 6 μ m). **B**, Quantification of the conditions shown in panel **A**. Confocal images were analyzed using ImageJ to quantify cholesterol levels based on Filipin staining. The mean intensity values of the detected filipin signals for each condition are shown in brackets, with the mock condition set to 1. Data are shown as mean \pm SD ($n = 4$). The statistical analysis was based on an unpaired, two-tailed t-test ($****p \leq 0.0001$). **C**, Representative confocal images following Filipin staining on stable U2OS cells overexpressing FGF2-GFP in a doxycycline-dependent manner. Images represent untreated cells, as well as cells treated with Cholesterol:Methyl- β -Cyclodextrin (1:10 molar ratio) complexes for 1 h in culture conditions. Filipin staining was performed on cells to visualize cholesterol. For each condition, GFP (to visualize FGF2-GFP) and filipin (to detect cholesterol) fluorescence are shown (Scale bar = 6 μ m). **D**, Quantification of the conditions shown in panel **C**. Confocal images were analyzed using ImageJ to quantify cholesterol levels based on Filipin staining. The mean intensity values of the detected filipin signals for each condition are shown in brackets, with the mock condition set to 1. Data are shown as mean \pm SD ($n = 4$). The statistical analysis was based on an unpaired, two-tailed t-test ($****p \leq 0.0001$).

I stained the membrane for a plasma membrane marker, the $\alpha 1$ subunit of the Na,K-ATPase (α -1), and an endoplasmic reticulum marker, calnexin (CNX). As depicted in Fig. 18, panel A, the membrane marker was enriched in the membrane fraction (PM), whereas CNX, even though still present in the membrane fraction, was present at very low levels compared to the input, especially considering the different percentage used for the two fractions (2% input and 50% membrane). With this western blot analysis, I validated the enrichment of the membrane

fraction for the analyzed samples. Lipid mass spec was performed at the lipidomic facility of BZH, in Britta Brügger's lab. This was performed for both plasma membrane fraction and input, to further validate the enrichment of the membrane fractions (based on cholesterol enrichment for the membrane fraction compared to the input, since cholesterol is enriched at plasma membranes). Lipid mass spec showed a significant 9 mol% increase of cholesterol levels in treated CHO K1 cells compared to the untreated condition (Fig. 18, panel B). For this analysis, I compared PM fractions and set the untreated condition to 1 for normalization. The PM fractions taken into account for this analysis were only the ones that showed an enrichment in both mass spec (cholesterol enrichment from input to PM) and western blotting (enrichment of PM marker and lower amounts of ER marker in PM fraction).

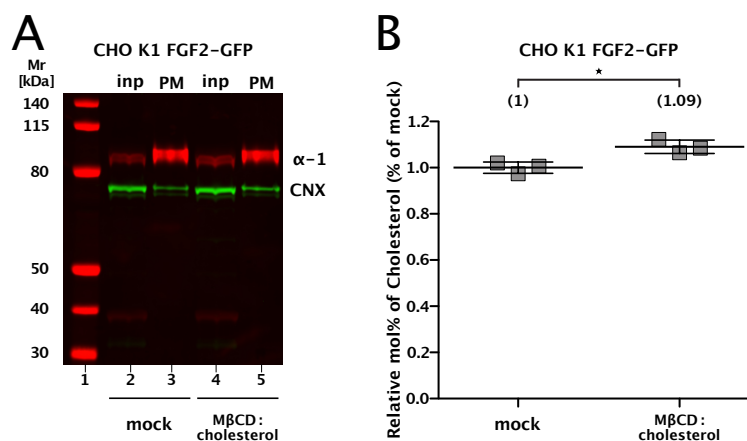


Fig. 18: Treating cells with cholesterol:Methyl-β-Cyclodextrin complexes enhances their cholesterol levels, based on lipid mass spectrometry. **A**, Representative western blot for membrane fractions validation. Input and membrane fractions of both untreated and cells treated with Cholesterol:Methyl-β-Cyclodextrin (1:10 molar ratio) complexes for 1 h in culture conditions, were blotted against a plasma membrane marker (the α-1 subunit of the Na,K-ATPase) to check for plasma membrane enrichment, and an ER marker (calnexin) to check for ER contamination of the plasma membrane fractions. **B**, Quantification of lipid mass spectrometry on CHO K1 samples for the conditions shown in panel A. The values represented on the graph are based on plasma membrane fractions, where ratios of cholesterol to PC were determined for both conditions, with the mock condition set to 1. Data are shown as mean ± SD (n = 3). The statistical analysis was based on an unpaired, two-tailed t- test (*p ≤ 0.05).

Thus, both analyses showed an increased level of cholesterol upon treatment with cholesterol:Methyl-β-Cyclodextrin complexes. Based on this procedure to enrich cholesterol, I quantified FGF2-GFP recruitment at the inner plasma membrane leaflet (Fig. 19), as well as FGF2-GFP secretion to cell surfaces (Fig. 20) via single molecule TIRF microscopy^{105,262}, in both CHO K1 and U2OS cell lines overexpressing FGF2-GFP in a doxycycline-dependent manner.

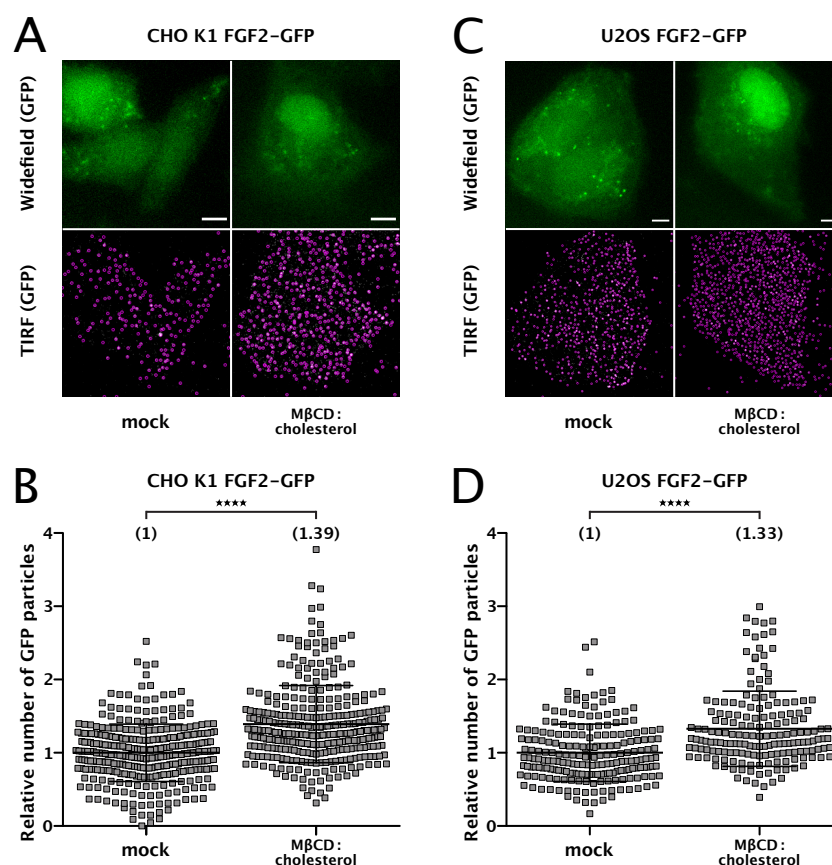


Fig. 19: Cellular cholesterol enrichment increases FGF2-GFP recruitment efficiency at the inner plasma membrane leaflet in living cells. **A**, Representative images of real-time single molecule TIRF recruitment assay conducted on a stable CHO K1 cell line overexpressing FGF2-GFP in a doxycycline-dependent manner. Images are shown as widefield, for the overall FGF2-GFP expression levels, and TIRF, for FGF2-GFP particles recruited to the inner plasma membrane leaflet (Scale bar = 6 μ m). They represent untreated cells, as well as cells treated with Cholesterol:Methyl- β -Cyclodextrin (1:10 molar ratio) complexes for 1 h in culture conditions. **B**, Quantification of real-time single molecule TIRF recruitment assay for the conditions shown in panel A, with the mock condition set to 1. Mean values are shown in brackets. Data are shown as mean \pm SD ($n = 4$). Statistical analysis was based on an unpaired, two-tailed t -test (**** $p \leq 0.0001$). **C**, Representative images of TIRF recruitment assay conducted on a stable U2OS cell line overexpressing FGF2-GFP in a doxycycline-dependent manner. Images are shown as widefield, for the overall FGF2-GFP expression levels, and TIRF, for FGF2-GFP particles recruited to the inner plasma membrane leaflet. They represent untreated cells, as well as cells treated with Cholesterol:Methyl- β -Cyclodextrin (1:10 molar ratio) complexes for 1 h in culture conditions. **D**, Quantification of real-time single molecule TIRF recruitment assay for the conditions shown in panel C, with the mock condition set to 1. Mean values are shown in brackets. Data are shown as mean \pm SD ($n = 4$). Statistical analysis was based on an unpaired, two-tailed t -test (**** $p \leq 0.0001$).

Regarding the analysis of recruitment efficiency, I took both widefield and TIRF images (Fig. 19, panel A). Widefield images allowed me to analyze total FGF2-GFP expression levels, while I used TIRF images to quantify individual FGF2-GFP particles per surface area in the vicinity of the plasma membrane. In both cell lines, FGF2-GFP recruitment efficiency was significantly enhanced following cholesterol enrichment. In particular, CHO K1 showed a 39% increase (Fig. 19, panel B) and U2OS a 33% increase (Fig. 19, panel D) compared to the untreated condition.

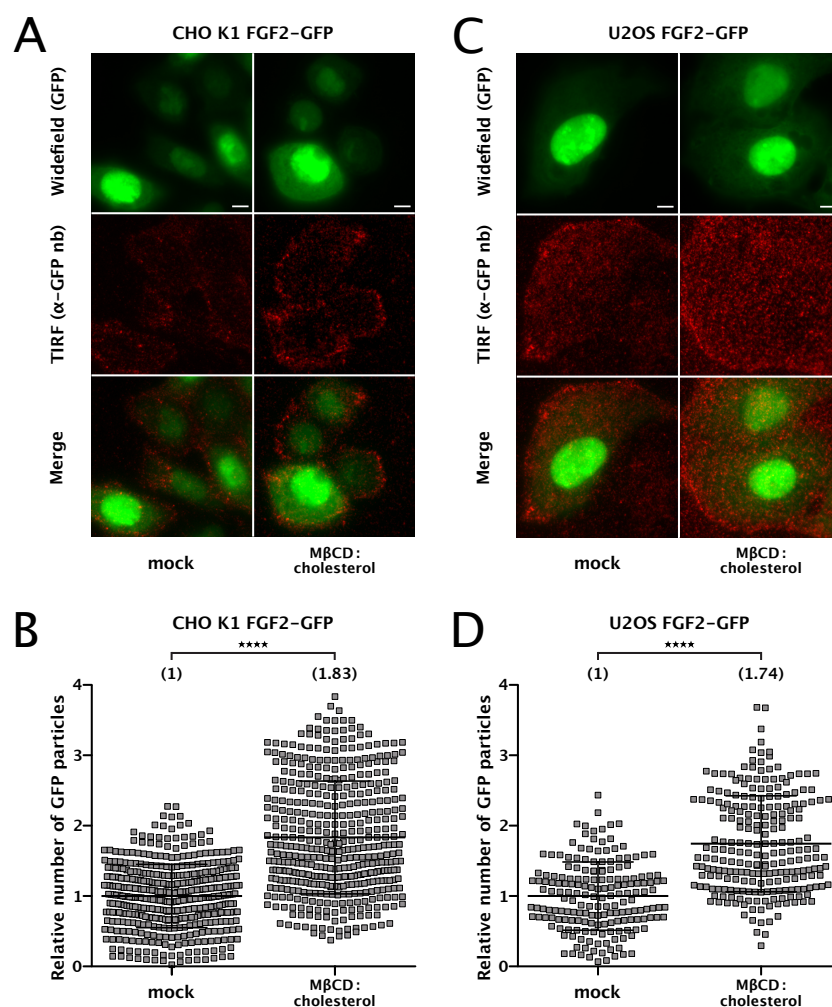


Fig. 20: Cellular cholesterol enrichment increases FGF2-GFP translocation from cells. A, Representative images of single molecule TIRF translocation assay conducted on a stable CHO K1 cell line overexpressing FGF2-GFP in a doxycycline-dependent manner. Images are shown as widefield, for the overall FGF2-GFP expression levels, TIRF, for translocated FGF2-GFP particles detected via membrane impermeable anti-GFP nanobodies labeled with Alexa-Fluor 647, and merge of the two channels (Scale bar = 6 μ m). They represent untreated cells, as well as cells treated with Cholesterol:Methyl- β -Cyclodextrin (1:10 molar ratio) complexes for 1 h in culture conditions. B, Quantification of single molecule TIRF translocation assay for the conditions shown in panel A, with the mock condition set to 1. Mean values are shown in brackets. Data are shown as mean \pm SD ($n = 4$). Statistical analysis was based on an unpaired, two-tailed t-test (**** $p \leq 0.0001$). C, Representative images of single molecule TIRF translocation assay conducted on a stable U2OS cell line overexpressing FGF2-GFP in a doxycycline-dependent manner. Images are shown as widefield, for the overall FGF2-GFP expression levels, TIRF, for translocated FGF2-GFP particles detected via membrane impermeable anti-GFP nanobodies labeled with Alexa-Fluor 647, and merge of the two channels. They represent untreated cells, as well as cells treated with Cholesterol:Methyl- β -Cyclodextrin (1:10 molar ratio) complexes for 1 h in culture conditions. D, Quantification of single molecule TIRF translocation assay for the conditions shown in panel C, with the mock condition set to 1. Mean values are shown in brackets. Data are shown as mean \pm SD ($n = 4$). Statistical analysis was based on an unpaired, two-tailed t-test (**** $p \leq 0.0001$).

In order to quantify translocation efficiency under conditions of increased cellular cholesterol levels, I once again employed single molecule TIRF translocation assay²⁶². I analyzed TIRF images to quantify the amount of nanobody particles on each cell surface, which I then normalized to cell surface area (μm^2). FGF2-GFP translocation efficiency across the plasma membrane significantly increased by 83% in CHO K1 (Fig. 20, panel B) cells and by 74% in U2OS cells (Fig. 20, panel D).

Since the idea behind this project was that cholesterol is a quite specific modulator of FGF2 unconventional secretion from cells, or more in general of type I UPS (also Tau secretion has been shown to be dependent on cholesterol⁶⁵), I also tested a conventionally secreted cargo for its translocation efficiency from cells upon cholesterol levels enrichment, to further challenge this hypothesis. The cargo I used is CD4-GFP, a transmembrane protein that reaches its localization following the classing ER-Golgi secretory pathway. Following cholesterol enrichment, I performed single molecule TIRF translocation assay²⁶² to evaluate whether there were differences in its translocation efficiency from CHO cells (Fig. 21).

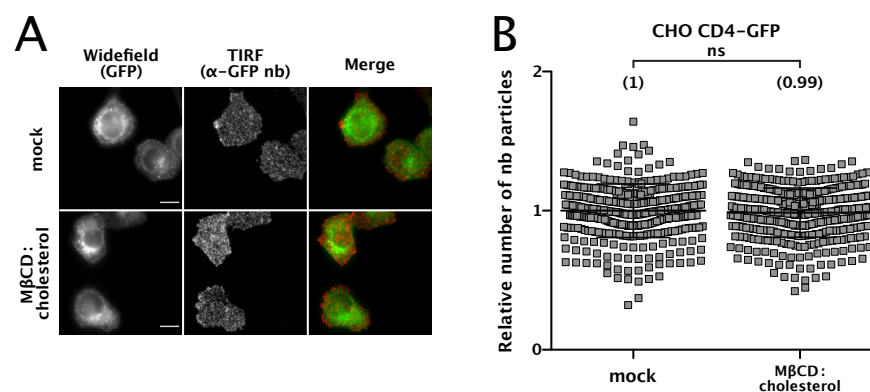


Fig. 21: Cellular cholesterol enrichment does not have an impact on CD4-GFP conventional secretion from cells. **A**, Representative images of TIRF translocation assay conducted on CHO K1 cells stably expressing CD4-GFP in a doxycycline-dependent manner, either untreated or treated with Cholesterol:Methyl- β -Cyclodextrin (1:10 molar ratio) complexes for 1 h in culture conditions. Images are shown as widefield, for the overall CD4-GFP expression levels, TIRF, for translocated CD4-GFP particles detected via membrane impermeable anti-GFP nanobodies labeled with Alexa-Fluor 647, and merge of the two channels (Scale bar = 6 μm). **B**, Quantification of single molecule TIRF translocation assay for the conditions shown in panel **A**, with the mock condition set to 1. Mean values are shown in brackets. Data are shown as mean \pm SD ($n = 4$). Statistical analysis was based on an unpaired, two-tailed t-test ($nsp > 0.05$).

After quantification and statistical analysis of 4 independent experiments, no significant differences could be observed between cholesterol enriched and untreated cells (Fig. 21, panel B). This suggested that cholesterol does not modulate the classical ER-Golgi pathway for protein secretion from cells.

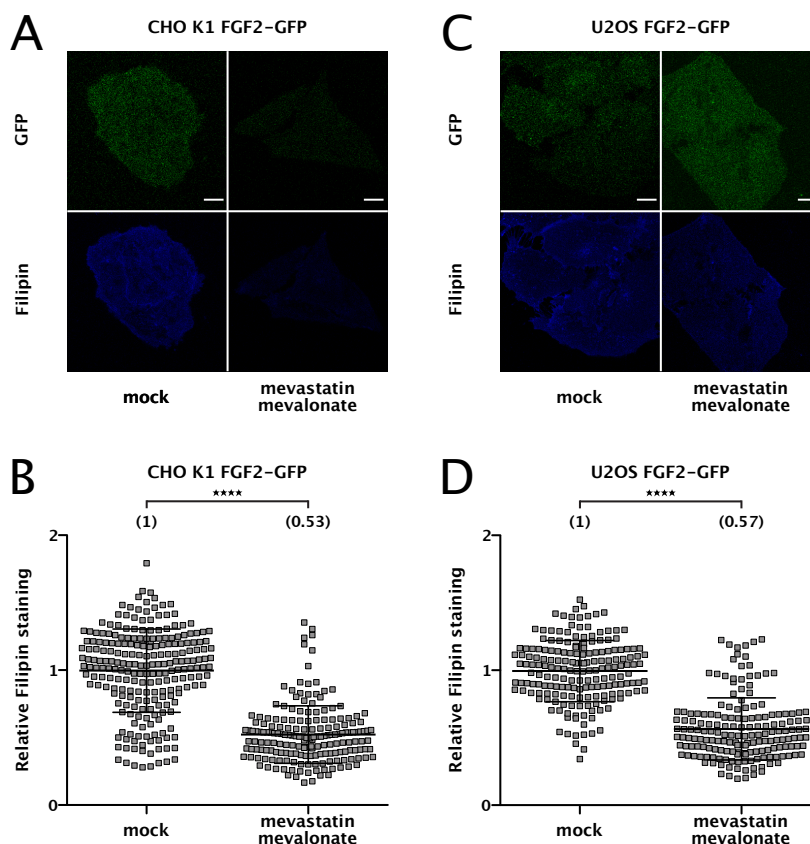


Fig. 22: Treating cells with mevastatin decreases their cholesterol levels, based on Filipin staining. **A**, Representative confocal images following Filipin staining on stable CHO K1 cells overexpressing FGF2-GFP in a doxycycline-dependent manner. Images represent untreated cells, as well as cells treated with 5 μ M mevastatin and 50 μ M mevalonate in the presence of de-lipidized serum, for 24 h in culture conditions. Filipin staining was performed on cells to visualize cholesterol. For each condition, GFP (to visualize FGF2-GFP) and filipin (to detect cholesterol) fluorescence are shown (Scale bar = 6 μ m). **B**, Quantification of the conditions shown in panel A. Confocal images were analyzed using ImageJ to quantify cholesterol levels based on Filipin staining. The mean intensity values of the detected filipin signals for each condition are shown in brackets, with the mock condition set to 1. Data are shown as mean \pm SD ($n = 4$). The statistical analysis was based on an unpaired, two-tailed t-test ($****p \leq 0.0001$). **C**, Representative confocal images following Filipin staining on stable U2OS cells overexpressing FGF2-GFP in a doxycycline-dependent manner. Images represent untreated cells, as well as cells treated with 5 μ M mevastatin and 50 μ M mevalonate in the presence of de-lipidized serum, for 24 h in culture conditions. Filipin staining was performed on cells to visualize cholesterol. For each condition, GFP (to visualize FGF2-GFP) and filipin (to detect cholesterol) fluorescence are shown (Scale bar = 6 μ m). **D**, Quantification of the conditions shown in panel C. Confocal images were analyzed using ImageJ to quantify cholesterol levels based on Filipin staining. The mean intensity values of the detected filipin signals for each condition are shown in brackets, with the mock condition set to 1. Data are shown as mean \pm SD ($n = 4$). The statistical analysis was based on an unpaired, two-tailed t-test ($****p \leq 0.0001$).

After demonstrating an effect for increased cholesterol levels on FGF2-GFP recruitment at the inner plasma membrane leaflet (Fig. 19) and translocation from cells (Fig. 20), I also studied the effect of cholesterol depletion from cellular plasma membranes. To achieve this, I treated

cells with mevastatin, combined with mevalonate, in the presence of Delipidated serum for 24 hours in culture conditions²⁷² (see materials and methods for details). Also in this case, I conducted these experiments in both CHO K1 and U2OS cells. The validation of this treatment for cholesterol removal was once again performed via Filipin staining and lipid mass spectrometry. I conducted confocal microscopy imaging after Filipin staining and quantified the mean intensity values for both mevastatin treated and untreated conditions in the two cell lines (Fig. 22). Cholesterol levels significantly decreased after mevastatin treatment by 47% in CHO K1 (Fig. 22, panel B) and 43% in U2OS (Fig. 22, panel D).

Lipid mass spectrometry was again performed by the BZH lipidomic facility, in Britta Brügger's lab. I provided them with input and membrane fractions samples of CHO K1 for mevastatin treated and untreated conditions. I also performed in parallel western blot analysis to further validate for membrane enrichment, as explained for the previous analysis. Quantification of mass spec results showed a significant 14 mol% reduction in cholesterol levels in CHO K1 cells treated with mevastatin compared to untreated cells (Fig. 23).

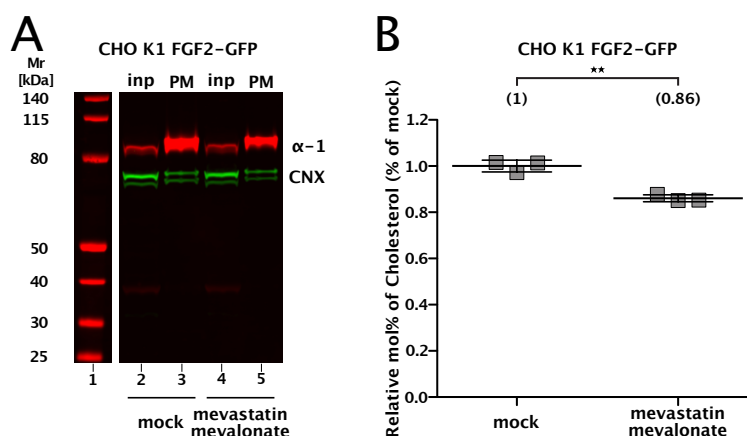


Fig. 23: Treating cells with mevastatin decreases their cholesterol levels, based on lipid mass spectrometry. A, Representative western blot for membrane fractions validation. Input and membrane fractions of both untreated and cells treated with 5 μ M mevastatin and 50 μ M mevalonate in the presence of de-lipidized serum, for 24 h in culture conditions, were blotted against a plasma membrane marker (the α -1 subunit of the Na,K-ATPase) to check for plasma membrane enrichment, and an ER marker (calnexin) to check for ER contamination of the plasma membrane fractions. B, Quantification of lipid mass spectrometry on CHO K1 samples for the conditions shown in panel A. The values represented on the graph are based on plasma membrane fractions, where ratios of cholesterol to PC were determined for both conditions, with the mock condition set to 1. Data are shown as mean \pm SD ($n = 3$). The statistical analysis was based on an unpaired, two-tailed t- test (** $p \leq 0.01$).

Both analyses showed a significant reduction of cholesterol levels after 24 hours mevastatin treatment. I then used this experimental procedure to quantify FGF2-GFP recruitment efficiency to the inner plasma membrane leaflet of living CHO K1 and U2OS cells, both

overexpressing FGF2-GFP in a doxycycline-dependent manner, employing TIRF microscopy^{105,262}. In this case, cholesterol reduction only mildly reduced FGF2-GFP recruitment efficiency, with a 9% significant decrease in CHO K1 cells (Fig. 24, panel B), and a 10% decrease in U2OS cells (Fig. 24, panel D), however not significant.

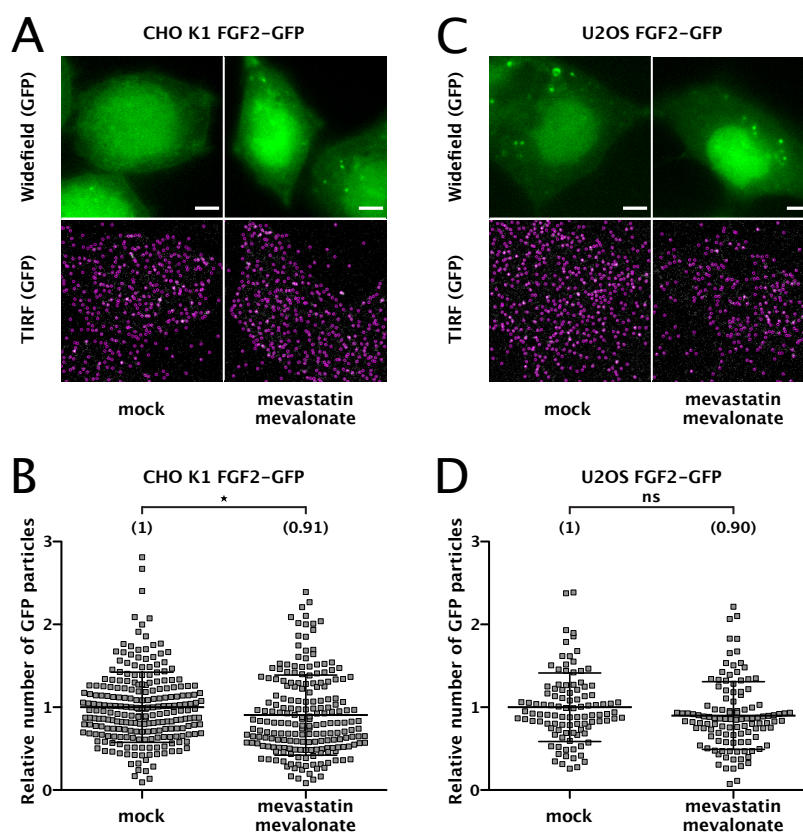


Fig. 24: Cellular cholesterol depletion reduces FGF2 recruitment at the inner plasma membrane leaflet in living cells. **A**, Representative images of real-time single molecule TIRF recruitment assay conducted on a stable CHO K1 cell line overexpressing FGF2-GFP in a doxycycline-dependent manner. Images are shown as widefield, for the overall FGF2-GFP expression levels, and TIRF, for FGF2-GFP particles recruited to the inner plasma membrane leaflet (Scale bar = 6 μ m). They represent untreated cells, as well as cells treated with 5 μ M mevastatin and 50 μ M mevalonate in the presence of de-lipidized serum, for 24 h in culture conditions. **B**, Quantification of real-time single molecule TIRF recruitment assay for the conditions shown in panel **A**, with the mock condition set to 1. Mean values are shown in brackets. Data are shown as mean \pm SD ($n = 4$). Statistical analysis was based on an unpaired, two-tailed t-test ($*p \leq 0.05$). **C**, Representative images of TIRF recruitment assay conducted on a stable U2OS cell line overexpressing FGF2-GFP in a doxycycline-dependent manner. Images are shown as widefield, for the overall FGF2-GFP expression levels, and TIRF, for FGF2-GFP particles recruited to the inner plasma membrane leaflet (Scale bar = 6 μ m). They represent untreated cells, as well as cells treated with 5 μ M mevastatin and 50 μ M mevalonate in the presence of de-lipidized serum, for 24 h in culture conditions. **D**, Quantification of real-time single molecule TIRF recruitment assay for the conditions shown in panel **C**, with the mock condition set to 1. Mean values are shown in brackets. Data are shown as mean \pm SD ($n = 4$). Statistical analysis was based on an unpaired, two-tailed t-test ($^{ns}p > 0.05$).

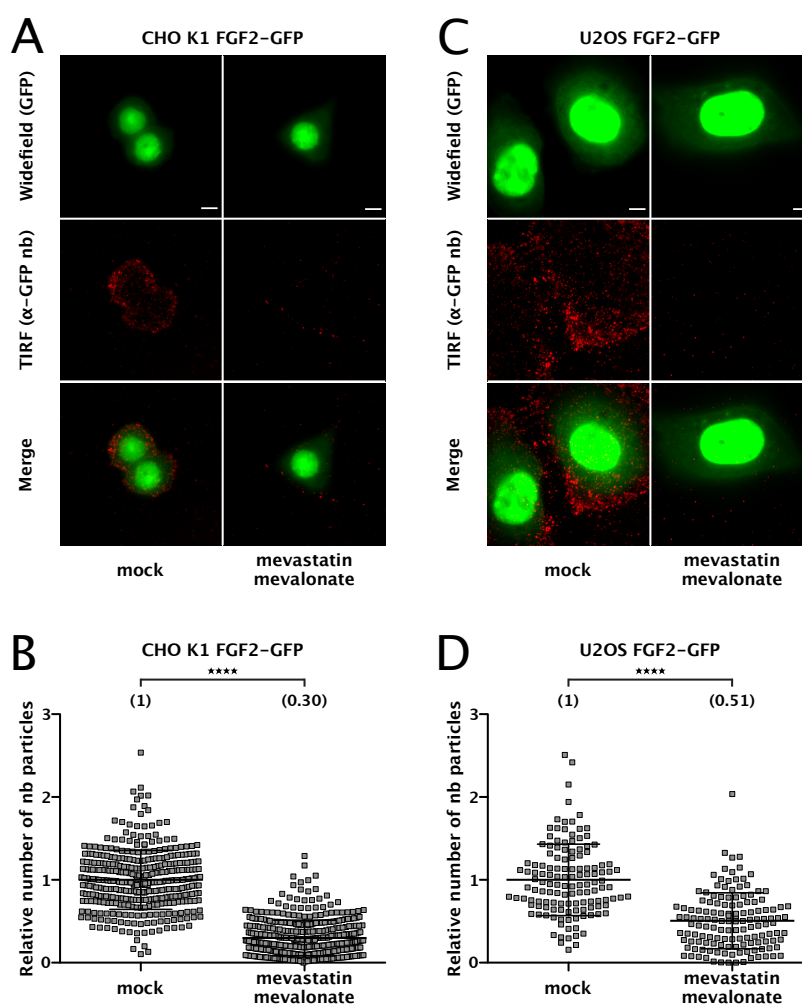


Fig. 25: Cellular cholesterol depletion reduces FGF2 recruitment at the inner plasma membrane leaflet in living cells. **A**, Representative images of TIRF translocation assay conducted on a stable CHO K1 cell line overexpressing FGF2-GFP in a doxycycline-dependent manner. Images are shown as widefield, for the overall FGF2-GFP expression levels, TIRF, for translocated FGF2-GFP particles detected via membrane impermeable anti-GFP nanobodies labeled with Alexa-Fluor 647, and merge of the two channels (Scale bar = 6 μ m). They represent untreated cells, as well as cells treated with 5 μ M mevastatin and 50 μ M mevalonate in the presence of de-lipidized serum, for 24 h in culture conditions. **B**, Quantification of real-time single molecule TIRF recruitment assay for the conditions shown in panel A, with the mock condition set to 1. Mean values are shown in brackets. Data are shown as mean \pm SD (n = 4). Statistical analysis was based on an unpaired, two-tailed t-test (****p \leq 0.0001). **C**, Representative images of TIRF translocation assay conducted on a stable U2OS cell line overexpressing FGF2-GFP in a doxycycline-dependent manner. Images are shown as widefield, for the overall FGF2-GFP expression levels, TIRF, for translocated FGF2-GFP particles detected via membrane impermeable anti-GFP nanobodies labeled with Alexa-Fluor 647, and merge of the two channels (Scale bar = 6 μ m). They represent untreated cells, as well as cells treated with 5 μ M mevastatin and 50 μ M mevalonate in the presence of de-lipidized serum, for 24 h in culture conditions. **D**, Quantification of real-time single molecule TIRF recruitment assay for the conditions shown in panel C, with the mock condition set to 1. Mean values are shown in brackets. Data are shown as mean \pm SD (n = 4). Statistical analysis was based on an unpaired, two-tailed t-test (****p \leq 0.0001).

Following the same experimental procedure for lowering cholesterol levels, I performed single molecule TIRF translocation assay on fixed CHO K1 and U2OS cells overexpressing FGF2-GFP

in a doxycycline-dependent manner²⁶². Reduced cholesterol levels caused a highly significant decrease of FGF2-GFP translocation to cell surfaces, with a 70% reduction in CHO K1 cells (Fig. 25, panel B) and a 49% reduction in U2OS cells (Fig. 25, panel D).

After proving an effect of cholesterol depletion from cells on FGF2-GFP translocation efficiency, I tested whether this effect would be specific for our protein of interest, similarly to what I observed for cholesterol enrichment, or if it would be a more general effect, affecting other cargo proteins secreted by conventional means. Also in this case, I made use of CHO cells overexpressing CD4-GFP in a doxycycline-dependent manner. After 4 biological replicates, CD4-GFP translocation efficiency, tested via single molecule TIRF microscopy, did not show any significant difference between mevastatin treated and untreated cells (Fig. 26, panel B). Together with the previous analysis showing no effect for CD4-GFP translocation from CHO cells enriched in their cholesterol levels (Fig. 26), these results showed that cholesterol does not play a role in modulating conventionally secreted proteins.

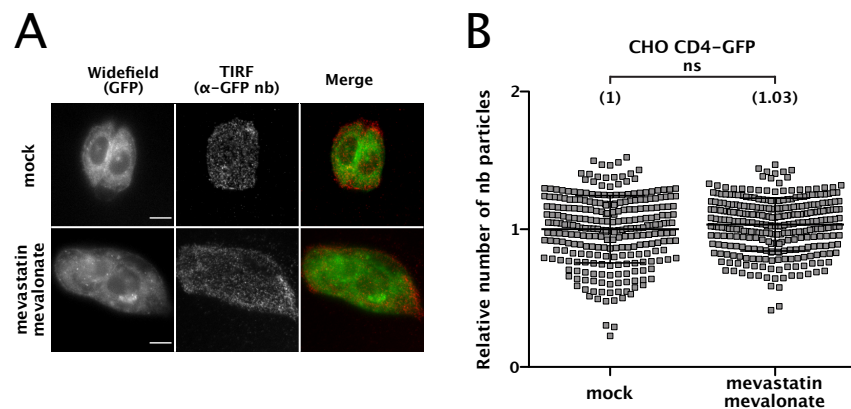


Fig. 26: Cellular cholesterol depletion does not have an impact on CD4-GFP conventional secretion from cells.

A, Representative images of TIRF translocation assay conducted on CHO K1 cells stably expressing CD4-GFP in a doxycycline-dependent manner, either untreated or treated with 5 μ M mevastatin and 50 μ M mevalonate in the presence of de-lipidized serum, for 24 h in culture conditions. Images are shown as widefield, for the overall CD4-GFP expression levels, TIRF, for translocated CD4-GFP particles detected via membrane impermeable anti-GFP nanobodies labeled with Alexa-Fluor 647, and merge of the two channels. **B**, Quantification of single molecule TIRF translocation assay for the conditions shown in panel A, with the mock condition set to 1. Mean values are shown in brackets. Data are shown as mean \pm SD ($n = 4$). Statistical analysis was based on an unpaired, two-tailed t-test. ^{ns} $p > 0.05$.

4.4.2 The role of sphingomyelin in the unconventional secretory pathway of FGF2

Similarly as for cholesterol, also sphingomyelin showed an effect when removed from PM like liposomes in terms of FGF2 binding¹¹¹. For this reason, I also focused on this lipid to better understand its role in the unconventional secretion of FGF2 from cells. In the context of sphingomyelin, to decrease its levels from cells, I made use of neutral sphingomyelinase (Sigma, S9396), an enzyme responsible for sphingomyelin degradation into ceramide and phosphocholine²⁷³. I used different concentrations of this enzyme and validated its efficiency in removing SM from CHO K1 by means of lipid mass spectrometry. I prepared samples as described for cholesterol analysis (for details, see methods). In brief, I enriched membrane fractions using the Minute™ Plasma Membrane Protein Isolation and Cell Fractionation Kit (Invent Biotechnologies), analyzed part of them by western blot analysis to check for PM enrichment and possible ER contaminations (Fig. 27, panel A) and sent them to the BZH lipidomic facility for lipid mass spectrometry (for details, see methods). In this case, I checked two different concentrations of nSMase for 4 hours in culture conditions. Lipid mass spectrometry showed a strongly significant reduction of SM levels in cells treated with either 0.1 U/ml or 0.5 U/mL nSMase, when compared with untreated cells (Fig. 27, panel B). Sphingomyelin levels are shown as mol% of the total plasma membrane lipids. 0.1 U/mL nSMase reduced sphingomyelin levels by 70 mol%, while 0.5 U/mL nSMase by around 80 mol%. Both reductions are highly significant compared to the mock condition, but they are not significantly different between each other, even though there is a clear tendency for a higher reduction with 0.5 U/mL. With these results, treatment of CHO K1 cells with nSMase was validated, and I could use this treatment to further investigate sphingomyelin impact on the unconventional secretion of FGF2.

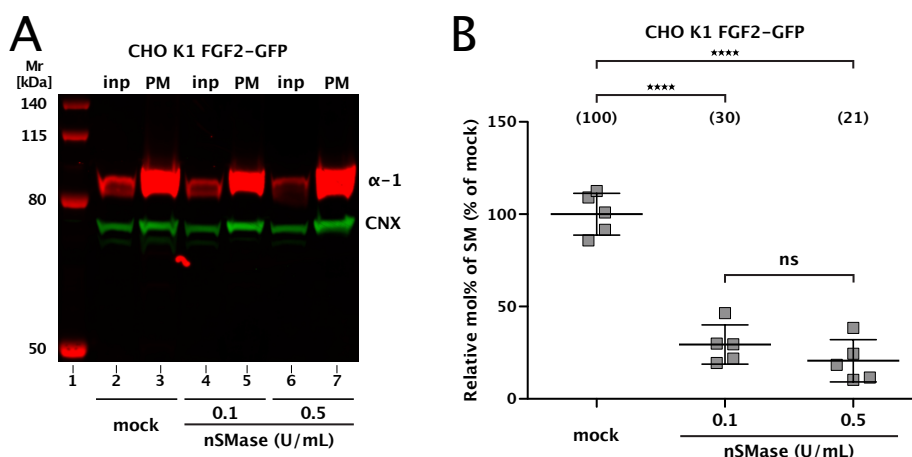


Fig. 27: Treating cells with neutral Sphingomyelinase (nSMase) decreases their sphingomyelin levels, based on lipid mass spectrometry. A, Representative western blot for membrane fractions validation. Input and membrane

Results

fractions of both untreated and cells treated with either 0.1 U/mL or 0.5 U/mL nSMase for 4 h in culture conditions, were blotted against a plasma membrane marker (the α -1 subunit of the Na,K-ATPase) to check for plasma membrane enrichment, and an ER marker (calnexin) to check for ER contamination of the plasma membrane fractions. **B**, Quantification of lipid mass spectrometry on CHO K1 samples for the conditions shown in panel A. The values represented on the graph are based on plasma membrane fractions, where sphingomyelin mol% was determined for all the conditions, with the mock condition set to 100%. Data are shown as mean \pm SD (n = 5). The statistical analysis was based on an unpaired, two-tailed t- test ($n^s p > 0.05$, $**** p \leq 0.0001$).

Based on this procedure to reduce cellular sphingomyelin levels, I performed cell surface biotinylation assay^{105,112,267} to assess the effect of SM reduction on FGF2-GFP secretion efficiency (Fig. 28, panel A). I treated cells with increasing concentrations of nSMase, 0.01 U/mL, 0.05 U/mL, 0.1 U/mL, 0.3 U/mL and 0.5 U/mL, for 4 hours in culture conditions and compared their FGF2-GFP secretion efficiency with untreated cells. Already at the lowest concentration of 0.01 U/mL nSMase, I found a significant 19% reduction of FGF2-GFP at cell surfaces compared to the untreated condition (Fig. 28, panel A, subpanel b). The effect of nSMase was concentration-dependent, as increasing amount of enzyme reduced more robustly FGF2-GFP secretion efficiency (Fig. 28, panel A, subpanel b). The strongest effect was achieved at the highest concentration of 0.5 U/mL nSMase, with a 52% reduction of secretion efficiency, going through a 30%, 40% and 47% reduction with 0.05 U/mL, 0.1 U/mL and 0.3 U/mL, respectively (Fig. 28, panel A, subpanel b). To further validate these results, I employed single molecule TIRF microscopy in combination with membrane-impermeable anti-GFP nanobodies to perform Translocation Assay²⁶². In this context, lowering SM levels by nSMase also triggered a concentration-dependent reduction in terms of FGF2-GFP translocation efficiency, even though not as linear as the one I observed with cell surface biotinylation assay. The lowest concentration of 0.01 U/mL already showed a highly significant reduction of FGF2-GFP translocation efficiency by 57% compared to untreated cells. This phenotype is probably linked to some technical problem, since it is very consistent throughout the 4 different biological replicates, however I was not able to determine the reason behind this. Nevertheless, the other concentrations of nSMase did show a concentration-dependent reduction of FGF2-GFP translocation efficiency, with 0.05 U/mL nSMase causing a significant drop of 31%, 0.1 U/mL significantly reducing FGF2-GFP translocation efficiency by 32%, and 0.3 U/mL and 0.5 U/mL nSMase affecting translocation efficiency by 67% and 55%, respectively (Fig. 28, panel B, subpanel b).

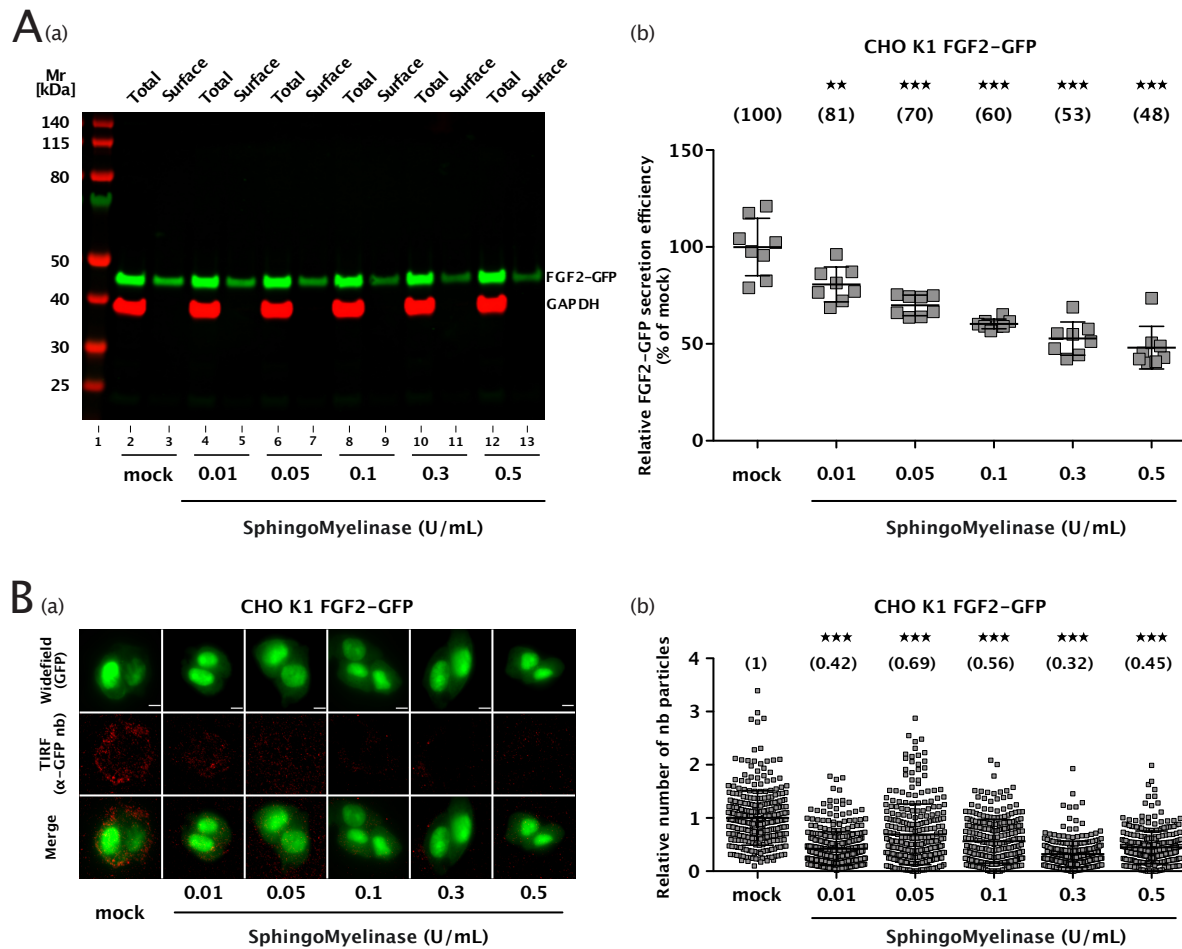


Fig. 28: Cellular sphingomyelin depletion reduces FGF2 secretion from cells. **A**, Cell surface biotinylation assay performed under conditions of decreased sphingomyelin levels. (a) Representative western blot analysis of cell surface biotinylation experiments, conducted on a stable CHO K1 cell line overexpressing FGF2-GFP in a doxycycline-dependent manner. Beyond the mock condition, cells were treated with increasing concentrations of neutral Sphingomyelinase (SMase): 0.01 U/mL, 0.05 U/mL, 0.1 U/mL, 0.3 U/mL, and 0.5 U/mL. SMase treatment was conducted for 4 h in culture conditions. Western blot analysis was conducted against GFP (to detect FGF2-GFP) and GAPDH (to check for cellular integrity during the assay, as well as a loading control). Total cell lysates (Total) and surface proteins eluted from streptavidin beads (Surface) were analyzed. (b), Quantification of cell surface biotinylation assay for conditions shown in subpanel (a), with the mock condition set to 100. Mean values are shown in brackets. Data are shown as mean \pm SD ($n = 4$). Statistical analysis was based on a one-way ANOVA test (** $p \leq 0.01$, *** $p \leq 0.001$). **B**, Single molecule TIRF translocation assay performed under conditions of decreased sphingomyelin levels. (a) Representative images of single molecule TIRF translocation assay conducted on a stable CHO K1 cell line overexpressing FGF2-GFP in a doxycycline-dependent manner. Images are shown as widefield, for the overall FGF2-GFP expression levels, TIRF, for translocated FGF2-GFP particles detected via membrane impermeable anti-GFP nanobodies labeled with Alexa-Fluor 647, and merge of the two channels (Scale bar = 6 μ m). They represent untreated cells, as well as cells treated with increasing concentrations of neutral Sphingomyelinase (SMase): 0.01 U/mL, 0.05 U/mL, 0.1 U/mL, 0.3 U/mL, and 0.5 U/mL. SMase treatment was conducted for 4 h in culture conditions. (b), Quantification of single molecule TIRF translocation assay for the conditions shown in subpanel (a), with the mock condition set to 1. Mean values are shown in brackets. Data are shown as mean \pm SD ($n = 4$). Statistical analysis was based on a one-way ANOVA test (** $p \leq 0.001$).

Combined with the biotinylation data, these results point at a role for sphingomyelin in the unconventional secretion of FGF2. To better understand the effect of sphingomyelin depletion from cells, I also tested FGF2-GFP recruitment efficiency via single molecule TIRF microscopy^{105,262} in intact CHO K1 cells. Interestingly, lowering sphingomyelin levels from cells, did not cause a phenotype at any concentration I tested (Fig. 29).

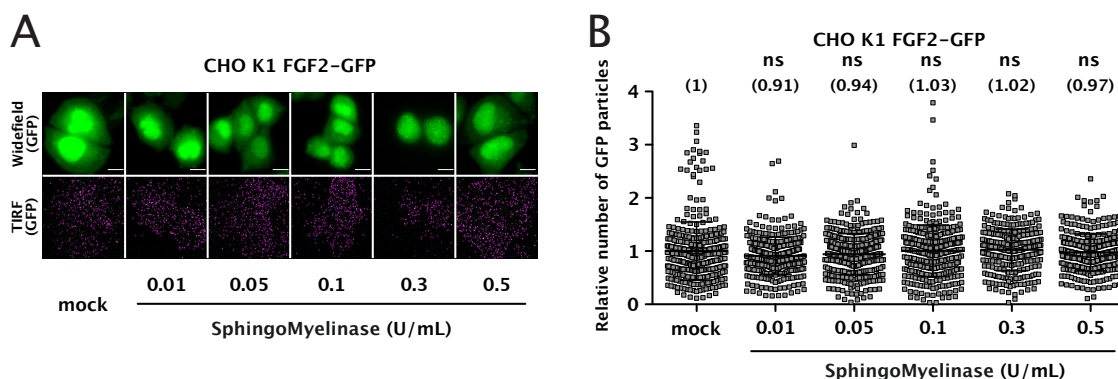


Fig. 29: Cellular sphingomyelin depletion does not have an impact on FGF2-GFP recruitment at the inner plasma membrane leaflet of living cells. **A**, Representative images of real-time single molecule TIRF recruitment assay conducted on a stable CHO K1 cell line overexpressing FGF2-GFP in a doxycycline-dependent manner. Images are shown as widefield, for the overall FGF2-GFP expression levels, and TIRF, for FGF2-GFP particles recruited to the inner plasma membrane leaflet (Scale bar = 6 μ m). They represent untreated cells, as well as cells treated with increasing concentrations of neutral Sphingomyelinase (SMase): 0.01 U/mL, 0.05 U/mL, 0.1 U/mL, 0.3 U/mL, and 0.5 U/mL. SMase treatment was conducted for 4 h in culture conditions. **B**, Quantification of real-time single molecule TIRF recruitment assay for the conditions shown in panel A, with the mock condition set to 1. Mean values are shown in brackets. Data are shown as mean \pm SD ($n = 4$). Statistical analysis was based on a one-way ANOVA test ($^{ns}p > 0.05$).

Once I methods). Lipid mass spectrometry, performed once again at the BZH lipidomic facility of Prof. Dr. Britta Brügger, showed a highly significant increase of sphingomyelin levels on treated versus untreated cells (Fig. 30, panel B). These results, showed as mol% sphingomyelin levels, proved an increase of around 140 mol% sphingomyelin in the plasma membrane of cells treated with Methyl- β -Cyclodextrin:sphingomyelin complexes compared to untreated cells. Also in this case, I conducted a western blot analysis and stained for α 1 and calnexin, to check for plasma membrane enrichment and ER contamination, respectively (Fig. 30, panel A).

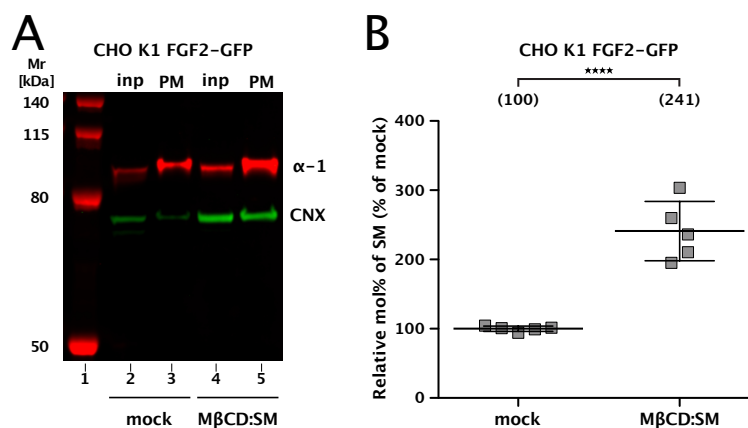


Fig. 30: Treating cells with sphingomyelin:Methyl-β-Cyclodextrin complexes enhances their sphingomyelin levels, based on lipid mass spectrometry. **A**, Representative western blot for membrane fractions validation. Input and membrane fractions of both untreated and cells treated with sphingomyelin:Methyl-β-Cyclodextrin (1:10 molar ratio) complexes for 1 h in culture conditions, were blotted against a plasma membrane marker (the α-1 subunit of the Na,K-ATPase) to check for plasma membrane enrichment, and an ER marker (calnexin) to check for ER contamination of the plasma membrane fractions. **B**, Quantification of lipid mass spectrometry on CHO K1 samples for the conditions shown in panel A. The values represented on the graph are based on plasma membrane fractions, where sphingomyelin mol% was determined for both conditions, with the mock condition set to 100%. Data are shown as mean ± SD (n = 3). The statistical analysis was based on an unpaired, two-tailed t- test (****p ≤ 0.0001).

After demonstrating a significant increase of cellular SM levels upon MβCD:SM complexes addition for 1 hour to cells, I used this procedure and quantified FGF2-GFP recruitment efficiency at the inner plasma membrane leaflet of living CHO K1 cells, employing single molecule TIRF microscopy^{105,262}. The increase was quite substantial, with, on average, twice as much FGF2-GFP particles at the inner plasma membrane leaflet of cells enriched in SM compared to untreated cells (Fig. 31, panel B). In this case, single cells showed an extremely high recruitment efficiency, with few cells showing over five times more FGF2-GFP particles at their inner leaflet compared to the average of particles found at untreated cells (Fig. 31, panel B).

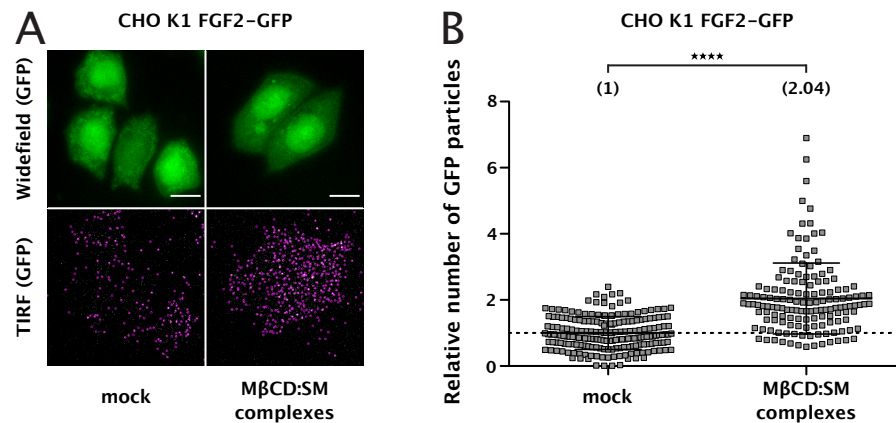


Fig. 31: Cellular sphingomyelin enrichment increases FGF2-GFP recruitment at the inner plasma membrane leaflet of living cells. **A**, Representative images of real-time single molecule TIRF recruitment assay conducted on a stable CHO K1 cell line overexpressing FGF2-GFP in a doxycycline-dependent manner. Images are shown as widefield, for the overall FGF2-GFP expression levels, and TIRF, for FGF2-GFP particles recruited to the inner plasma membrane leaflet (Scale bar = 6 μ m). They represent untreated cells, as well as cells treated with sphingomyelin:Methyl- β -Cyclodextrin (1:10 molar ratio) complexes for 1 h in culture conditions. **B**, Quantification of real-time single molecule TIRF recruitment assay for the conditions shown in panel A, with the mock condition set to 1. Mean values are shown in brackets. Data are shown as mean \pm SD ($n = 4$). Statistical analysis was based on a one-way ANOVA test (**** $p \leq 0.0001$).

On the same conditions of enriched cellular SM levels, I performed single molecule TIRF Translocation Assay²⁶² (Fig. 32, panel A), and cell surface biotinylation assay^{105,112,267} (Fig. 32, panel B). After quantification of four TIRF biological replicates, I observed a highly significant increase of 91% FGF2-GFP translocation efficiency in cells enriched in SM compared to untreated cells (Fig. 32, panel A, subpanel b). In cell surface biotinylation assay, I observed a similar phenotype, with a significant increase of 79% in terms of secretion efficiency compared to untreated cells (Fig. 32, panel B, subpanel b).

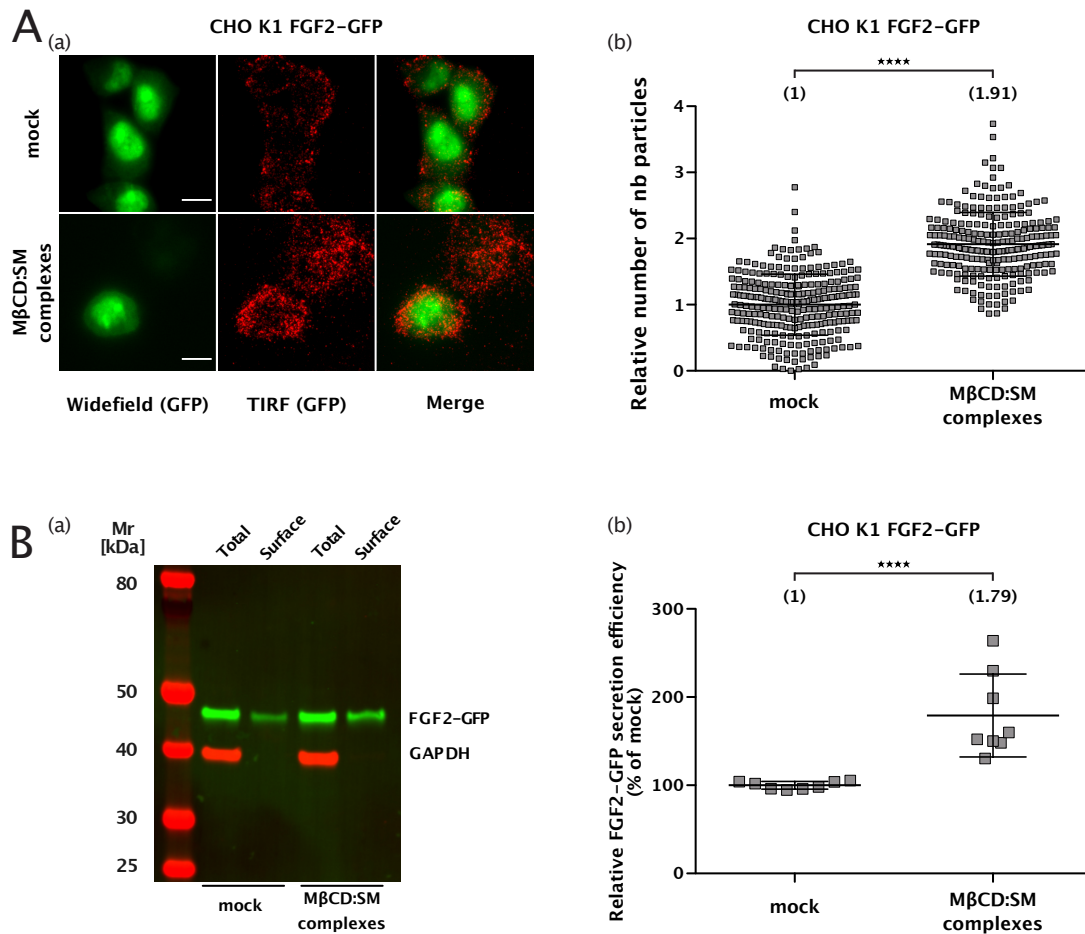


Fig. 32: Cellular sphingomyelin enrichment increases FGF2-GFP secretion efficiency from cells. **A**, Single molecule TIRF translocation assay performed under conditions of enriched sphingomyelin levels. (a) Representative images of single molecule TIRF translocation assay conducted on a stable CHO K1 cell line overexpressing FGF2-GFP in a doxycycline-dependent manner. Images are shown as widefield, for the overall FGF2-GFP expression levels, TIRF, for translocated FGF2-GFP particles detected via membrane impermeable anti-GFP nanobodies labeled with Alexa-Fluor 647, and merge of the two channels (Scale bar = 6 μ m). They represent untreated cells, as well as cells treated with Sphingomyelin:Methyl- β -Cyclodextrin (1:10 molar ratio) complexes for 1 h in culture conditions. (b), Quantification of single molecule TIRF translocation assay for the conditions shown in panel (a), with the mock condition set to 1. Mean values are shown in brackets. Data are shown as mean \pm SD (n = 4). Statistical analysis was based on an unpaired, two-tailed t-test (****p \leq 0.0001). **B**, Cell surface biotinylation assay performed under conditions of enriched sphingomyelin levels. (a) Representative western blot analysis of cell surface biotinylation experiments, conducted on a stable CHO K1 cell line overexpressing FGF2-GFP in a doxycycline-dependent manner. Beyond the mock condition, cells were treated with Sphingomyelin:Methyl- β -Cyclodextrin (1:10 molar ratio) complexes for 1 h in culture conditions. Western blot analysis was conducted against GFP (to detect FGF2-GFP) and GAPDH (to check for cellular integrity during the assay, as well as a loading control). Total cell lysates (Total) and surface proteins eluted from streptavidin beads (Surface) were analyzed. (b) Quantification of cell surface biotinylation assay for conditions shown in subpanel (a), with the mock condition set to 100. Mean values are shown in brackets. Data are shown as mean \pm SD (n = 4). Statistical analysis was based on an unpaired, two-tailed t-test (****p \leq 0.0001).

Thus, while lowering plasma membrane SM levels only affected FGF2–GFP translocation efficiency, but not its recruitment to the inner leaflet, increasing plasma membrane SM levels strongly increased both parameters, pointing at a strong effect for SM in the regulation of the unconventional secretion of FGF2.

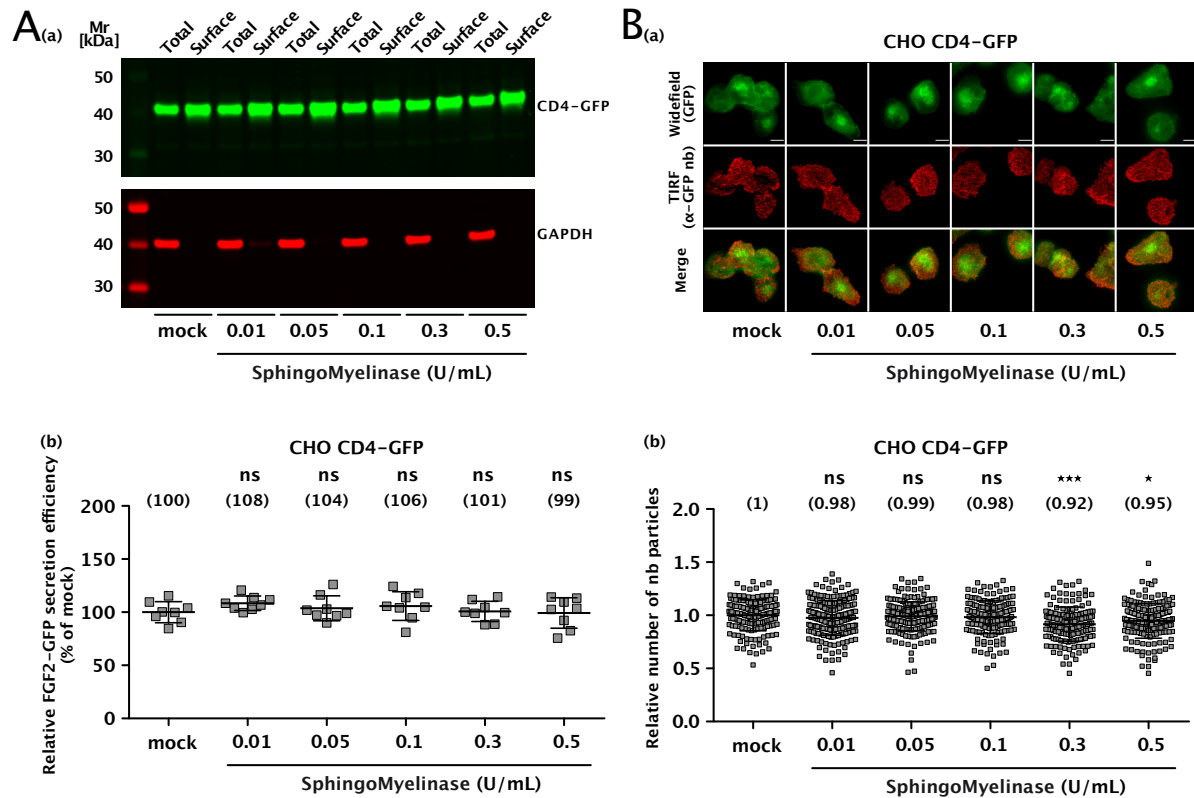


Fig. 33: Cellular sphingomyelin depletion does not interfere with CD4–GFP secretion from cells. **A**, Cell surface biotinylation assay performed under conditions of decreased sphingomyelin levels. **(a)** Representative western blot analysis of cell surface biotinylation experiments, conducted on a stable CHO cell line overexpressing CD4–GFP in a doxycycline–dependent manner. Beyond the mock condition, cells were treated with increasing concentrations of neutral Sphingomyelinase (SMase): 0.01 U/mL, 0.05 U/mL, 0.1 U/mL, 0.3 U/mL, and 0.5 U/mL. SMase treatment was conducted for 4 h in culture conditions. Western blot analysis was conducted against GFP (to detect CD4–GFP) and GAPDH (to check for cellular integrity during the assay, as well as a loading control). Total cell lysates (Total) and surface proteins eluted from streptavidin beads (Surface) were analyzed. **(b)**, Quantification of cell surface biotinylation assay for conditions shown in subpanel (a), with the mock condition set to 100. Mean values are shown in brackets. Data are shown as mean \pm SD ($n = 4$). Statistical analysis was based on a one–way ANOVA test ($^{ns}p > 0.05$). **B**, Single molecule TIRF translocation assay performed under conditions of decreased sphingomyelin levels. **(a)** Representative images of TIRF translocation assay conducted on a stable CHO cell line overexpressing CD4–GFP in a doxycycline–dependent manner. Images are shown as widefield, for the overall CD4–GFP expression levels, TIRF, for translocated CD4–GFP particles detected via membrane impermeable anti–GFP nanobodies labeled with Alexa–Fluor 647, and merge of the two channels (Scale bar = 6 μ m). They represent untreated cells, as well as cells treated with increasing concentrations of neutral Sphingomyelinase (SMase): 0.01 U/mL, 0.05 U/mL, 0.1 U/mL, 0.3 U/mL, and 0.5 U/mL. SMase treatment was conducted for 4 h in culture conditions. **(b)**, Quantification of single molecule TIRF translocation assay for the conditions shown in subpanel (a), with the mock condition set to 1. Mean values are shown in brackets. Data are shown as mean \pm SD ($n = 4$). Statistical analysis was based on a one–way ANOVA test ($^{ns}p > 0.05$, $^*p \leq 0.01$, $^{***}p \leq 0.001$).

Like for the cholesterol investigation, I tested a protein secreted by conventional means, CD4–GFP, in the context of altered SM levels. I performed these experiments with both assays to test secretion efficiency, cell surface biotinylation assay^{105,112,267} (Fig. 33, panel A) and single molecule TIRF translocation assay²⁶² (Fig. 33, panel B), in conditions of both reduced and enriched sphingomyelin levels. Sphingomyelin depletion did not cause any phenotype in terms of CD4–GFP secretion efficiency in cell surface biotinylation assay (Fig. 33, panel A, subpanel b). When studied via single molecule TIRF microscopy, only higher concentrations of nSMase caused a mild phenotype of 92% and 95% at 0.3 U/mL and 0.5 U/mL, respectively, when compared to untreated cells, set to 1 (Fig. 33, panel B, subpanel b). Lower concentrations of nSMase did not cause any phenotype (Fig. 33, panel B, subpanel b), similarly to what I observed with cell surface biotinylation assay.

As shown in figure 34, cellular Sphingomyelin enrichment did not cause a phenotype as well, neither when investigated via cell surface biotinylation assay (Fig. 34, panel A), nor via single molecule TIRF translocation assay (Fig. 34, panel panel B). These results pointed out that, like what I already observed for cholesterol, also sphingomyelin does not seem to play a role in the ER/Golgi–dependent conventional pathway for protein secretion, but it is rather a quite specific modulator of type I unconventional secretion of FGF2.

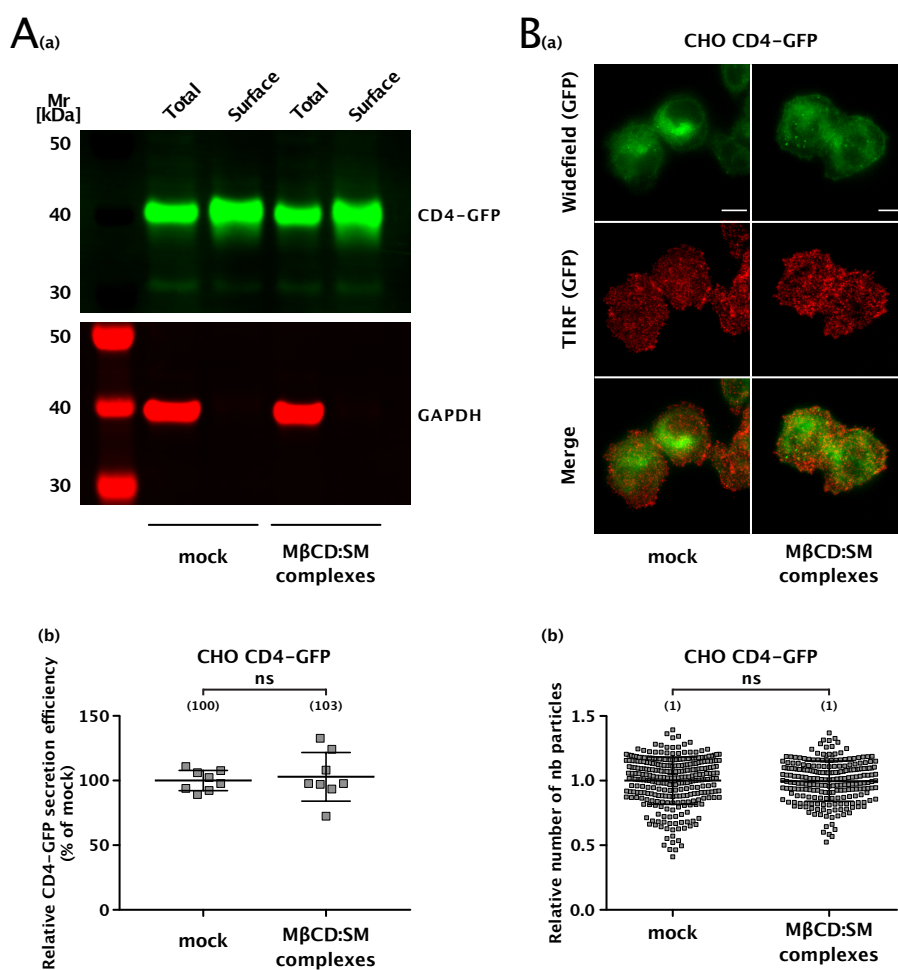


Fig. 34: Cellular sphingomyelin enrichment does not interfere with CD4-GFP secretion from cells. **A**, Cell surface biotinylation assay performed under conditions of decreased sphingomyelin levels. **(a)** Representative western blot analysis of cell surface biotinylation experiments, conducted on a stable CHO cell line overexpressing CD4-GFP in a doxycycline-dependent manner. Beyond the mock condition, cells were treated with Sphingomyelin:Methyl- β -Cyclodextrin (1:10 molar ratio) complexes for 1 h in culture conditions. Western blot analysis was conducted against GFP (to detect CD4-GFP) and GAPDH (to check for cellular integrity during the assay, as well as a loading control). Total cell lysates (Total) and surface proteins eluted from streptavidin beads (Surface) were analyzed. **(b)**, Quantification of cell surface biotinylation assay for conditions shown in subpanel **(a)**, with the mock condition set to 100. Mean values are shown in brackets. Data are shown as mean \pm SD ($n = 4$). Statistical analysis was based on an unpaired, two-tailed t -test ($nsp > 0.05$). **B**, Single molecule TIRF translocation assay performed under conditions of decreased sphingomyelin levels. **(a)** Representative images of TIRF translocation assay conducted on a stable CHO cell line overexpressing CD4-GFP in a doxycycline-dependent manner. Images are shown as widefield, for the overall CD4-GFP expression levels, TIRF, for translocated CD4-GFP particles detected via membrane impermeable anti-GFP nanobodies labeled with Alexa-Fluor 647, and merge of the two channels (Scale bar = 6 μ m). They represent untreated cells, as well as cells treated with Sphingomyelin:Methyl- β -Cyclodextrin (1:10 molar ratio) complexes for 1 h in culture conditions. **(b)**, Quantification of single molecule TIRF translocation assay for the conditions shown in subpanel **(a)**, with the mock condition set to 1. Mean values are shown in brackets. Data are shown as mean \pm SD ($n = 4$). Statistical analysis was based on an unpaired, two-tailed t -test ($nsp > 0.05$).

5. Discussion

5.1 The $\alpha 1$ subunit of the Na,K-ATPase is the first physical contact of FGF2 at the inner plasma membrane leaflet

The Na,K-ATPase is one of the last components discovered to play a role in the unconventional secretory pathway of FGF2. The first hint in this direction came from the observation that ouabain, a well-known inhibitor of the Na,K-ATPase pertaining to the cardiac glycoside family, was found to inhibit FGF2 secretion from cells²⁶⁹. Furthermore, a mutant form of the Na,K-ATPase which is insensitive to ouabain was capable of rescuing FGF2 secretion from cells in the presence of this cardiac glycoside¹⁰⁹. More recently, the $\alpha 1$ subunit of the Na,K-ATPase was reported as one of the strongest hits in a genome-wide RNAi screen designed to find out proteins whose knock down inhibits FGF2 secretion from cells¹⁰⁴. The purification of a soluble, small molecular weight subdomain of the cytosolic part of the Na,K-ATPase which was found to be both necessary and sufficient for binding FGF2 ($\alpha 1$ -subCD3)¹⁰⁵, allowed for NMR spectroscopy in order to analyze binding epitopes between FGF2 and $\alpha 1$ -subCD3. Based on this, two lysine residues were identified (K54 and K60) on FGF2 surface. These residues, when mutated, impaired the binding between purified FGF2 and $\alpha 1$ -subCD3¹⁰⁵. The replacement of these lysine residues by glutamates on FGF2 in cell-based experiments, caused an impact on both FGF2 recruitment to the inner plasma membrane leaflet and translocation from cells¹⁰⁵ (Fig. 7, 8, and 9). When investigated together with mutations in the PI(4,5)P₂ binding pocket¹¹¹, a mutant form of FGF2 which was already known to have a strong phenotype for FGF2 secretion from cells¹¹², this did not show any phenotype for FGF2 recruitment to the inner leaflet (Fig. 9)¹⁰⁵. When mutations in the PI(4,5)P₂ binding pocket were combined with mutations of the two lysine residues (K54/60E), this did not further affect FGF2 recruitment efficiency compared to mutations restricted to lysine 54 and lysine 60 (Fig. 9). This was direct evidence that, even though in reconstitution experiments $\alpha 1$ is not needed for FGF2 recruitment to PI(4,5)P₂ containing liposomes^{110,111}, in cells it is essential for efficient recruitment to the inner plasma membrane leaflet and translocation from cells. This result also revealed the order of interactions of FGF2 at the inner leaflet of the plasma membrane during its unconventional secretion, with the $\alpha 1$ subunit of the Na,K-ATPase being the first physical contact of FGF2 at the membrane and preceding the interaction with PI(4,5)P₂¹⁰⁵. Therefore, these data point at $\alpha 1$ being a landing platform for FGF2 to reach the inner plasma membrane leaflet. Beyond this, FGF2 interaction with $\alpha 1$ may be a prerequisite for its subsequent binding to PI(4,5)P₂, which is essential for oligomerization and membrane pore formation. This could be caused by a role of $\alpha 1$ in FGF2 dimerization, which would increase avidity for PI(4,5)P₂, facilitating its subsequent binding. At this stage of our investigation, there is still no conclusive data on the oligomeric state of FGF2 during its interaction with $\alpha 1$.

With cross-linking experiments with purified FGF2 and $\alpha 1$ -subCD3, performed by Hans-Michael Müller, we showed the preferential formation of a heterodimer over FGF2 homodimers¹⁰⁵. Nevertheless, higher molecular weight hetero-oligomers could be observed, suggesting a potential 2:1 interaction between FGF2 and $\alpha 1$ -subCD3. As already mentioned, these experiments were performed with $\alpha 1$ -subCD3, the minimal binding partner of FGF2. $\alpha 1$ -subCD3 is both necessary and sufficient for FGF2 binding¹⁰⁵, but it is not to be excluded that other cytoplasmic areas of the Na,K-ATPase play a role in a possible dimerization of FGF2 based on this interaction. For this reason, it will be interesting to test purified domains including not only $\alpha 1$ -subCD3, but also broader areas of the cytoplasmic part of $\alpha 1$, such as $\alpha 1$ -CD1-3 (a soluble fusion protein connecting the first three cytoplasmic loops of $\alpha 1$) and $\alpha 1$ -CD3 (the third cytoplasmic loop of $\alpha 1$)¹⁰⁴, as well as full-length Na,K-ATPase. Furthermore, a subsequent set of cross-linking experiments performed in living cells will be crucial to better understand the stoichiometry of this interaction under physiological conditions. Another interesting hypothesis, for which there are also no data at this point, but it will for sure be an interesting project for future investigations, is that this interaction between FGF2 and $\alpha 1$ not only serves as a physical contact for FGF2 to reach the plasma membrane, and perhaps to drive FGF2 dimerization, but it has a modulatory effect on $\alpha 1$. This hypothesis is based on the consideration that, even if very transient with the whole process taking 200 ms on average²⁶², with our current model for FGF2 unconventional secretion, a lipidic membrane pore is formed. A modulation of the Na,K-ATPase might be necessary to maintain the voltage gradient across the plasma membrane during FGF2 secretion. In future investigations, a possible way to test this hypothesis might be to follow ATPase activity of Na,K-ATPase in living cells, comparing different conditions such as presence and absence of FGF2 (taking advantage of doxycycline-inducible system for protein expression)²⁷⁴, and comparison between wild-type FGF2 and a mutant form not capable of efficient binding to $\alpha 1$ (K54/60E)¹⁰⁵. These experiments could be performed in the presence and absence of ouabain, an inhibitor of the Na,K-ATPase, to differentiate between ATPase activities coming from the Na,K-ATPase and other ATPases²⁷⁵. Another possible way to test this hypothesis (FGF2 modulating $\alpha 1$ ATPase activity to maintain the voltage gradient during translocation events) will be to directly check for membrane potential on cells expressing various forms of FGF2 (wild-type and K54/60E), and again in the presence and absence of FGF2. This might be achieved employing a newly-designed DNA-based fluorescent reporter that is able to quantify membrane potential, that the developers named *Voltair*²⁷⁶. Always considering the role of $\alpha 1$, in experiments performed to test how ouabain affects FGF2 unconventional secretion, I found a strong impact on FGF2 secretion following ouabain-induced inhibition of the Na,K-ATPase (Fig. 10), and a milder effect on FGF2 recruitment to the inner plasma membrane leaflet (Fig. 11). It is noteworthy that the strongest phenotype I found for FGF2 recruitment in the presence of ouabain (64%) is very similar to the one I observed for the mutant FGF2 form not being able to interact with $\alpha 1$ (68%) (Fig. 9). When

considering secretion efficiency, I observed a similar phenotype for this mutant form of FGF2 (K54/60E) with two independent assays, cell surface biotinylation assay (Fig. 7) and single molecule TIRF Translocation assay (Fig. 8). From this point of view, experiments performed in the presence of ouabain to study FGF2 translocation efficiency from cells, showed a substantial stronger phenotype at high concentrations of the inhibitor (100 μ M), with a phenotype below 40% (Fig. 10). I consider the different translocation phenotype of ouabain treated cells compared with the one of cells expressing a mutant FGF2 form not being able to efficiently interact with α 1 (K54/60E) to be the most interesting. A possible way to interpret this difference could be to link it with the previous hypothesis of a double role for α 1 in the unconventional secretion of FGF2. On the one hand, α 1 acts as a landing platform for FGF2 efficient recruitment at the inner plasma membrane leaflet, and this would be directly linked with the phenotype observed for K54/60E FGF2 (Fig. 7, 8, and 9); on the other hand, a modulation of α 1 would be necessary for FGF2 translocation events. The latter would be directly linked to the strong translocation phenotype observed for ouabain treated cells (Fig. 10). In this scenario, ouabain would not only prevent α 1 modulation from FGF2, but would also inhibit α 1 physiological functions, causing a stronger phenotype beyond the one observable by impairing α 1 interaction with FGF2. It is of course also important to take into account that ouabain has a number of pleiotropic effects, and there is the risk to overinterpret results coming from it. This could have led to a very strong phenotype not exclusively derived from α 1 inhibition, but rather from other pleiotropic effects that ouabain treatment might cause. Would it be nonetheless interesting to further investigate this, together with the previous hypothesis for other possible roles of α 1 beyond being the first physical contact for FGF2 at the inner plasma membrane leaflet.

5.2 Two different roles for two cysteine residues?

Two surface cysteine residues (C77 and C95) have been shown in a previous study to be exclusively present in FGF2 and absent in the other FGF family members carrying a signal peptide for the ER/Golgi-dependent secretory pathway¹¹². These two cysteines are involved in PI(4,5)P₂-dependent oligomerization of FGF2, and their replacement by alanine residues cause the inability of FGF2 to get secreted from cells¹¹² (Fig. 12). In a parallel project of this study, I tried to better understand the single contribution of these two residues, using cell lines expressing single mutant forms of FGF2 (C77A and C95A), together with cells expressing a double mutant form of FGF2 (C77/95A). In all assays taken into account, substitution of cysteine in position 95 caused a stronger phenotype compared with substitution of cysteine 77, both for FGF2 recruitment to the inner plasma membrane leaflet (Fig. 14) and translocation to cell surfaces (Fig. 12 and 13). As shown in figure 11, FGF2-GFP recruitment efficiency does not differ between the double cysteine mutant and the single substitution of cysteine 95, but it does differ compared with the single substitution of cysteine 77, for which recruitment is

less affected, but still impaired compared with wild-type cells. This could imply that, for double substitution of the two cysteine residues, the contribution of cysteine 77 is neglectable compared to the one of cysteine 95 in terms of recruitment (as cysteine 95 and double cysteine mutant have the same phenotype). It is however noteworthy that the phenotype I observed for both single substitution of cysteine 95 and double cysteine substitution is comparable to the highest phenotype I ever observed in TIRF recruitment assay, specifically the one I observed for the mutant form of FGF2-GFP with an impaired binding to the $\alpha 1$ subunit of the Na,K-ATPase [FGF2 (K54/60E)-GFP] (Fig. 8). This could point at a limit of the assay, with a maximum observable recruitment phenotype around this range. The phenotypes observed in the two secretion assays I have used (cell surface biotinylation assay and TIRF translocation assay) are very comparable taking into account single mutant forms of FGF2 (C77A and C95A), with a phenotype close to 80% for C77A and one close to 35% for C95A (Fig. 12 and 13). Interestingly, when considering double substitutions of these cysteine residues to alanine residues (C77/95A), an important difference could be observed between TIRF translocation assay and cell surface biotinylation assay. In the latter assay, the double cysteine mutant form of FGF2 was found to be incapable to translocate across the plasma membrane; in TIRF translocation assay, this mutant form of FGF2 showed a weaker phenotype compared with C95A expressing cells, with an over than 60% average number of particles found at cell surfaces compared with wild-type cells (Fig. 13). This different phenotype based on the assay being used was not new for this particular mutant form of FGF2 (C77/95A), it has also been observed by a former PhD student who developed both FGF2 recruitment and translocation TIRF assay, Dr. Eleni Dimou (unpublished data). A possible explanation for this could be linked to the inability of this double cysteine mutant to form oligomers, but my recent finding that single substitution of cysteine 95 triggers a stronger phenotype than double substitution (Fig. 13), seems to go in another direction. To this day there is not a satisfying explanation for this observation, but it must be something linked to this particular mutant form, since single substitution forms behaved in a similar way in both secretion assays (Fig. 12 and 13). It is notable that differences between TIRF translocation assay and cell surface biotinylation assay have been observed for a number of studies, showing often a stronger phenotype in TIRF than in biotinylation (opposed to what it has been observed in this cysteine project). A possible explanation for this has been put forward that is linked to the different size of nanobodies or antibodies, and biotin, the latter being much smaller. The size of biotin could allow it to go deeper in proximity to cell surfaces, within the heparan sulfate proteoglycan's chains meshwork, and to then recognize a different population of translocated FGF2. An extension to this hypothesis is that biotin could even recognize membrane-inserted FGF2 oligomers, prior to FGF2 translocation events. This might explain how with antibody/nanobody-based assays, like the TIRF translocation assay used in this study, or surface staining FACS assay, another well-established assay used in our laboratory, the

phenotype observed is often stronger compared to the same conditions studied with cell surface biotinylation assay.

In a previous part of the project, cysteine 77 was believed to play a role in FGF2 oligomerization together with cysteine 95, with the formation of disulfide bridges¹¹². More recently, there has been evidence pointing at cysteine 95 to be the only residue involved in the formation of disulfide bridges (experiments performed by Dr. Hans-Michael Müller, data not shown). Nonetheless, cysteine 77 has a role in the unconventional secretion of FGF2, as its substitution cause a phenotype in both recruitment and translocation assays (Fig. 12, 13, and 14). The most likely reason behind this is linked to its position within FGF2. Cysteine 77 is in very close proximity to the two lysine residues (K54/60E) involved in the interaction between FGF2 and the α 1 subunit of the Na,K-ATPase. In a preliminary part of this study, this cysteine residue has been also taken into consideration for its possible interaction with α 1, and I generated cell lines expressing a mutant form of FGF2 where cysteine 77 is replaced by alanine (table 1). When NMR spectroscopy was performed to map binding epitopes on FGF2 for α 1-subCD3, cysteine 77 could not be examined, since a mutant form of FGF2 was used, carrying serine residues in substitution of cysteine residues in position 77 and 95, to avoid formation of FGF2 oligomers (cysteine 77 was believed to play a role in disulfide bridge formation together with cysteine 95). We anyway took cysteine 77 into consideration for a possible role in this interaction, and a former PhD student, Dr. Cyril Legrand, performed biochemical binding assays *in vitro* to test binding efficiencies between α 1-subCD3 and various mutant forms of recombinant FGF2, including C77A, C95A, and C77/95A (unpublished results). Both mutant forms of FGF2 carrying a single substitution for either cysteine 77 or cysteine 95 showed a loss of binding towards α 1-subCD3 between 30% to 40% compared with wild-type recombinant FGF2 with two independent assays (Alpha® Screen assay and pulldown assay). Recombinant FGF2 carrying substitutions of both cysteine residues could hardly be found to interact with α 1-subCD3. On the one hand, these results may point at dimerized FGF2 interacting with α 1, since the double cysteine mutant could not interact with it. On the other hand, since it is quite clear today that the cysteine residue driving this interaction is solely the one in position 95, C95A single mutant should also have the same phenotype, if the inability to dimerize would be the only explanation. A straightforward explanation would be for cysteine in position 77 to be part of the interaction with α 1, and therefore already showing a phenotype when replaced by alanine. Substitution of both cysteine residues would then have the strongest phenotype carrying both the inability to dimerize (coming from substitution of cysteine 95) and a lower binding efficiency to α 1 (coming from substitution of cysteine 77).

5.3 A possible involvement of liquid-ordered domains on the unconventional secretion of FGF2

In this thesis, a substantial part of my focus regarded membrane lipid composition, and how its changes would affect the unconventional secretion of FGF2. The starting point of this investigation derived from earlier observations pointing at a modulatory role of the lipid environment for FGF2 membrane recruitment. In this study, both cholesterol and sphingomyelin appeared to play a role in PI(4,5)P₂-dependent FGF2 membrane recruitment, with a drop in FGF2 membrane recruitment in their absence. These observations were conducted with *in vitro* assays, and I aimed at studying the modulatory role of cholesterol and sphingomyelin using cell-based assays. In experiments performed under cellular cholesterol enrichment, a condition that I achieved employing cholesterol:Methyl- β -Cyclodextrin complexes, both FGF2 recruitment at the inner plasma membrane leaflet (Fig. 19) and FGF2 translocation to cell surfaces (Fig. 20) appeared to be enhanced. I observed this phenomenon with two different cell lines, CHO K1 and the human U2OS cell line. In a subsequent set of experiments, evaluating the same parameters under the opposite conditions of reduced cellular cholesterol levels (achieved through mevastatin treatment), I observed a substantial reduction in FGF2 translocation to cell surfaces (Fig. 25), while FGF2 recruitment to the inner plasma membrane leaflet was only mildly affected, but still significantly reduced in CHO K1 cells (U2OS cells also showed a reduction, but it did not turn out to be significant) (Fig. 24). Together, these results showed a modulatory effect of cholesterol towards both FGF2 recruitment to the inner leaflet and FGF2 translocation to cell surfaces, with cholesterol enrichment enhancing both parameters (Fig. 19 and Fig. 20, respectively), and cholesterol depletion having a negative effect on both translocation and recruitment, with the last one being only mildly affected (Fig. 25 and Fig. 24, respectively).

Manipulation of cellular sphingomyelin levels showed relatively similar effects, with some differences in the FGF2 recruitment results. To reach sphingomyelin depletion, I made use on neutral Sphingomyelinase (nSMase), the plasma membrane-resident enzyme responsible for sphingomyelin degradation. Following treatment with nSMase, I evaluated FGF2 translocation efficiency to cell surfaces with two independent assays (cell surface biotinylation assay and single molecule TIRF translocation assay). Both of them reported a decrease in FGF2 translocation efficiency under conditions of reduced membrane sphingomyelin levels, which turned out to be concentration-dependent (Fig. 28). Regarding FGF2 recruitment to the inner plasma membrane leaflet, cellular sphingomyelin reduction did not produce significant changes compared to the untreated condition (Fig. 29). To study the effect of increased sphingomyelin levels, I once again made use of M β CD, this time complexed with sphingomyelin. Under these conditions, FGF2 recruitment to the inner plasma membrane leaflet increased with a factor of 2 (Fig. 31). Similarly, following cellular sphingomyelin levels enrichment, FGF2 translocation to cell surfaces was found to be increased in a highly

significant manner with two independent assays (cell surface biotinylation assay and single molecule TIRF translocation assay) (Fig. 32). As well as cholesterol, sphingomyelin proved to be an important modulator of the unconventional secretory pathway of FGF2. It has been known in literature that cholesterol and sphingomyelin have an intimate relationship within each other in biological membranes. There are studies that report an interplay of each other, e.g., increasing sphingomyelin levels would also indirectly increase cholesterol levels, and reducing sphingomyelin levels would also decrease cholesterol levels. This possibility was taken into account in this investigation, and lipid mass spectrometry following treatment to manipulate cellular sphingomyelin levels was conducted not only on sphingomyelin, but also on cholesterol and all the other lipids.

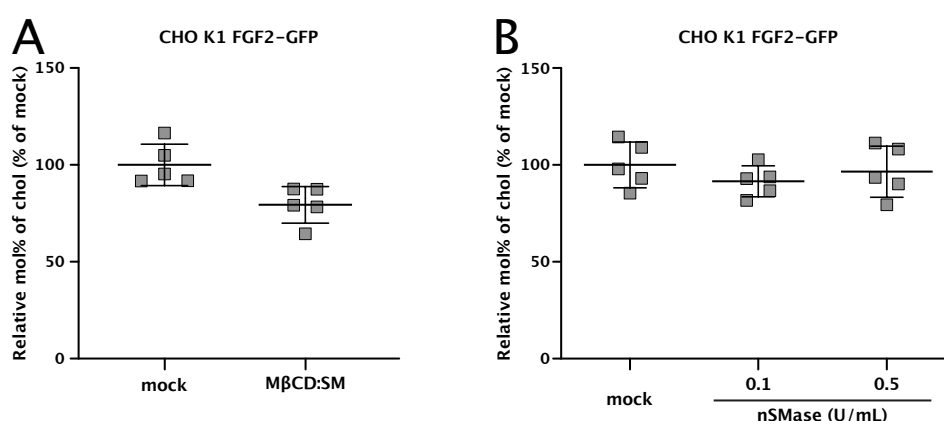


Figure 35: Manipulating cellular sphingomyelin levels does not have an impact on cellular cholesterol levels, based on lipid mass spectrometry. A, Quantification of lipid mass spectrometry on CHO K1 cells treated with sphingomyelin:Methyl- β -Cyclodextrin (1:10 molar ratio) complexes for 1 h in culture conditions (same samples shown in Fig. 30). The values represented on the graph are based on plasma membrane fractions, where ratios of cholesterol to PC were determined for both conditions as mol%, with the mock condition set to 100%. Data are shown as mean \pm SD (n = 5). B, Quantification of lipid mass spectrometry on CHO K1 cells treated with either 0.1 U/mL or 0.5 U/mL nSMase for 4 h in culture conditions (same samples shown in Fig. 27). The values represented on the graph are based on plasma membrane fractions, where ratios of cholesterol to PC were determined for all conditions as mol%, with the mock condition set to 100%. Data are shown as mean \pm SD (n = 5).

In fact, a full lipidomic analysis was performed. As shown in figure 35, cholesterol levels did not increase upon sphingomyelin enrichment, and did not decrease following sphingomyelin depletion. This means that the phenotypes observed in this investigation are to be linked entirely to sphingomyelin levels manipulation, and not on cholesterol.

As mentioned before, in 2017, the unconventional secretion of FGF2 has been reconstituted *in vitro* using purified components. In these experiments, PI(4,5)P₂ and heparin resulted necessary and sufficient to reconstitute FGF2 translocation across Giant Uni-lamellar Vesicles

(GUVs). In this assay, several minutes were needed to observe a substantial amount of FGF2 translocation across the GUVs membranes. In a recent study, FGF2 secretion was observed in real-time in living cells using a single molecule TIRF assay. In this context, the average time for FGF2 translocation to occur in living cells, starting from the point when FGF2 is recruited to the inner leaflet, was of about 200 ms, showing a substantial difference in terms of kinetics when compared to *in vitro* experiments.

This great difference could be explained, at least partially, by the different complexity in which *in vitro* and cell-based assays take place. In GUVs, additional components of the FGF2 secretion machinery, such as the $\alpha 1$ subunit of the Na,K-ATPase and Tec kinase, were absent, as, in this context, the sole presence of PI(4,5)P₂ and heparin was enough to trigger FGF2 translocation events. Beyond that, PI(4,5)P₂ was not asymmetrically distributed between the two leaflets as it is in cells (where its only, or predominantly, present in the inner leaflet), and heparin was added as a soluble component in the lumen of GUVs, while in a cellular context heparan sulfate chains of proteoglycans are membrane-proximal, a behaviour that is particularly pronounced in GPC1, that we recently found to be the dedicated HSPG for FGF2 secretion¹¹⁴, where the distance between heparan sulfate chains and the membrane outer leaflet is of about 3 nm¹⁰³.

An additional possible explanation for this difference in the kinetic of FGF2 translocation in cell-based vs *in vitro* experiments could come from the presence of nanodomains in cell membranes, in which the components of the FGF2 secretion machinery would be present in close proximity, allowing for a fast translocation. As previously discussed, liquid-ordered domains in the plasma membrane are known to be enriched in sphingomyelin and cholesterol. The modulatory effect on the unconventional secretion of FGF2 of these two lipid components of the plasma membrane could be a hint for a compartmentalization of the machinery involved in this pathway in liquid-ordered nanodomains. Another hint in this direction comes from the recent finding of Glypican 1 (GPC1) as a rate-limiting factor component of FGF2 secretion. It has been known for several years that Heparan Sulphate Proteoglycans (HSPGs) are essential components of the unconventional secretion machinery of FGF2^{46,103,110,114}, but, until a recent study, it was not clear whether there was a dedicated HSPG for FGF2 secretion. A Bio-ID screen conducted in our lab, under supervision of Dr. Eleni Dimou, to identify so far unknown components involved in the secretion of FGF2, showed GPC1 as the strongest hit. GPC1 is a GPI-anchored HSPG, and proteins that interact with the plasma membrane through a GPI anchor are known to localize in liquid-ordered domains. I employed single molecule TIRF microscopy to evaluate FGF2 translocation efficiency under conditions of GPC1 overexpression. I conducted these experiments in two different conditions, either at high or low FGF2 expression levels. Experiments performed under high FGF2 expression levels showed a quite strong increase of FGF2 secretion efficiency for cells overexpressing GPC1 versus wild-type cells (Fig. 15). This phenotype was consistent with the one observed under the same conditions using an independent cell surface biotinylation assay. Combination of

high resolution TIRF microscopy and high affinity α -GFP nanobodies (for details, see Materials and Methods) allowed to check for FGF2 secretion efficiency also under conditions of low FGF2 expression levels. Under these conditions, FGF2 translocation efficiency raised more than four times compared to wild-type cells, denoting a stronger impact on this pathway when only limiting amounts of FGF2 are present.

Thus, in this thesis, two plasma membrane components, cholesterol and sphingomyelin, and a protein, GPI-anchored GPC1, which are known to partition into liquid-ordered domains, were proven to play an important role in the unconventional secretion of FGF2. In addition to these three components of the unconventional secretion machinery of FGF2, also the Na,K-ATPase, which was found in this study to be the first physical contact of FGF2 at the inner plasma membrane leaflet, could partition into liquid ordered domains . There are different ways how this could happen, the most likely of which are palmitoylation or interaction with sphingomyelin. To test these hypothesis, new experiments have been already planned, employing techniques such as DRM fractions preparation and DuoLink proximity ligation assay (PLA). One of the possible options involves the use of 2-bromopalmitate, which inhibits protein palmitoylation and, therefore, would affect the Na,K-ATPase localization into liquid-ordered domains, if palmitoylation were the driving force. In regards of sphingomyelin, the approaches I optimized within this thesis to both deplete and enrich sphingomyelin levels in cells (section 4.4.2) will be used to evaluate their impact on Na,K-ATPase localization into liquid-ordered domains. Future investigations will be necessary to accumulate further evidence for structural organization in nanodomains of the FGF2 unconventional secretion machinery.

5.4 Lipidomic analysis

Within the project regarding how membrane composition affects the unconventional secretion of FGF2, I had a collaboration with the BZH lipidomic facility of Prof. Dr. Britta Brügger. As explained before, this collaboration consisted in lipid mass spectrometry of samples treated to either enrich or deplete their cholesterol/sphingomyelin levels. For the quantification of samples in which I manipulated sphingomyelin levels (section 4.4.2), they conducted a whole lipidomic analysis of those samples, and therefore, beyond checking the specific amount of sphingomyelin and cholesterol (which results have been discussed previously), they checked for every single lipid species present in the sample. These results were interesting because they gave the actual plasma membrane lipidic composition of CHO K1 cells, and it was interesting to compare this with the plasma membrane-like composition used in our laboratory for liposomes. The graphs in figure 36 show the lipid composition of untreated CHO K1 cells found in this study (panel A), and the plasma membrane-like lipid composition currently used in our lab. The two compositions are actually pretty similar, with the biggest difference concerning a higher sphingomyelin concentration on PM-like liposomes compared to CHO K1 cells, at the expense of phosphatidyl ethanolamine.

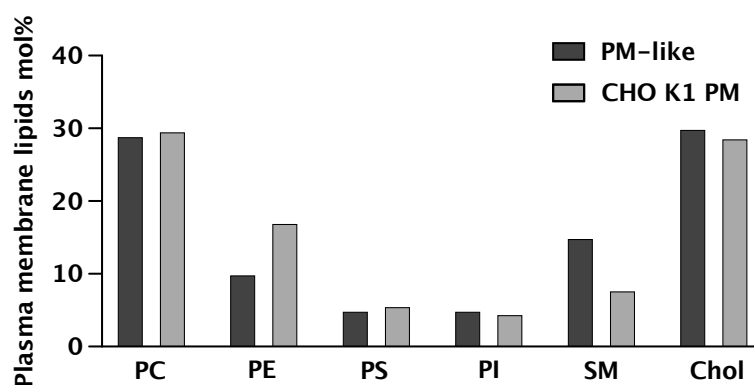


Figure 36: Comparison between PM-like lipid composition of liposomes, and CHO K1 plasma membrane lipid composition, based on lipid mass spectrometry. PC, phosphatidylcholine; PE, phosphatidylethanolamine, PS, phosphatidylserine, PI, phosphatidylinositol, SM, sphingomyelin, and Chol, cholesterol.

6 Conclusion and future perspective

In conclusion, in this study several aspects of the unconventional secretory pathway of FGF2 have been elucidated. First, I found the $\alpha 1$ subunit of the Na,K-ATPase to be the first physical contact of FGF2 at the inner plasma membrane leaflet, preceding its interaction with PI(4,5)P₂. This implies the interaction of FGF2 with $\alpha 1$ at the inner plasma membrane leaflet to be indispensable an efficient interaction with PI(4,5)P₂, in contrast to what has been observed in *in vitro* experiments, in which FGF2 is capable of binding PI(4,5)P₂-containing liposomes without any auxiliary factor^{111,113}. As previously discussed, this interaction with $\alpha 1$ could also be important for a modulation of the Na,K-ATPase in the context of FGF2 translocation events, in which transient membrane pores are generated. Beyond the interaction with $\alpha 1$, within this thesis I focused on other aspects of the unconventional secretion of FGF2. As discussed before, there are two surface cysteine residues on FGF2 (cysteine 77 and cysteine 95) that has been for long a mystery within our lab, since it was clear they had an impact on FGF2 oligomerization and secretion from cells, but it was not clear which was the specific contribution of each single cysteine. Within this study, I contributed to elucidate their single contribution in a cellular context, in which they are involved in both recruitment and secretion. Specifically, the mutation of both cysteine residues has the strongest phenotype in terms of secretion, with contribution coming mainly from cysteine 95, but also from cysteine 77, for which it is being clearer a role in the interaction with $\alpha 1$, whereas cysteine 95 should be the exclusive cysteine residue involved in FGF2 dimerization through the formation of a disulfide bridge.

Membrane properties were also found to be of crucial importance for this secretory pathway. For both cholesterol and sphingomyelin, in fact, I found a strong involvement in recruitment and translocation of FGF2 from cells. This could possibly point at an involvement of liquid-ordered domains in the unconventional secretion of FGF2, also when considering the importance of GPC1 (a GPI-anchored protein, as discussed before, then therefore should be located in liquid-ordered domains) in its unconventional secretion.

During this thesis, recruitment and translocation TIRF assays have been optimized and used in several different projects to evaluate different aspects of the unconventional secretion of FGF2. A big improvement has been achieved through the employment of high affinity, membrane impermeable anti-GFP nanobodies (Chromotek), with a KD of 1 pM. The characteristics of this reagent allowed me to use them at a way higher concentration compared to the former nanobodies used to establish this assay, which were custom-made in the laboratory of Helge Ewers, at the Freie Universität in Berlin. This particular aspect allowed to perform TIRF translocation experiments even in the absence of doxycycline and therefore at a low FGF2-GFP expression level. With this approach I have been able to study FGF2-GFP translocation efficiency in the context of GPC1 overexpression under conditions of different

FGF2–GFP expression levels. This allowed me to find a way larger impact of GPC1 on this process when FGF2–GFP is present in low amounts, which contributed to the conclusion that GPC1 is the dedicated HSPG for the unconventional secretion of FGF2.

These assays, beyond the projects they have already been used in, give the opportunity to a number of applications. One future project that could not be completed during this study involves a high affinity PI(4,5)P₂ sensor, based on the Pleckstrin Homology domain of phospholipase C δ 1 (PH–PLC– δ 1). The hypothesis behind this project is based on the current model for the unconventional secretion of FGF2, in which the accumulation of PI(4,5)P₂ molecules destabilizes the lipid bilayer and favor the formation of a toroidal lipidic membrane pore in which a FGF2 oligomer can span the membrane and finally reach the extracellular space, being resolved by membrane–proximal heparan sulfate chains on HSPGs. In this model, PI(4,5)P₂ molecules interact with FGF2 also inside the toroidal pore, and we hypothesized that a few PI(4,5)P₂ molecules could reach the outer leaflet during this process. To challenge this hypothesis, this high affinity PI(4,5)P₂ sensor will be used to detect PI(4,5)P₂ molecules at the outer leaflet at sites of FGF2 translocation, detected via anti–GFP nanobodies under the TIRF setup employed for single molecule translocation assay. This PI(4,5)P₂ sensor is fused with HALO–tag, and this will be employed to stain the protein with a specific membrane impermeable Halo dye. Another option to perform these experiments could be to use a different FGF2 fusion protein, for example FGF2–Spot (Chromotek), instead of FGF2–GFP. This would increase the options for color combinations, since with FGF2–GFP two channels are already taken (GFP and far–red for the anti–GFP nanobodies). These experiments will be performed with a TIRF microscope able to image two different channels at the same time, to simultaneously image translocated FGF2–GFP particles and PI(4,5)P₂ molecules at the outer leaflet. A TIRF setup like this is available in the laboratory of Helge Ewers at the Freie Universität in Berlin, since with the one I used for all the projects within this work at the ZMBH imaging facility is only possible to image one channel at a time.

7. References

1. Rothman, J. E. *Mechanisms of intracellular protein transport*.
2. Rothman, J. E. & Wieland, F. T. *Protein Sorting by Transport Vesicles*.
<https://www.science.org>.
3. science.271.5255.1526.
4. Aviram, N. & Schuldiner, M. Targeting and translocation of proteins to the endoplasmic reticulum at a glance. *J Cell Sci* **130**, 4079–4085 (2017).
5. Rapoport, T. A. Protein translocation across the eukaryotic endoplasmic reticulum and bacterial plasma membranes. *Nature* vol. 450 663–669 Preprint at <https://doi.org/10.1038/nature06384> (2007).
6. Walter, P., Ibrahimi, I. & Blobel, G. *Translocation of Proteins Across the Endoplasmic Reticulum I. Signal Recognition Protein (SRP) Binds to In-Vitro-Assembled Polysomes Synthesizing Secretory Protein*. *THE JOURNAL OF CELL BIOLOGY* vol. 91 <http://rupress.org/jcb/article-pdf/91/2/545/1075402/545.pdf> (1981).
7. Walter, P. & Blobel, G. *Translocation of Proteins Across the Endoplasmic Reticulum II. Signal Recognition Protein (SRP) Mediates the Selective Binding to Microsomal Membranes of In-Vitro-Assembled Polysomes Synthesizing Secretory Protein*. *THE JOURNAL OF CELL BIOLOGY* vol. 91 <http://rupress.org/jcb/article-pdf/91/2/551/1075421/551.pdf> (1981).
8. Walter, P. & Blobel, G. *Translocation of Proteins Across the Endoplasmic Reticulum III. Signal Recognition Protein (SRP) Causes Signal Sequence-dependent and Site-specific Arrest of Chain Elongation that is Released by Microsomal Membranes*. *THE JOURNAL OF CELL BIOLOGY* vol. 91 <http://rupress.org/jcb/article-pdf/91/2/557/1075435/557.pdf> (1981).
9. Gilmore, R., Blobel, G. & Walter, P. *Protein Translocation Across the Endoplasmic Reticulum. I. Detection in the Microsomal Membrane of a Receptor for the Signal Recognition Particle*. vol. 95 <http://rupress.org/jcb/article-pdf/95/2/463/1402487/463.pdf> (1982).
10. Halic, M. & Beckmann, R. The signal recognition particle and its interactions during protein targeting. *Current Opinion in Structural Biology* vol. 15 116–125 Preprint at <https://doi.org/10.1016/j.sbi.2005.01.013> (2005).
11. Shan, S. O., Schmid, S. L. & Zhang, X. Signal recognition particle (SRP) and SRP receptor: A new paradigm for multistate regulatory GTPases. *Biochemistry* **48**, 6696–6704 (2009).
12. Giirlich', D. & Rapoport, T. A. *Protein Translocation into Proteoliposomes Reconstituted from Purified Components of the Endoplasmic Reticulum Membrane*. *Cell* vol. 75 (1993).
13. Jackson, R. C. & Blobel, G. *Post-translational cleavage of presecretory proteins with an extract of rough microsomes from dog pancreas containing signal peptidase activity (deoxycholate extraction/signal peptide/latency)*. *Cell Biology* vol. 74 <https://www.pnas.org> (1977).
14. Gogala, M. *et al.* Structures of the Sec61 complex engaged in nascent peptide translocation or membrane insertion. *Nature* **506**, 107–110 (2014).
15. Pfeffer, S. *et al.* Structure of the native Sec61 protein-conducting channel. *Nat Commun* **6**, (2015).

16. Li, L. *et al.* Crystal structure of a substrate-engaged SecY protein-translocation channel. *Nature* **531**, 395–399 (2016).
17. McGilvray, P. T. *et al.* An ER translocon for multi-pass membrane protein biogenesis. *Elife* **9**, 1–43 (2020).
18. Tyedmers, J., Lerner, M., Wiedmann, M., Volkmer, J. & Zimmermann, R. Polypeptide-binding proteins mediate completion of co-translational protein translocation into the mammalian endoplasmic reticulum. *EMBO Rep* **4**, 505–510 (2003).
19. Brodsky, J. L., Goekeler, J. & Schekmantt, R. *BiP and Sec63p are required for both co- and posttranslational protein translocation into the yeast endoplasmic reticulum (DnaJ/heat shock proteins/70-kDa heat shock protein)*. *Cell Biology* vol. 92 <https://www.pnas.org> (1995).
20. Pfeffer, S. *et al.* Structure of the mammalian oligosaccharyl-transferase complex in the native ER protein translocon. *Nat Commun* **5**, (2014).
21. Freedman, R. B. *The formation of protein disulphide bonds*. *Current Opinion in Structural Biology* vol. 5 (1995).
22. Ast, T., Cohen, G. & Schuldiner, M. A network of cytosolic factors targets SRP-independent proteins to the endoplasmic reticulum. *Cell* **152**, 1134–1145 (2013).
23. Viotti, C. ER to Golgi-Dependent Protein Secretion: The Conventional Pathway. *Methods Mol. Biol.* **1459**, 3–29 (2016).
24. Ellgaard, L. & Helenius, A. Quality control in the endoplasmic reticulum. *Nature Reviews Molecular Cell Biology* vol. 4 181–191 Preprint at <https://doi.org/10.1038/nrm1052> (2003).
25. Gomez-Navarro, N. & Miller, E. Protein sorting at the ER-Golgi interface. *Journal of Cell Biology* **215**, 769–778 (2016).
26. Béthune, J. & Wieland, F. T. Assembly of COPI and COPII Vesicular Coat Proteins on Membranes. (2018) doi:10.1146/annurev-biophys.
27. Peotter, J., Kasberg, W., Pustova, I. & Audhya, A. COPII-mediated trafficking at the ER/ERGIC interface. *Traffic* vol. 20 491–503 Preprint at <https://doi.org/10.1111/tra.12654> (2019).
28. Szul, T. & Sztul, E. COPII and COPI traffic at the ER-Golgi interface. *Physiology* **26**, 348–364 (2011).
29. Appenzeller-Herzog, C. & Hauri, H. P. The ER-Golgi intermediate compartment (ERGIC): In search of its identity and function. *J Cell Sci* **119**, 2173–2183 (2006).
30. Brandizzi, F. & Barlowe, C. Organization of the ER-Golgi interface for membrane traffic control. *Nature Reviews Molecular Cell Biology* vol. 14 382–392 Preprint at <https://doi.org/10.1038/nrm3588> (2013).
31. Hanisch, F.-G., Reis, C. A., Clausen, H. & Paulsen, H. *Evidence for glycosylation-dependent activities of polypeptide N-acetylgalactosaminyltransferases rGalNAc-T2 and-T4 on mucin glycopeptides*. *Glycobiology* vol. 11 (2001).
32. 1-s2.0-S0955067400001162-main.
33. Bannykh, S. I. & Balch, W. E. *Mini-Review Membrane Dynamics at the Endoplasmic Reticulum-Golgi Interface*. *The Journal of Cell Biology* vol. 138 <http://rupress.org/jcb/article-pdf/138/1/1/1270804/14551.pdf> (1997).
34. Mironov, A. A., Weidman, P. & Luini, A. *Mini-Review Variations on the Intracellular Transport Theme: Maturing Cisternae and Trafficking Tubules*. *The Journal of Cell Biology* vol. 138 <http://www.jcb.org> (1997).

35. Glick, B. S., Elston, T. & Oster, G. *Hypothesis A cisternal maturation mechanism can explain the asymmetry of the Golgi stack. FEBS 19132 FEBS Letters* vol. 414 (1997).
36. Marsh, B. J., Volkmann, N., Mcintosh, J. R. & Howell, K. E. *Direct continuities between cisternae at different levels of the Golgi complex in glucose-stimulated mouse islet beta cells.* <https://www.pnas.org> (2004).
37. Trucco, A. *et al.* Secretory traffic triggers the formation of tubular continuities across Golgi sub-compartments. *Nat Cell Biol* **6**, 1071–1081 (2004).
38. Park, K., Ju, S., Kim, N. & Park, S. Y. The Golgi complex: a hub of the secretory pathway. *BMB Rep* **54**, 246–252 (2021).
39. Ponnambalam, S. & Baldwin, S. A. Constitutive protein secretion from the trans-Golgi network to the plasma membrane. *Molecular Membrane Biology* vol. 20 129–139 Preprint at <https://doi.org/10.1080/0968768031000084172> (2003).
40. Jamora, C. Regulated secretion. *Genome Biol* **1**, (2000).
41. *TALKING POINT.* (1990).
42. Nickel, W. Pathways of unconventional protein secretion. *Current Opinion in Biotechnology* vol. 21 621–626 Preprint at <https://doi.org/10.1016/j.copbio.2010.06.004> (2010).
43. Dimou, E. & Nickel, W. Unconventional mechanisms of eukaryotic protein secretion. *Current Biology* vol. 28 R406–R410 Preprint at <https://doi.org/10.1016/j.cub.2017.11.074> (2018).
44. Rabouille, C., Malhotra, V. & Nickel, W. Diversity in unconventional protein secretion. *J Cell Sci* **125**, 5251–5255 (2012).
45. Rabouille, C. Pathways of Unconventional Protein Secretion. *Trends in Cell Biology* vol. 27 230–240 Preprint at <https://doi.org/10.1016/j.tcb.2016.11.007> (2017).
46. Steringer, J. P. & Nickel, W. A direct gateway into the extracellular space: Unconventional secretion of FGF2 through self-sustained plasma membrane pores. *Seminars in Cell and Developmental Biology* vol. 83 3–7 Preprint at <https://doi.org/10.1016/j.semcd.2018.02.010> (2018).
47. Auron, P. E. *et al.* *Nucleotide sequence of human monocyte interleukin 1 precursor cDNA.* vol. 81 <https://www.pnas.org> (1984).
48. Furutani, Y. *et al.* *Volume 13 Number 16 1985 Nucleic Acids Cloning and characterization of the cDNAs for human and rabbit interleukin-1 precursor.*
49. Cruz-Garcia, D., Malhotra, V. & Curwin, A. J. Unconventional protein secretion triggered by nutrient starvation. *Seminars in Cell and Developmental Biology* vol. 83 22–28 Preprint at <https://doi.org/10.1016/j.semcd.2018.02.021> (2018).
50. Sitia, R. & Rubartelli, A. The unconventional secretion of IL-1 β : Handling a dangerous weapon to optimize inflammatory responses. *Seminars in Cell and Developmental Biology* vol. 83 12–21 Preprint at <https://doi.org/10.1016/j.semcd.2018.03.011> (2018).
51. Martin-Sanchez, F. *et al.* Inflammasome-dependent IL-1 β release depends upon membrane permeabilisation. *Cell Death Differ* **23**, 1219–1231 (2016).
52. Ding, J. *et al.* Pore-forming activity and structural autoinhibition of the gasdermin family. *Nature* **535**, 111–116 (2016).
53. Liu, X. *et al.* Inflammasome-activated gasdermin D causes pyroptosis by forming membrane pores. *Nature* **535**, 153–158 (2016).
54. Pallotta, M. T. & Nickel, W. FGF2 and IL-1 β - Explorers of unconventional secretory pathways at a glance. *J Cell Sci* **133**, (2020).

55. Rayne, F. *et al.* Phosphatidylinositol-(4,5)-bisphosphate enables efficient secretion of HIV-1 Tat by infected T-cells. *EMBO Journal* **29**, 1348–1362 (2010).
56. Ensoli, B., Barillari, G., Zaki Salahuddin, S., GaDo, R. C. & WongStaal, F. *Tat protein of HIV-1 stimulates growth of cells derived from Kaposi's sarcoma lesions of AIDS patients.* (1990).
57. Ghafouri, M., Amini, S., Khalili, K. & Sawaya, B. E. HIV-1 associated dementia: Symptoms and causes. *Retrovirology* vol. 3 Preprint at <https://doi.org/10.1186/1742-4690-3-28> (2006).
58. Mele, A. R. *et al.* Defining the molecular mechanisms of HIV-1 Tat secretion: PtdIns(4,5)P₂ at the epicenter. *Traffic* vol. 19 655–665 Preprint at <https://doi.org/10.1111/tra.12578> (2018).
59. Agostini, S. *et al.* Inhibition of Non Canonical HIV-1 Tat Secretion Through the Cellular Na⁺,K⁺-ATPase Blocks HIV-1 Infection. *EBioMedicine* **21**, 170–181 (2017).
60. Stewart, S. E., Ashkenazi, A., Williamson, A., Rubinsztein, D. C. & Moreau, K. Transbilayer phospholipid movement facilitates the translocation of annexin across membranes. *J Cell Sci* **131**, (2018).
61. Lizarbe, M. A., Barrasa, J. I., Olmo, N., Gavilanes, F. & Turnay, J. Annexin-phospholipid interactions. Functional implications. *International Journal of Molecular Sciences* vol. 14 2652–2683 Preprint at <https://doi.org/10.3390/ijms14022652> (2013).
62. Gerke, V., Creutz, C. E. & Moss, S. E. Annexins: Linking Ca²⁺ signalling to membrane dynamics. *Nature Reviews Molecular Cell Biology* vol. 6 449–461 Preprint at <https://doi.org/10.1038/nrm1661> (2005).
63. Gerke, V. & Moss, S. E. Annexins: From Structure to Function. (2002) doi:10.1152/physrev.00030.2001.-Annexins.
64. Katsinelos, T. *et al.* Unconventional Secretion Mediates the Trans-cellular Spreading of Tau. *Cell Rep* **23**, 2039–2055 (2018).
65. Merezko, M. *et al.* Secretion of Tau via an Unconventional Non-vesicular Mechanism. *Cell Rep* **25**, 2027-2035.e4 (2018).
66. Merezko, M., Uronen, R. L. & Huttunen, H. J. The Cell Biology of Tau Secretion. *Frontiers in Molecular Neuroscience* vol. 13 Preprint at <https://doi.org/10.3389/fnmol.2020.569818> (2020).
67. Ketchum, C. J., Schmidt, W. K., Rajendrakumar, G. v., Michaelis, S. & Maloney, P. C. The Yeast a-factor Transporter Ste6p, a Member of the ABC Superfamily, Couples ATP Hydrolysis to Pheromone Export. *Journal of Biological Chemistry* **276**, 29007–29011 (2001).
68. Kuchler, K., Sterne, R. E. & Thorner, J. *Saccharomyces cerevisiae* STE6 gene product: a novel pathway for protein export in eukaryotic cells. *EMBO Journal* **8**, 3973–3984 (1989).
69. Claus, S., Jezierska, S. & van Bogaert, I. N. A. Protein-facilitated transport of hydrophobic molecules across the yeast plasma membrane. *FEBS Letters* vol. 593 1508–1527 Preprint at <https://doi.org/10.1002/1873-3468.13469> (2019).
70. Mambula, S. S. & Calderwood, S. K. Heat induced release of Hsp70 from prostate carcinoma cells involves both active secretion and passive release from necrotic cells. *International Journal of Hyperthermia* **22**, 575–585 (2006).
71. Mambula, S. S. & Calderwood, S. K. Heat Shock Protein 70 Is Secreted from Tumor Cells by a Nonclassical Pathway Involving Lysosomal Endosomes. *The Journal of Immunology* **177**, 7849–7857 (2006).

72. Kinseth, M. A. *et al.* The Golgi-Associated Protein GRASP Is Required for Unconventional Protein Secretion during Development. *Cell* **130**, 524–534 (2007).
73. Subramani, S. & Malhotra, V. Non-autophagic roles of autophagy-related proteins. *EMBO Reports* vol. 14 143–151 Preprint at <https://doi.org/10.1038/embor.2012.220> (2013).
74. Curwin, A. J. *et al.* ESCRT-III drives the final stages of CUPS maturation for unconventional protein secretion. doi:10.7554/eLife.16299.001.
75. Cruz-Garcia, D. *et al.* Remodeling of secretory compartments creates CUPS during nutrient starvation. *Journal of Cell Biology* **207**, 695–703 (2014).
76. Bruns, C., Mccaffery, J. M., Curwin, A. J., Duran, J. M. & Malhotra, V. Biogenesis of a novel compartment for autophagosome-mediated unconventional protein secretion. *Journal of Cell Biology* **195**, 979–992 (2011).
77. Cruz-Garcia, D. *et al.* A diacidic motif determines unconventional secretion of wild-type and ALS-linked mutant SOD1. *Journal of Cell Biology* **216**, 2691–2700 (2017).
78. Rubartelli, A., Cozzolino, F., Talio, M. & Sitia, R. A novel secretory pathway for interleukin-1 β , a protein lacking a signal sequence. *EMBO Journal* **9**, 1503–1510 (1990).
79. Mackenzie, A. *et al.* *Per-regaux and Gabel. Immunity* vol. 8 <http://www.immunity.com/> (2001).
80. Dupont, N. *et al.* Autophagy-based unconventional secretory pathway for extracellular delivery of IL-1 β . *EMBO Journal* **30**, 4701–4711 (2011).
81. Zhang, M., Kenny, S. J., Ge, L., Xu, K. & Schekman, R. Translocation of interleukin-1 β into a vesicle intermediate in autophagy-mediated secretion. *Elife* **4**, (2015).
82. Andrei, C. *et al.* *The Secretory Route of the Leaderless Protein Interleukin 1 Involves Exocytosis of Endolysosome-related Vesicles. Molecular Biology of the Cell* vol. 10 (1999).
83. Qu, Y., Franchi, L., Nunez, G. & Dubyak, G. R. Nonclassical IL-1 β Secretion Stimulated by P2X7 Receptors Is Dependent on Inflammasome Activation and Correlated with Exosome Release in Murine Macrophages. *The Journal of Immunology* **179**, 1913–1925 (2007).
84. Zhang, M. *et al.* A Translocation Pathway for Vesicle-Mediated Unconventional Protein Secretion. *Cell* **181**, 637-652.e15 (2020).
85. Gee, H. Y., Noh, S. H., Tang, B. L., Kim, K. H. & Lee, M. G. Rescue of Δ f508-CFTR trafficking via a GRASP-dependent unconventional secretion pathway. *Cell* **146**, 746–760 (2011).
86. Amaral, M. D. *CFTR and Chaperones Processing and Degradation. Journal of Molecular Neuroscience* vol. 41 <http://www.genet.> (2004).
87. Turcios, N. L. Cystic fibrosis lung disease: An overview. *Respir Care* **65**, 233–251 (2020).
88. Schweigerer, L. *et al.* *Capillary endothelial cells express basic fibroblast growth factor, a mitogen that promotes their own growth. Lindsay. K. & Noble. M. 1. Neurosci* vol. 34 (1967).
89. Seghezzi, G. *et al.* *Fibroblast Growth Factor-2 (FGF-2) Induces Vascular Endothelial Growth Factor (VEGF) Expression in the Endothelial Cells of Forming Capillaries: An Autocrine Mechanism Contributing to Angiogenesis. The Journal of Cell Biology* vol. 141 <http://www.jcb.org> (1998).

90. Vasiliasuskas, D. & Stern, C. D. Patterning the embryonic axis: FGF signaling and how vertebrate embryos measure time. *Cell* vol. 106 133–136 Preprint at [https://doi.org/10.1016/S0092-8674\(01\)00442-1](https://doi.org/10.1016/S0092-8674(01)00442-1) (2001).
91. Beenken, A. & Mohammadi, M. The FGF family: Biology, pathophysiology and therapy. *Nature Reviews Drug Discovery* vol. 8 235–253 Preprint at <https://doi.org/10.1038/nrd2792> (2009).
92. Chen, Y. *et al.* FGF2-mediated reciprocal tumor cell-endothelial cell interplay contributes to the growth of chemoresistant cells: a potential mechanism for superficial bladder cancer recurrence. *Tumor Biology* **37**, 4313–4321 (2016).
93. Jimenez-Pascual, A., Mitchell, K., Siebzehnrubl, F. A. & Lathia, J. D. FGF2: a novel druggable target for glioblastoma? *Expert Opinion on Therapeutic Targets* vol. 24 311–318 Preprint at <https://doi.org/10.1080/14728222.2020.1736558> (2020).
94. Schlessinger, J. *Cell Signaling by Receptor Review Tyrosine Kinases receptor) are monomers in the cell membrane. Ligand binding induces dimerization of these receptors re-sulting in autophosphorylation of their cytoplasmic do.* *Cell* vol. 103 (2000).
95. Schlessinger, J. *et al.* *Crystal Structure of a Ternary FGF-FGFR-Heparin Complex Reveals a Dual Role for Heparin in FGFR Binding and Dimerization D3 that plays an important role in determining ligand-receptor specificity (reviewed by Jaye et al Each of the FGFRs binds to a unique subset of FGFs accounting for the tight regulation and diversity in response to FGF stimulation (Ornitz. Medicine et al vol. 6 (2000).*
96. Häcker, U., Nybakken, K. & Perrimon, N. Heparan sulphate proteoglycans: The sweet side of development. *Nature Reviews Molecular Cell Biology* vol. 6 530–541 Preprint at <https://doi.org/10.1038/nrm1681> (2005).
97. Renko, M., Quarto, N., Morimoto, T. & Rifkin, D. B. *Nuclear and Cytoplasmic Localization of Different Basic Fibroblast Growth Factor Species.* *JOURNAL OF CELLULAR PHYSIOLOGY* vol. 144 (1990).
98. Sheng, Z., Lewis, J. A. & Chirico, W. J. Nuclear and nucleolar localization of 18-kDa fibroblast growth factor-2 is controlled by C-terminal signals. *Journal of Biological Chemistry* **279**, 40153–40160 (2004).
99. Mignatti, P. & Rifkin, D. 6. *Release of Basic Fibroblast Growth Factor, an Angiogenic Factor Devoid of Secretory Signal Sequence: A Trivial Phenomenon or a Novel Secretion Mechanism? Journal of Cellular Biochemistry* vol. 47 (1991).
100. Micnatti, P., Morimoto, T. & Rifkin, D. B. *Basic Fibroblast Growth Factor, a Protein Devoid of Secretory Signal Sequence, Is Released by Cells via a Pathway Independent of the Endoplasmic Reticulum-Colgi Complex.* *JOURNAL OF CELLULAR PHYSIOLOGY* vol. 151 (1992).
101. Nickel, W. Unconventional secretory routes: Direct protein export across the plasma membrane of mammalian cells. *Traffic* vol. 6 607–614 Preprint at <https://doi.org/10.1111/j.1600-0854.2005.00302.x> (2005).
102. Nickel, W. Unconventional secretion: An extracellular trap for export of fibroblast growth factor 2. *J Cell Sci* **120**, 2295–2299 (2007).
103. Sparn, C., Meyer, A., Saleppico, R. & Nickel, W. Unconventional secretion mediated by direct protein self-translocation across the plasma membranes of mammalian cells. *Trends in Biochemical Sciences* vol. 47 699–709 Preprint at <https://doi.org/10.1016/j.tibs.2022.04.001> (2022).

104. Zacherl, S. *et al.* A Direct Role for ATP1A1 in Unconventional Secretion of Fibroblast Growth Factor 2. *Journal of Biological Chemistry* **290**, 3654–3665 (2015).
105. Legrand, C. *et al.* The Na,K-ATPase acts upstream of phosphoinositide PI(4,5)P2 facilitating unconventional secretion of Fibroblast Growth Factor 2. *Commun Biol* **3**, (2020).
106. Ebert, A. D. *et al.* Tec-Kinase-Mediated Phosphorylation of Fibroblast Growth Factor 2 is Essential for Unconventional Secretion. *Traffic* **11**, 813–826 (2010).
107. la Venuta, G. *et al.* Small molecule inhibitors targeting tec kinase block unconventional secretion of fibroblast growth factor 2. *Journal of Biological Chemistry* **291**, 17787–17803 (2016).
108. Florkiewicz, R. Z., Anchin, J. & Baird, A. *The Inhibition of Fibroblast Growth Factor-2 Export by Cardenolides Implies a Novel Function for the Catalytic Subunit of Na,K-ATPase**. <http://www.jbc.org/> (1998).
109. Dahl, J. P., Binda, A., Canfield, V. A. & Levenson, R. Participation of Na,K-ATPase in FGF-2 secretion: Rescue of ouabain-inhibitable FGF-2 secretion by ouabain-resistant Na,K-ATPase α subunits. *Biochemistry* **39**, 14877–14883 (2000).
110. Steringer, J. P. *et al.* Key steps in unconventional secretion of fibroblast growth factor 2 reconstituted with purified components. (2017) doi:10.7554/eLife.28985.001.
111. Temmerman, K. *et al.* A direct role for phosphatidylinositol-4,5-bisphosphate in unconventional secretion of fibroblast growth factor 2. *Traffic* **9**, 1204–1217 (2008).
112. Müller, H. M. *et al.* Formation of disulfide bridges drives oligomerization, membrane pore formation, and translocation of fibroblast growth factor 2 to cell surfaces. *Journal of Biological Chemistry* **290**, 8925–8937 (2015).
113. Temmerman, K. & Nickel, W. A novel flow cytometric assay to quantify interactions between proteins and membrane lipids. *J Lipid Res* **50**, 1245–1254 (2009).
114. Sparn, C. *et al.* Glypican-1 drives unconventional secretion of Fibroblast Growth Factor 2. *Elife* **11**, (2022).
115. Lolicato, F. & Nickel, W. A Role for Liquid-Ordered Plasma Membrane Nanodomains Coordinating the Unconventional Secretory Pathway of Fibroblast Growth Factor 2? *Frontiers in Cell and Developmental Biology* vol. 10 Preprint at <https://doi.org/10.3389/fcell.2022.864257> (2022).
116. Skou, J. C. *The Influence of Some Cations on an Adenosine Triphosphatase from Peripheral Nerves*. *J Am Soc Nephrol* vol. 9 (1957).
117. Bublitz, M., Morth, J. P. & Nissen, P. P-type ATPases at a glance. *Journal of Cell Science* vol. 124 3917 Preprint at <https://doi.org/10.1242/jcs.102921> (2011).
118. Lopina, O. D., Tverskoi, A. M., Klimanova, E. A., Sidorenko, S. V. & Orlov, S. N. Ouabain-Induced Cell Death and Survival. Role of α 1-Na,K-ATPase-Mediated Signaling and $[Na^+]_i/[K^+]_i$ -Dependent Gene Expression. *Frontiers in Physiology* vol. 11 Preprint at <https://doi.org/10.3389/fphys.2020.01060> (2020).
119. Clausen, M. v., Hilbers, F. & Poulsen, H. The structure and function of the Na,K-ATPase isoforms in health and disease. *Frontiers in Physiology* vol. 8 Preprint at <https://doi.org/10.3389/fphys.2017.00371> (2017).
120. Geering, K. Function of FXYD proteins, regulators of Na,K-ATPase. *Journal of Bioenergetics and Biomembranes* vol. 37 387–392 Preprint at <https://doi.org/10.1007/s10863-005-9476-x> (2005).
121. Garty, H. & Karlish, S. J. D. FXYD Proteins: Tissue-Specific Regulators of the Na,K-ATPase. *Semin Nephrol* **25**, 304–311 (2005).

122. Blanco, G. Na,K-ATPase Subunit Heterogeneity as a Mechanism for Tissue-Specific Ion Regulation. *Semin Nephrol* **25**, 292–303 (2005).
123. Scheiner-Bobis, G. The sodium pump. Its molecular properties and mechanics of ion transport. *European Journal of Biochemistry* vol. 269 2424–2433 Preprint at <https://doi.org/10.1046/j.1432-1033.2002.02909.x> (2002).
124. Beggah, A. T., Jaunin, P. & Geering, K. Role of glycosylation and disulfide bond formation in the β subunit in the folding and functional expression of Na,K-ATPase. *Journal of Biological Chemistry* **272**, 10318–10326 (1997).
125. Tokhtaeva, E., Munson, K., Sachs, G. & Vagin, O. N-Glycan-Dependent Quality Control of the Na,K-ATPase β 2 Subunit. *Biochemistry* **49**, 3116–3128 (2010).
126. Gregersen, J. L., Mattle, D., Fedosova, N. U., Nissen, P. & Reinhard, L. Isolation, crystallization and crystal structure determination of bovine kidney Na⁺,K⁺-ATPase. *Acta Crystallographica Section:F Structural Biology Communications* **72**, 282–287 (2016).
127. Schneeberger, A. & Apell, H.-J. *Ion Selectivity of the Cytoplasmic Binding Sites of the Na,K-ATPase: I. Sodium Binding is Associated with a Conformational Rearrangement.*
128. Stolz, M. *et al.* Structural changes in the catalytic cycle of the Na⁺,K⁺-ATPase studied by infrared spectroscopy. *Biophys J* **96**, 3433–3442 (2009).
129. Leone, F. A., Furriel, R. P. M., McNamara, J. C., Horisberger, J. D. & Borin, I. A. Cation transport coupled to ATP hydrolysis by the (Na, K)-ATPase: An integrated, animated model. *Biochemistry and Molecular Biology Education* **38**, 276–279 (2010).
130. Castillo, J. P. *et al.* Mechanism of potassium ion uptake by the Na⁺/K⁺-ATPase. *Nat Commun* **6**, (2015).
131. 4220691.
132. Qiu, L. Y. *et al.* Reconstruction of the complete ouabain-binding pocket of Na,K-ATPase in gastric H,K-ATPase by substitution of only seven amino acids. *Journal of Biological Chemistry* **280**, 32349–32355 (2005).
133. Li, Y. Q. *et al.* Conversion of the low affinity ouabain-binding site of non-gastric H,K-ATPase into a high affinity binding site by substitution of only five amino acids. *Journal of Biological Chemistry* **281**, 13533–13539 (2006).
134. Dostanic-Larson, I. *et al.* Physiological role of the 1-and 2-isoforms of the Na-K-ATPase and biological significance of their cardiac glycoside binding site. *Am J Physiol Regul Integr Comp Physiol* **290**, 524–528 (2006).
135. 15685783.
136. Dmitrieva, R. I. & Doris, P. A. Cardiotonic Steroids: Potential Endogenous Sodium Pump Ligands with Diverse Function11. *Exp Biol Med* **227**, 561–569 (2002).
137. Goto, A., Yamada, K., Ishii, M. & Sugimoto, T. Digitalis-like activity in human plasma: Relation to blood pressure and sodium balance. *Am J Med* **89**, 420–426 (1990).
138. Mathews, W. R. *et al.* *Mass Spectral Characterization of an Endogenous Digitalislike Factor From Human Plasma.* <http://ahajournals.org>.
139. Schneider, R. *et al.* Bovine adrenals contain, in addition to ouabain, a second inhibitor of the sodium pump. *Journal of Biological Chemistry* **273**, 784–792 (1998).
140. Kawamura, A. *et al.* *On the structure of endogenous ouabain.* *Biochemistry* vol. 96 www.pnas.org. (1999).
141. Goto, A. *et al.* *ISOLATION OF A URINARY DIGITALIS-LIKE FACTOR INDISTINGUISHABLE FROM DIGOXIN. BIOCHEMICAL AND BIOPHYSICAL RESEARCH COMMUNICATIONS* vol. 173 (1990).

142. Lichtstein', D. *et al.* Identification of digitalis-like compounds in human cataractous lenses. *Eur. J. Biochem* vol. 216 (1993).
143. Bravený, P. *Heart, calcium and time. Exp Clin Cardiol* vol. 7 (2002).
144. Kaplan, J. H. Biochemistry of Na,K-ATPase. *Annu Rev Biochem.* **71**, 511–535 (2002).
145. pericles_17496632834.
146. Haas, M., Askari, A. & Xie, Z. Involvement of Src and epidermal growth factor receptor in the signal-transducing function of Na⁺/K⁺-ATPase. *Journal of Biological Chemistry* **275**, 27832–27837 (2000).
147. Yuan, Z. *et al.* Na/K-ATPase Tethers Phospholipase C and IP3 Receptor into a Calcium-regulatory Complex. *Mol Biol Cell* **16**, 4034–4045 (2005).
148. Haas, M., Wang, H., Tian, J. & Xie, Z. Src-mediated inter-receptor cross-talk between the Na⁺/K⁺-ATPase and the epidermal growth factor receptor relays the signal from ouabain to mitogen-activated protein kinases. *Journal of Biological Chemistry* **277**, 18694–18702 (2002).
149. Segall, L., Javaid, Z. Z., Carl, S. L., Lane, L. K. & Blostein, R. Structural basis for α 1 versus α 2 isoform-distinct behavior of the Na,K-ATPase. *Journal of Biological Chemistry* **278**, 9027–9034 (2003).
150. Liu, L. *et al.* Role of caveolae in ouabain-induced proliferation of cultured vascular smooth muscle cells of the synthetic phenotype. *Am J Physiol Heart Circ Physiol* **287**, 2173–2182 (2004).
151. Wang, X. Q. *et al.* Apoptotic insults impair Na⁺, K⁺-ATPase activity as a mechanism of neuronal death mediated by concurrent ATP deficiency and oxidant stress. *J Cell Sci* **116**, 2099–2110 (2003).
152. Zhang, S. *et al.* Distinct role of the N-terminal tail of the Na,K-ATPase catalytic subunit as a signal transducer. *Journal of Biological Chemistry* **281**, 21954–21962 (2006).
153. Liang, M., Cai, T., Tian, J., Qu, W. & Xie, Z. J. Functional characterization of Src-interacting Na/K-ATPase using RNA interference assay. *Journal of Biological Chemistry* **281**, 19709–19719 (2006).
154. Yuan, Z. *et al.* Na/K-ATPase Tethers Phospholipase C and IP3 Receptor into a Calcium-regulatory Complex. *Mol Biol Cell* **16**, 4034–4045 (2005).
155. Li, J., Zelenin, S., Aperia, A. & Aizman, O. Low doses of ouabain protect from serum deprivation-triggered apoptosis and stimulate kidney cell proliferation via activation of NF- κ B. *Journal of the American Society of Nephrology* **17**, 1848–1857 (2006).
156. Xie, Z. & Askari, A. Na⁺/K⁺-ATPase as a signal transducer. *European Journal of Biochemistry* vol. 269 2434–2439 Preprint at <https://doi.org/10.1046/j.1432-1033.2002.02910.x> (2002).
157. 14993422.
158. 12619881.
159. Katoh, M. & Nakagama, H. FGF Receptors: Cancer Biology and Therapeutics. *Med Res Rev* **34**, 280–300 (2014).
160. Lemmon, M. A. & Schlessinger, J. *Regulation of signal transduction and signal diversity by receptor oligomerization.* (1994).
161. Zehe, C., Engling, A., Wegehingel, S., Schä, T. & Nickel, W. Cell-surface heparan sulfate proteoglycans are essential components of the unconventional export machinery of FGF-2. www.pnas.org/cgi/doi/10.1073/pnas.0605997103 (2006).
162. Esko, J. D., Stewart, T. E. & Taylor, W. H. *Animal cell mutants defective in glycosaminoglycan biosynthesis (Chinese hamster ovary cells/replica*

- plating/proteoglycans/sulfation/xylosyltransferase*). *Biochemistry* vol. 82 <https://www.pnas.org> (1985).
163. Sarrazin, S., Lamanna, W. C. & Esko, J. D. Heparan sulfate proteoglycans. *Cold Spring Harb Perspect Biol* **3**, 1–33 (2011).
 164. Filmus, J., Capurro, M. & Rast, J. Glypicans. *Genome Biology* vol. 9 Preprint at <https://doi.org/10.1186/gb-2008-9-5-224> (2009).
 165. Svensson, G., Linse, S. & Mani, K. Chemical and thermal unfolding of glypican-1: Protective effect of heparan sulfate against heat-induced irreversible aggregation. *Biochemistry* **48**, 9994–10004 (2009).
 166. Paulick, M. G. & Bertozzi, C. R. The glycosylphosphatidylinositol anchor: A complex membrane-anchoring structure for proteins. *Biochemistry* vol. 47 6991–7000 Preprint at <https://doi.org/10.1021/bi8006324> (2008).
 167. Chatterjee, S. & Mayor, S. *The GPI-anchor and protein sorting*. *CMLS, Cell. Mol. Life Sci* vol. 58 (2001).
 168. Capurro, M. I., Xiang, Y.-Y., Lobe, C. & Filmus, J. *Glypican-3 Promotes the Growth of Hepatocellular Carcinoma by Stimulating Canonical Wnt Signaling*. <http://aacrjournals.org/cancerres/article-pdf/65/14/6245/2534283/6245-6254.pdf>.
 169. Capurro, M. I. *et al.* Glypican-3 Inhibits Hedgehog Signaling during Development by Competing with Patched for Hedgehog Binding. *Dev Cell* **14**, 700–711 (2008).
 170. Kreuger, J., Perez, L., Giraldez, A. J. & Cohen, S. M. *Opposing Activities of Dally-like Glypican at High and Low Levels of Wingless Morphogen Activity*. *Developmental Cell* vol. 7 (2004).
 171. Belenkaya, T. Y. *et al.* *Drosophila Dpp Morphogen Movement Is Independent of Dynamin-Mediated Endocytosis but Regulated by the Glypican Members of Heparan Sulfate Proteoglycans* (Entchev *et al* Teleman and Cohen, 2000). *Drosophila wings arise from wing imaginal discs that are subdivided into anterior (A) and posterior (P) compartments. During wing disc*. *Cell* vol. 119 <http://www.> (2004).
 172. Han, C. H., Belenkaya, T. Y., Wang, B. & Lin, X. *Drosophila glypicans control the cell-to-cell movement of Hedgehog by a dynamin-independent process*. *Development* **131**, 601–611 (2004).
 173. Akiyama, T. *et al.* Dally regulates Dpp morphogen gradient formation by stabilizing Dpp on the cell surface. *Dev Biol* **313**, 408–419 (2008).
 174. Raman, R., Venkataraman, G., Ernst, S., Sasisekharan, V. & Sasisekharan, R. Structural specificity of heparin binding in the fibroblast growth factor family of proteins. **100**, (2002).
 175. Gerrit van Meer, Dennis R. Voelker & Gerald W. Feigenson. *Membrane lipids: where they are and how they behave*. www.nature.com/reviews/molcellbio (2008).
 176. Shimizu, T. Lipid mediators in health and disease: Enzymes and receptors as therapeutic targets for the regulation of immunity and inflammation. *Annual Review of Pharmacology and Toxicology* vol. 49 123–150 Preprint at <https://doi.org/10.1146/annurev.pharmtox.011008.145616> (2009).
 177. Nakamura, M. T., Yudell, B. E. & Loor, J. J. Regulation of energy metabolism by long-chain fatty acids. *Progress in Lipid Research* vol. 53 124–144 Preprint at <https://doi.org/10.1016/j.plipres.2013.12.001> (2014).
 178. Saliba, A. E., Vonkova, I. & Gavin, A. C. The systematic analysis of protein-lipid interactions comes of age. *Nature Reviews Molecular Cell Biology* vol. 16 753–761 Preprint at <https://doi.org/10.1038/nrm4080> (2015).

179. Yamashita, A. *et al.* Acyltransferases and transacylases that determine the fatty acid composition of glycerolipids and the metabolism of bioactive lipid mediators in mammalian cells and model organisms. *Progress in Lipid Research* vol. 53 18–81 Preprint at <https://doi.org/10.1016/j.plipres.2013.10.001> (2014).
180. Suzuki, J., Umeda, M., Sims, P. J. & Nagata, S. Calcium-dependent phospholipid scrambling by TMEM16F. *Nature* **468**, 834–840 (2010).
181. Ohvo, H., Rekilä, R., Ramstedt, B., Leppimäki, P. L. & Slotte, J. P. *Cholesterol interactions with phospholipids in membranes*. www.elsevier.com/locate/plipres.
182. de Boer, J. F., Kuipers, F. & Groen, A. K. Cholesterol Transport Revisited: A New Turbo Mechanism to Drive Cholesterol Excretion. *Trends in Endocrinology and Metabolism* vol. 29 123–133 Preprint at <https://doi.org/10.1016/j.tem.2017.11.006> (2018).
183. Yeagle, P. L. *Modulation of membrane function by cholesterol*. *Biochimie* vol. 73 (1991).
184. Haines, T. H. *Do sterols reduce proton and sodium leaks through lipid bilayers?* *Progress in Lipid Research* vol. 40 www.elsevier.com/locate/plipres* (2001).
185. Rajendran, L. & Simons, K. Lipid rafts and membrane dynamics. *J Cell Sci* **118**, 1099–1102 (2005).
186. Simons, K. & Ikonen, E. *Functional rafts in cell membranes*. *Nature @ Macmillan Publishers Ltd* vol. 387 (1997).
187. Repa, J. J. & Mangelsdorf, D. J. *THE ROLE OF ORPHAN NUCLEAR RECEPTORS IN THE REGULATION OF CHOLESTEROL HOMEOSTASIS*. *Annu. Rev. Cell Dev. Biol* vol. 16 www.annualreviews.org (2000).
188. Mullen, P. J., Yu, R., Longo, J., Archer, M. C. & Penn, L. Z. The interplay between cell signalling and the mevalonate pathway in cancer. *Nature Reviews Cancer* vol. 16 718–731 Preprint at <https://doi.org/10.1038/nrc.2016.76> (2016).
189. Göbel, A., Rauner, M., Hofbauer, L. C. & Rachner, T. D. Cholesterol and beyond - The role of the mevalonate pathway in cancer biology. *Biochimica et Biophysica Acta - Reviews on Cancer* vol. 1873 Preprint at <https://doi.org/10.1016/j.bbcan.2020.188351> (2020).
190. Bloch, K. *The Biological Synthesis of Cholesterol*. <https://www.science.org> (1965).
191. Simons, K. & Ikonen, E. *How Cells Handle Cholesterol*. *Biochem. Biophys. Res. Commun* vol. 349 <https://www.science.org> (1994).
192. Peter, P. T. & Maciej, B. Statins: Then and Now. *METHODIST DEBAKEY CARDIOVASC J* **15**, 23–31 (2019).
193. Davignon, J. & Mabile, L. Mechanisms of action of statins and their pleiotropic effect. *Ann Endocrinol* **62**, 101–112 (2001).
194. Ohashi, K. *et al.* Early Embryonic Lethality Caused by Targeted Disruption of the 3-Hydroxy-3-methylglutaryl-CoA Reductase Gene. *Journal of Biological Chemistry* **278**, 42936–42941 (2003).
195. Endo, A., Kuroda, M. & Tsujita, Y. ML-236A, ML-236B and ML-236C, new inhibitors of cholesterol synthesis produced by *Penicillium citrinum*. *J Antibiot* **29**, 1346–1348 (1976).
196. Brown, A. G., Smale, T. C., King, J., Hasenkamp, R. & Thompson, R. H. Crystal and molecular structure of compactin, a new antifungal metabolite from *Penicillium brevicompactum*. *J Chem Soc Perkin* **1**, 1165–1170 (1976).
197. Endo, A., Kuroda, M. & Tanzawa, K. *COMPETITIVE INHIBITION OF 3-HYDROXY-3-METHYLGLUTARYL COENZYME A REDUCTASE BY ML-236A AND ML-236B FUNGAL METABOLITES, HAVING HYPOCHOLESTEROLEMIC ACTIVITY*.

198. Wächtershäuser, A., Akoglu, B. & Stein, J. *HMG-CoA reductase inhibitor mevastatin enhances the growth inhibitory effect of butyrate in the colorectal carcinoma cell line Caco-2*. (2001).
199. Mahammad, S. & Parmryd, I. *Cholesterol Depletion using Methyl- β -cyclodextrin*.
200. Zidovetzki, R. & Levitan, I. *Use of cyclodextrins to manipulate plasma membrane cholesterol content: evidence, misconceptions and control strategies*.
201. George Whitfield, B. B. *et al. Isolation and Properties of Filipin 4799 [Contribution from the Upjohn Filipin, an Antifungal Antibiotic: Isolation and Properties. J. Antibiotics (Japan), Ser. A vol. 20 https://pubs.acs.org/sharingguidelines (1955)*.
202. Kim, J. do, Han, J. W., Hwang, I. C., Lee, D. & Kim, B. S. Identification and biocontrol efficacy of *Streptomyces mihaensis* producing filipin III against *Fusarium wilt*. *J Basic Microbiol* **52**, 150–159 (2012).
203. Barreales, E. G., Payero, T. D., de Pedro, A. & Aparicio, J. F. Phosphate effect on filipin production and morphological differentiation in *Streptomyces filipinensis* and the role of the PhoP transcription factor. *PLoS One* **13**, (2018).
204. Maxfield, F. R. & Wüstner, D. Analysis of Cholesterol Trafficking with Fluorescent Probes. in *Methods in Cell Biology* vol. 108 367–393 (Academic Press Inc., 2012).
205. Gimpl, G. & Gehrig-Burger, K. Probes for studying cholesterol binding and cell biology. *Steroids* vol. 76 216–231 Preprint at <https://doi.org/10.1016/j.steroids.2010.11.001> (2011).
206. Kruth, H. S. *et al.* Type C Niemann-Pick disease. Abnormal metabolism of low density lipoprotein in homozygous and heterozygous fibroblasts. *Journal of Biological Chemistry* **261**, 16769–16774 (1986).
207. Carter, H. E., Glick, F. J., Norris, W. P. & Phillips, G. E. *BIOCHEMISTRY OF THE SPHINGOLIPIDES* III. STRUCTURE OF SPHINGOSINE*.
208. Mandon, E. C., Ehses, I., Rother, J., van Echten, G. & Sandhoff, K. *THE JOURNAL OF BIOLOGICAL CHEMISTRY Subcellular Localization and Membrane Topology of Serine Palmitoyltransferase, 3-Dehydrosphinganine Reductase, and Sphinganine N-Acyltransferase in Mouse Liver*. vol. 267 (1992).
209. Yasuda, S., Nishijima, M. & Hanada, K. Localization, topology, and function of the LCB1 subunit of serine palmitoyltransferase in mammalian cells. *Journal of Biological Chemistry* **278**, 4176–4183 (2003).
210. Pewzner-Jung, Y., Ben-Dor, S. & Futerman, A. H. When do Lasses (longevity assurance genes) become CerS (ceramide synthases)? Insights into the regulation of ceramide synthesis. *Journal of Biological Chemistry* vol. 281 25001–25005 Preprint at <https://doi.org/10.1074/jbc.R600010200> (2006).
211. Lahiri, S. *et al.* Kinetic characterization of mammalian ceramide synthases: Determination of Km values towards sphinganine. *FEBS Lett* **581**, 5289–5294 (2007).
212. Riebeling, C., Allegood, J. C., Wang, E., Merrill, A. H. & Futerman, A. H. Two Mammalian Longevity Assurance Gene (LAG1) Family Members, *trh1* and *trh4*, Regulate Dihydroceramide Synthesis Using Different Fatty Acyl-CoA Donors. *Journal of Biological Chemistry* **278**, 43452–43459 (2003).
213. Laviad, E. L. *et al.* Characterization of ceramide synthase 2: Tissue distribution, substrate specificity, and inhibition by sphingosine 1-phosphate. *Journal of Biological Chemistry* **283**, 5677–5684 (2008).
214. Venkataraman, K. *et al.* Upstream of growth and differentiation factor 1 (*uog1*), a mammalian homolog of the yeast longevity assurance gene 1 (LAG1), regulates N-

- stearoyl-sphinganine (C18-(dihydro)ceramide) synthesis in a fumonisin B1-independent manner in mammalian cells. *Journal of Biological Chemistry* **277**, 35642–35649 (2002).
215. Mizutani, Y., Kihara, A. & Igarashi, Y. Mammalian Lass6 and its related family members regulate synthesis of specific ceramides. *Biochemical Journal* **390**, 263–271 (2005).
216. Mizutani, Y., Kihara, A., Chiba, H., Tojo, H. & Igarashi, Y. 2-Hydroxy-ceramide synthesis by ceramide synthase family: Enzymatic basis for the preference of FA chain length. *J Lipid Res* **49**, 2356–2364 (2008).
217. Mizutani, Y., Kihara, A. & Igarashi, Y. LASS3 (longevity assurance homologue 3) is a mainly testis-specific (dihydro)ceramide synthase with relatively broad substrate specificity. *Biochemical Journal* **398**, 531–538 (2006).
218. Kentaro, H. *et al.* Molecular machinery for non-vesicular trafficking of ceramide. *Nature* **426**, 803–809 (2003).
219. Gault, C. R., Obeid, L. M. & Hannun, Y. A. *An overview of sphingolipid metabolism: from synthesis to breakdown.*
220. Ichikawa, S., SAKIYAMA, H., Suzuki, G., I-p Jwa Hidari, K. & Hirabayashi, Yoshi. *Expression cloning of a cDNA for human ceramide glucosyltransferase that catalyzes the first glycosylation step of glycosphingolipid synthesis (glucosylceramide/glucocerebroside/glucosylceramide synthase/melanoma).* vol. 93 <https://www.pnas.org> (1996).
221. Breiden Bernadette and Sandhoff, K. Ganglioside Metabolism and Its Inherited Diseases. in *Gangliosides: Methods and Protocols* (ed. Sonnino Sandro and Prinetti, A.) 97–141 (Springer New York, 2018). doi:10.1007/978-1-4939-8552-4_5.
222. Tafesse, F. G., Ternes, P. & Holthuis, J. C. M. The multigenic sphingomyelin synthase family. *Journal of Biological Chemistry* vol. 281 29421–29425 Preprint at <https://doi.org/10.1074/jbc.R600021200> (2006).
223. Dieter, W., Rudi, M., Anderer, Z. F. A. & Kanfer, J. N. *THE ROLE OF ENDOGENOUS PHOSPHATIDYLCHOLINE AND CERAMIDE IN THE BIOSYNTHESIS OF SPHINGOMYELIN IN MOUSE FIBROBLASTS.*
224. Marggraf, W.-D., Anderer, F. A. & Kanfer, J. N. *THE FORMATION OF SPHINGOMYELIN FROM PHOSPHATIDYLCHOLINE IN PLASMA MEMBRANE PREPARATIONS FROM MOUSE FIBROBLASTS.* *Biochimica et Biophysica Acta* vol. 664 (1981).
225. Bernert, J. T. & David Ullman, M. *BIOSYNTHESIS OF SPHINGOMYELIN FROM erythro-CERAMIDES AND PHOSPHATIDYLCHOLINE BY A MICROSOMAL CHOLINEPHOSPHOTRANSFERASE.* *Biochimica et Biophysica Acta* vol. 666 (1981).
226. David, M. & Radin, N. S. *The Enzymatic Formation of Sphingomyelin from Ceramide and Lecithin in Mouse Liver**. *THE JOURNAL OF BIOLOGICAL CHEMISTRY* vol. 249 (1974).
227. Kamil, B., Anna, F., Anna, S., Sławomir, P. & Halina, C. Regulation of sphingomyelin metabolism. *Pharmacological Reports* vol. 68 570–581 Preprint at <https://doi.org/10.1016/j.pharep.2015.12.008> (2016).
228. Adada, M., Luberto, C. & Canals, D. Inhibitors of the sphingomyelin cycle: Sphingomyelin synthases and sphingomyelinases. *Chemistry and Physics of Lipids* vol. 197 45–59 Preprint at <https://doi.org/10.1016/j.chemphyslip.2015.07.008> (2016).
229. Duan, R. D. *et al.* Purification, localization, and expression of human intestinal alkaline sphingomyelinase. *J Lipid Res* **44**, 1241–1250 (2003).

230. Schissel, S. L., Keesler, G. A., Schuchman, E. H., Williams, K. J. & Tabas, I. *The Cellular Trafficking and Zinc Dependence of Secretory and Lysosomal Sphingomyelinase, Two Products of the Acid Sphingomyelinase Gene**. <http://www.jbc.org> (1998).
231. Schissel, S. L., Schuchman ¶, E. H., Williams, K. J. & Tabas, I. *Zn 2-stimulated Sphingomyelinase Is Secreted by Many Cell Types and Is a Product of the Acid Sphingomyelinase Gene**. (1996).
232. Brady, R. O., Kanfer, J. N., Mock, M. B. & Fredrickson, D. S. *THE METABOLISM OF SPHINGOMYELIN, H. EVIDENCE OF AN ENZYMATIC DEFICIENCY IN NIEMANN-PICK DISEASE*. vol. 4 <https://www.pnas.org>.
233. Schneider, P. B. & Kennedy, E. P. *Sphingomyelinase in normal human spleens and in spleens from subjects with Niemann-Pick disease*. (1967).
234. Schuchman, E. H. & Desnick, R. J. Types A and B Niemann-Pick disease. *Molecular Genetics and Metabolism* vol. 120 27–33 Preprint at <https://doi.org/10.1016/j.ymgme.2016.12.008> (2017).
235. Hofmann, K., Tomiuk, S., Wolff, G. & Stoffel, W. *Cloning and characterization of the mammalian brain-specific, Mg 2-dependent neutral sphingomyelinase*. *National Institutes of Health* www.ch.embnet.org/software/TMPREDform.html (2000).
236. Tani, M. & Hannun, Y. A. Neutral sphingomyelinase 2 is palmitoylated on multiple cysteine residues: Role of palmitoylation in subcellular localization. *Journal of Biological Chemistry* **282**, 10047–10056 (2007).
237. Sezgin, E., Levental, I., Mayor, S. & Eggeling, C. The mystery of membrane organization: Composition, regulation and roles of lipid rafts. *Nature Reviews Molecular Cell Biology* vol. 18 361–374 Preprint at <https://doi.org/10.1038/nrm.2017.16> (2017).
238. Stier, A. & Sackmann, E. Heterogeneous lipid distribution in liver microsomal membranes. *Biochim Biophys Acta* **311**, 400–408 (1973).
239. Israelachvili, J. N., Marčelja, S. & Horn, R. G. Physical principles of membrane organization. *Q Rev Biophys* **13**, 121–200 (1980).
240. Karnovsky, M. J., Kleinfeld, A. M., Hoover, R. L. & Klausner, R. D. *The Concept of Lipid Domains in Membranes*. <http://rupress.org/jcb/article-pdf/94/1/1/1076005/1.pdf>.
241. Fantini, J., Garmy, N., Mahfoud, R. & Yahi, N. Lipid rafts: structure, function and role in HIV, Alzheimer's and prion diseases. *Expert reviews in molecular medicine* vol. 4 1–22 Preprint at <https://doi.org/10.1017/S1462399402005392> (2002).
242. Parton, R. G. & Simons, K. Digging into Caveolae. *Science (1979)* **269**, 1398–1399 (1995).
243. Brown, D. A. & Rose, J. K. Sorting of GPI-anchored proteins to glycolipid-enriched membrane subdomains during transport to the apical cell surface. *Cell* **68**, 533–544 (1992).
244. Magee, A. I. & Parmryd, I. *Detergent-resistant membranes and the protein composition of lipid rafts*. *Genome Biology* vol. 4 <http://genomebiology.com/2003/4/11/234> (2003).
245. Parton, R. G., Tillu, V. A. & Collins, B. M. *Caveolae*. *R402 Current Biology* vol. 28 (2018).
246. Kurzchalia, T. v. & Parton, R. G. Membrane microdomains and caveolae. *Curr. Opin. Cell Biol.* **11**, 424–431 (1999).
247. Danielsen, E. M. & van Deurs, B. *A Transferrin-like GPI-linked Iron-binding Protein in Detergent-insoluble Noncaveolar Microdomains at the Apical Surface of Fetal*

- Intestinal Epithelial Cells*. <http://rupress.org/jcb/article-pdf/131/4/939/1265363/939.pdf>.
248. Sargiacomo, M., Sudol, M., Tang, Z. & Lisanti, M. P. *Signal Transducing Molecules and Glycosyl-phosphatidylinositol-Minked Proteins Form a Caveolin-rich Insoluble Complex in MDCK Cells*. <http://rupress.org/jcb/article-pdf/122/4/789/1258349/789.pdf>.
 249. Simons, K. & Toomre, D. *LIPID RAFTS AND SIGNAL TRANSDUCTION. NATURE REVIEWS / MOLECULAR CELL BIOLOGY* vol. 1 www.nature.com/reviews/molcellbio (2000).
 250. Rajendran, L. *et al. Asymmetric localization of flotillins reggies in preassembled platforms confers inherent polarity to hematopoietic cells*. www.pnas.org/cgi/doi/10.1073/pnas.1331629100.
 251. Lolicato, F. & Nickel, W. A Role for Liquid-Ordered Plasma Membrane Nanodomains Coordinating the Unconventional Secretory Pathway of Fibroblast Growth Factor 2? *Frontiers in Cell and Developmental Biology* vol. 10 Preprint at <https://doi.org/10.3389/fcell.2022.864257> (2022).
 252. la Venuta, G., Zeitler, M., Steringer, J. P., Müller, H. M. & Nickel, W. The startling properties of fibroblast growth factor 2: How to exit mammalian cells without a signal peptide at hand. *Journal of Biological Chemistry* vol. 290 27015–27020 Preprint at <https://doi.org/10.1074/jbc.R115.689257> (2015).
 253. Fish, K. N. Total internal reflection fluorescence (TIRF) microscopy. *Current Protocols in Cytometry* Preprint at <https://doi.org/10.1002/0471142956.cy1218s50> (2009).
 254. Ambrose, E. J. A Surface Contact Microscope for the study of Cell Movements. *Nature* **178**, 1194–1194 (1956).
 255. Mattheyses, A. L. & Axelrod, D. Direct measurement of the evanescent field profile produced by objective-based total internal reflection fluorescence. *J Biomed Opt* **11**, 014006 (2006).
 256. Brunstein, M., Teremetz, M., Héroult, K., Tourain, C. & Oheim, M. Eliminating unwanted far-field excitation in objective-type TIRF. Part I. Identifying sources of nonevanescant excitation light. *Biophys J* **106**, 1020–1032 (2014).
 257. Ambrose, W. P., Goodwin, P. M. & Nolan, J. P. *Single-Molecule Detection With Total Internal Reflection Excitation: Comparing Signal-to-Background and Total Signals in Different Geometries*. *Cytometry* vol. 36 (1999).
 258. Fairlamb, M. S., Whitaker, A. M., Bain, F. E., Spies, M. & Freudenthal, B. D. Construction of a three-color prism-based tirf microscope to study the interactions and dynamics of macromolecules. *Biology (Basel)* **10**, (2021).
 259. Gibbs, D. R., Kaur, A., Megalathan, A., Sapkota, K. & Dhakal, S. Build your own microscope: Step-by-step guide for building a prism-based tirf microscope. *Methods and Protocols* vol. 1 1–16 Preprint at <https://doi.org/10.3390/mps1040040> (2018).
 260. Friedman, L. J., Chung, J. & Gelles, J. Viewing dynamic assembly of molecular complexes by multi-wavelength single-molecule fluorescence. *Biophys J* **91**, 1023–1031 (2006).
 261. Sako, Y., Minoguchi, S. & Yanagida, T. *Single-molecule imaging of EGFR signalling on the surface of living cells*. *NATURE CELL BIOLOGY* vol. 2 (2000).
 262. Dimou, E. *et al.* Single event visualization of unconventional secretion of FGF2. *Journal of Cell Biology* **218**, 683–699 (2019).
 263. Mattheyses, A. L., Simon, S. M. & Rappoport, J. Z. Imaging with total internal reflection fluorescence microscopy for the cell biologist. *Journal of Cell Science* vol. 123 3621–3628 Preprint at <https://doi.org/10.1242/jcs.056218> (2010).

264. Davis, M. W. & Jorgensen, E. M. ApE, A Plasmid Editor: A Freely Available DNA Manipulation and Visualization Program. *Frontiers in Bioinformatics* **2**, (2022).
265. Schindelin, J. *et al.* Fiji: An open-source platform for biological-image analysis. *Nature Methods* vol. 9 676–682 Preprint at <https://doi.org/10.1038/nmeth.2019> (2012).
266. Tinevez, J. Y. *et al.* TrackMate: An open and extensible platform for single-particle tracking. *Methods* **115**, 80–90 (2017).
267. Sparn, C. *et al.* Glypican-1 drives unconventional secretion of Fibroblast Growth Factor 2. doi:10.1101/2021.11.11.468179.
268. Temmerman, K. *et al.* A direct role for phosphatidylinositol-4,5-bisphosphate in unconventional secretion of fibroblast growth factor 2. *Traffic* **9**, 1204–1217 (2008).
269. Florkiewicz, R. Z., Anchin, J. & Baird, A. *The Inhibition of Fibroblast Growth Factor-2 Export by Cardenolides Implies a Novel Function for the Catalytic Subunit of Na⁺,K⁺-ATPase**. <http://www.jbc.org/> (1998).
270. Akimova, O. A. *et al.* Critical role of the α 1-Na⁺, K⁺-ATPase subunit in insensitivity of rodent cells to cytotoxic action of ouabain. *Apoptosis* **20**, 1200–1210 (2015).
271. Norman, A. W., Demel, R. A., de Kruyff, B. & van Deepen, L. L. M. *Issw of &r& 25. THE JOURNAL OF B~LOGICAL CHEMISTRY* vol. 247 (1972).
272. Heidasch, R. *et al.* Intramembrane protease SPP defines a cholesterol-regulated switch of the mevalonate pathway. doi:10.1101/2021.07.19.452877.
273. Clarke, C. J. *et al.* The extended family of neutral sphingomyelinases. *Biochemistry* **45**, 11247–11256 (2006).
274. Engling, A. *et al.* Biosynthetic FGF-2 is targeted to non-lipid raft microdomains following translocation to the extracellular surface of CHO cells. *J Cell Sci* **115**, 3619–3631 (2002).
275. Pôças, E. S. C., Touza, N. A., da Silva, A. J. M., Costa, P. R. R. & Noël, F. Synergistic interaction between ouabain and 8-methoxy-3,9-dihydroxy coumestan, a non-steroidal synthetic inhibitor of Na⁺,K⁺-ATPase. *Life Sci* **81**, 1199–1204 (2007).
276. Saminathan, A. *et al.* A DNA-based voltmeter for organelles. *Nat Nanotechnol* **16**, 96–103 (2021).

8. Acknowledgments

After more than five years of scientific research in Heidelberg, there are several people I would like to acknowledge.

First of all, I would like to thank Prof. Dr. Walter Nickel. I am really grateful I had the chance to work with you Walter. You were able to understand my difficulties at the beginning and never stopped encouraging me and giving me positive feedbacks. I really understood what it means to be a scientist working together with you, and I also understood the big difference there is between positive and negative evidence. I cannot thank you enough for all the support you gave me throughout these years, not only with scientific advices, but also for personal issues. Many thanks!

I would like to thank Dr. Maria Teresa Pallotta. Teresa, you gave me a big opportunity putting me in contact with Walter. You also convinced me to try this experience, and told me that I would not regret work together with a decent person like Walter. You were indeed right, many thanks again!

About my university studies in Italy, I would also like to thank Prof. Dr. Ursula Grohmann. She has been a real guidance during the last year of the bachelor, and during the master in Perugia. It was really inspiring for me following your lectures and discussing with you about new issues on pharmacology and immunology. I am very grateful you even gave me the chance to give a lecture in one of your courses together with you. I am really sorry you are no longer with us. It has been a big loss for everyone who got the pleasure to meet you and to work with you, and for the scientific community as well. I will always keep a warm memory of you! Coming to other members of our group, I would like to start thanking Dr. Eleni Dimou and Dr. Taxiarchis Katsinelos. Eleni, you had a big impact on my PhD work, it goes without saying that most of this would not have been possible without you. Beyond teaching me a wonderful TIRF assay that you were able to establish yourself, you have been an example for me during the first months of this experience, together with Akis. I understood quite soon that I was working with two very great scientists, and I tried to take as many suggestions as possible from you. My hope is that, during these last months, I have done the same for the new generation of PhD students in our lab.

A big help also came from Sabine Wegehingel, I learned the vast majority of the biochemical and cell-based assays I have used during this PhD from you. I really enjoyed working together with you and learning several techniques from you, you were always very patient and positive. At the beginning of my path here, your approach to the daily work really helped me a lot, thanks again!

I would also like to thank Annalena Meyer. It has been a pleasure for me working with you, being neighbors in the lab with our benches, sharing buffers, protocols and advices. For a

couple of years, the work has been fun even when experiments did not go the best way, and that is mainly because of you Annalena. Many thanks also for proofreading this thesis. Many thanks to Dr. Fabio Lolicato. We shared projects and fun moments in the lab, as well as outside the lab. The lab has been indeed more fun ever since you joined, especially in the late afternoons and in the evenings, when we have been often the only ones around, doing experiments in a very joyful atmosphere!

I would like to also thank Dr. Hans-Michael Müller for his experienced advices in the lab, as well as for all the conversations we had about gardening, Italian cuisine and wines. Many thanks to all the other members of the Nickel group as well. Dr. Sebastian Unger, Dr. Mennatallah Ahmed, Dr. Cyril Legrand, Dr. Alina Muschko, Dr. Carola Sparn, and Stephani Schmitz, who already left the lab, and Dr. Julia Steringer, Daniel Beyer, Jaime Fernandez Sobaberas, the newly arrived Ali Lashkari and Manpreet Kaur, who are still part of this group. I would also like to thank two students who have been part of the group inside and outside the lab, Zeynep Kilcan and Elena Miari.

Many thanks to Barbara Schröter and Anke Heymann, who helped me a lot with all the bureaucracy and with their awesome organization skills.

I would like to further acknowledge Dr. Holger Lorenz and Christian Hoert from the ZMBH Imaging Facility for their help with the TIRF microscope.

Many thanks to Prof. Dr. Thomas Söllner and Prof. Dr. Oliver Fackler for their inspiring suggestions and scientific advices throughout my PhD thesis, and for agreeing, together with Prof. Dr. Matthias Mayer, to be part of the committee of this thesis defense.

I would also like to thank Prof. Dr. Britta Brügger, whose kind and brilliant suggestions helped me a lot during the two final project of this thesis.

Also, I am quite happy that the Schuck group joined our floor in this last year. You guys brought a friendly and international atmosphere in this environment, it has been a pleasure sharing the floor with all of you!

Coming to friends outside the lab, a big thank you goes to Alessandra Albertelli and to Cinthia Amaya Ramirez. Alessandra, you made me feel home from the very first day we met, in the 2018's Christmas markets. Thank you for being present throughout the up and downs of these years. And Cinthia, from the start of my PhD you tried to include me in social events and always tried to not make me feel alone, understanding my position better than anybody else. Thanks again to both of you!

Very important for me have been also Fabio Lolicato and Alessandra Griffo. Fabio, beyond sharing many projects and fun moments in the lab, we shared many experiences outside the lab as well, and I could always count on you and Alessandra during these last three years. Many thanks to Federica Fiorentino! I really enjoyed working with you in our cell culture for years and, beyond that, it has been really nice sharing many coffee breaks at the BZH and at the Botanik, talking about our respective experiences and sharing our concerns about the future in these last months.

I am also very happy I had the chance to meet such a good person like Giulia Ruffini in the last year. It was a happy surprise for me to find out that we used to go to the very same place, Grottammare, on holidays as kids (and still now as adults!). I really enjoy talking about cuisine and Italy in general, and I will not forget that my last visit in Berlin for our SFB meeting has been really nice mainly because of your presence, thanks again!

Thanks a lot to Federica Scollo, who I had the pleasure to meet during her visit to our lab in 2021. I am really happy we managed to stay in contact after you left Heidelberg, both for superficial and deeper conversations. I hope we could celebrate something soon about “our” FC Juventus, instead of suffering and texting each other about our opinions on Juve’s football games.

I would also like to thank Francesco Muraca, for all the beers and dinners we had together with Fabio, as well as the German course, and Janathan Altuzar, for being part of many fun evenings with Cinthia and Alessandra, and many others with Annalena.

Finally, even if not in Heidelberg, a big thank you goes to my best friend in the world Francesca Mecarelli. You are the main reason why, after recent events, I still believe in the word “friendship”. Nothing else is needed to explain your importance in my life.

Last but not most important, I would like to thank my family. Mamma, with your sacrifices you allowed me, together with dad, to live this experience, and you always encouraged me to continue this experience in difficult times, even if you would have preferred for me to live closer to you two. Thanks a lot for always being a supportive and reliable presence in my life. Many thanks to my sister Elisa, being ten years older than me you have always been a big reference for me. Thanks to you and to my brother-in-law, Mirko, also for bringing to life two wonderful kids, Diego and Matteo. Diego, you always fancy a lot my presence, and you were pretty sorry when I moved to Germany, when you were only six years old. I am sorry about that, but I hope you are still enjoying the time we are spending together during my summer and Christmas holidays at home. Matteo, it is always a pity for me to be able to spend so little time with you in your early years. I hope I am still passing something to you in the little time we can spend together.

And, of course, the biggest thank you goes to my father, Alvaro. Papà, from the very beginning of this experience you encouraged me to continue and to keep going during the difficulties I had at the beginning, being completely alone in a foreign country. I cannot thank you enough for all the sacrifices you and mom made for me, my sister, and my nephews. Your absence is felt more and more every day. Not everybody here was able to understand what this meant to me, and the impact your absence had on me. Luckily, I also found many people and friends who tried to understand what I was going through, and what I am still going through after more than a year. I will try my best to keep the promise I made to you a few days before you passed away, you can be sure of that!